COMBUSTION AND EMISSIONS CHARACTERISTICS OF METHANOL, METHANOL-WATER, AND GASOLINE-METHANOL BLENDS IN A SPARK IGNITION ENGINE

by

JULIAN A. LORUSSO

B.S.M.E., Purdue University
(1974)

SUBMITTED IN PARTIAL FULFILLMENT
OF THE REQUIREMENTS FOR THE
DEGREE OF

MASTER OF SCIENCE IN MECHANICAL ENGINEERING

at the

MASSACHUSETTS INSTITUTE OF TECHNOLOGY

May 1976

Signature of Author . . . . . .
Department of Mechanical Engineering,

Certified by . . . . . .
Thesis Supervisor

Accepted by . . . . . .
Chairman, Department Committee on Graduate Students

COMBUSTION AND EMISSIONS CHARACTERISTICS OF METHANOL, METHANOL-WATER, AND GASOLINE-METHANOL BLENDS IN A SPARK IGNITION ENGINE

by

JULIAN A. LORUSSO

Submitted to the Department of Mechanical Engineering on May 17,1976 in partial fulfilment of the requirements for the Degree of Master of Science.

ABSTRACT

Depletion of U.S. and global petroleum reserves has excited interest in synthetic-fuel replacements for petroleum. For automotive application, where gasoline would be replaced, synthetic gasoline and methanol produced from shale rock and/or coal appear to be the most practical alternatives.

Combustion characteristics -- kernel development, ignition delay, combustion duration, turbulent flame speed, thermal efficiency, energy efficiency and exhaust emissions -- are studied using a CFR engine. Indolene clear is used as a base fuel for all comparisons. 10% water-90% methanol, 15% methanol-85% indolene, and pure methanol are studied. Base operating conditions are at 1600 RPM, 53 psi imep, with MBT spark timing. A large constant temperature (180°F) fuel-air mixing chamber is used to insure mixture homogeneity and eliminate effects due to varying latent heats of vaporization. At a constant speed and load, equivalence ratio is varied to determine the practical lean limit of each fuel. Also, variation of spark advance relative to MBT, and compression ratio are investigated in the lean region where significant gains in energy efficiency and emissions quality are anticipated.

Kernel development, ignition delay, and combustion duration are shown to vary with equivalence ratio and fuel type, with methanol fuels exhibiting fastest burn rates. Turbulent flame speeds are calculated, and results are presented as a function of equivalence ratio, mass fraction burned, and normalized flame radius. Indicated thermal efficiencies and exhaust emissions levels are presented as functions of equivalence ratio, spark advance, and compression ratio. Special attention is given to the variation of thermodynamic properties calculated from measured pressure-time histories to explain differences in combustion characteristics observed.

Data presented is an attempt to produce an extended data base on methanol fuels so that trade-offs between consumer costs and efficiency gains can be done in a scientific - rational manner.

Thesis Supervisor: Rodney J. Tabaczynski
Title: Lecturer in Mechanical Engineering

ACKNOWLEDGMENTS

Completion of this paper would have been impossible without help from many people along the way. In general, it's a great feeling to be done, and I thank God for the strength and confidence he has given me to bring me this far in my career.

My first professional acknowledgment goes to my advisors Rod Tabaczysnki and John Heywood, for extending to me this great opportunity. Particularly I would like to thank Rod for his superb guidance, good humor, and patience along the way.

As a first personal acknowledgment, my thanks and appreciation go to my parents, Mary and Matthew LoRusso, for their inexhaustible supply of encouragement and support throughout my academic years, and for being two of the greatest parents anyone could ask for.

Next is my fiancee, Judy Catlin, who I thank for her patience through all the long hours I have not been able to spend with her in the past few months, for her encouragement to do my best, and most important, for being herself.

To my relatives and friends at home, I thank for all the help and encouragement throughout my academic years; particularly my Uncle, Louis Comis, may he rest in peace, for all his professional advice, and for introducing me to the engineering profession.

Next, I must thank Don Fitzgerald, our mechanical engineer in the Sloan Lab, for his most helpful assistance in the emissions measurements, and for being a really great guy.

To our Sloan Lab technicians, Larry Johnson, William Finley, and Sal Albino, I thank for their help and guidance in experimental techniques

and for being three of the greatest people ever.

My next thanks goes to Colin Ferguson, for his most helpful assistance in setting up the data analysis programs, and for an enjoyable acquaintance as a fellow student of the combustion sciences.

My friends in the Sloan Lab I would like to thank next for all the pleasant day-to-day consultations, and for being some really down-to-earth people.

To Professors N.M. Laurendeau, A.R. Spaulding, and V.W. Goldschmidt, Purdue University, I enjoy extending my thanks for their most appreciated help and guidance in my undergraduate years; particularly, Norm Laurendeau for introducing me to the combustion sciences.

My thanks to my friends at Purdue, especially the Phi Psi's, for much encouragement and great friendship.

To the Rome Strip Steel Co., Rome, N.Y., and personnel, for the financial support of my undergraduate education, and for much encouragement along the way, I am sincerely grateful.

Some other professional acknowledgments go to Joe Rife, Sloan Automotive Lab; Joe Harrington, Marjorie Roberts, and George Lavoie, Ford Motor Co.; and John P. Longwell, Exxon Research for some helpful suggestions.

Finally, my thanks go to Rosemary Carpenter for her typing skills and effort in the final draft, and Sharon Richardson for the typing of many supporting documents.

This work was supported by the Energy Laboratory, MIT, and John Hawley.

TABLE OF CONTENTS

TABLE OF CONTENTS (Contd.)

LIST OF TABLES

LIST OF FIGURES

LIST OF FIGURES (Contd.)

LIST OF FIGURES (Contd.)

LIST OF FIGURES (Contd.)

1. INTRODUCTION

Transportation and industrial uses of petroleum comprise roughly 23% and 7.5% of the total energy consumed in the U.S., respectively, where % of petroleum used in transportation is used as gasoline in automotive application (1,2). Recently methanol has received increased attention as a synthetic replacement to petroleum-derived fuels. Interest is centered around methanol's ability to be produced from abundant U.S. coal reserves, and it's potential for exhibiting significant emissions quality and energy conversion efficiency advantages when burned in various combustion devices.

Information in the literature is plentiful for automotive use of methanol; however, few systematic studies exist on combustion properties of ethanol, gasoline-methanol blends, and methanol-water blends. The objective of this study is to obtain more quantitative information on the combustion characteristics (kernel development, ignition delay, combustion duration, turbulent flame speed, thermal efficiency) and exhaust emissions characteristics of Methanol fuels. Indolene Clear is used as a base fuel for all comparisons, and the fuels studied are pure methanol, a 15% methanol-85% indolene blend, and a 10% water-90% methanol blend.

A thermodynamic analysis of the combustion process for oxygenated fuels is carried out in a Cooperative Fuel Research (CPR) engine. This approach requires accurate measurement of cylinder pressure versus crank angle, mass flow rates of fuel and air inducted, residual mole fractions, exhaust gas specie concentrations, and engine

performance data. Special attention is given to variations of thermodynamic properties for burned and unburned gases and relative burning rates during the combustion process to explain differences in the indicated thermal efficiency, lean misfire limits, and exhaust emissions levels for the various fuels.

A review of physical properties of methanol fuels and a review of performance in a spark ignition engine is first presented. In order to help put into perspective the systems nature of the process of converting to synthetic fuels, a section on methanol's potential for commercial application as a motor fuel is presented. This section, although more qualitative in nature, is presented to provide some perspective to the general problems of utilization alternate fuels.

2. A REVIEW OF THE PERFORMANCE OF METHANOL FUELS IN SPARK IGNITION ENGINES

2.1 Physical Properties

Before discussing the performance of methanol fuels in a spark ignition engine, some important physical properties of these fuels will be compared with those of indolene. Physical properties can be categorized as: 1) properties of a synthetic fuel stimulating its use because of its similarity to gasoline, and 2) properties of a synthetic fuel either stimulating or complicating its use because of its dissimilarity to gasoline. Table 1 lists the properties of the fuels studied.

Properties of methanol fuels similar to gasoline* would imply that few design changes in automotive technology would be required and engine performance would not be changed significantly. Methanol is a liquid at room temperature and temperatures well below freezing. It's energy content (volume or mass basis) implies that fuel storage in an automobile for a reasonable driving range is practical. Values of other properties such as liquid density, coefficient of expansion, surface tension, absolute viscosity, and specific heat of liquid are close in value to those of indolene.

Properties dissimilar to gasoline imply that design changes and new technology may be required; also, engine performance may be significantly altered. The properties advantageous to methanol's use are its better octane characteristics, wider and leaner flammability limits, and faster flame propagation speeds. These properties can

*The term "gasoline" is used interchangeably with "indolene."

generally contribute to improved thermal efficiency, emissions quality, and equal to or greater power output compared to that possible for indolene. Methanol's (as well as a methanol-water or a gasoline-methanol blend) latent heat of vaporization appears to improve octane quality, NO_x emissions, and volumetric efficiency due to the cooling of the unburned mixture. High latent heats of vaporization can also be a disadvantage in fuel/air mixing, especially in cold start situations (discussed next). Other disadvantageous properties of methanol (also methanol-water blends) are different fuel/air stoichiometry, lower heat of combustion, and low vapor pressure. The stoichiometric fuel/air ratio and the latent heat of vaporization are roughly 2 1/4 and 3 1/3 times that of gasoline, respectively. This implies that the carburetion and intake manifold systems would have to be modified to supply 2 1/4 times the additional fuel flow and roughly eight times the manifold heating to attain the proper degree of fuel/air mixture preparation. Assuring adequate performance of methanol and methanol-water blends in cold start situations will involve special design considerations. Methanol's single boiling point characteristics, low vapor pressure, and high latent heat of vaporization cause cold starts to be impossible at ambient temperatures below 50°F without starting fuel systems (discussed also in Section 5) (3,4). Gasoline-methanol blends have problems with phase separation and increased volatility. Roughly .5% water present in a 15% methanol-gasoline blend would completely separate the methanol from the gasoline forcing the

engine to be inoperable (5,6). A 3 psig increase in Reid vapor pressure would also result requiring modifications to the fuel system to handle the more volatile fuel mixture (5, 6, 7). Although not listed in Table 1, the use of any of the methanol fuels will also require additional fuel system corrosion precautions due to methanol's increased solvency and corrosion properties.

2.2 Discussion of Performance in a Spark Ignition Engine

The output of a spark ignition engine depends primarily upon the quantities of air and fuel inducted, spark timing relative to top dead center (TDC), inlet mixture temperature, compression ratio, shaft speed, oil temperature, and coolant temperature. A review of the performance of methanol in a spark ignition engine, i.e., output power, indicated specific fuel consumption, thermal efficiency, exhaust emissions, lean misfire limits, burning characteristics, and octane quality advantages, will be presented. Discussion will be centered around single cylinder engine (CFR and CLR) experiments since dependent variables that govern engine output can be effectively controlled; consequently, a better understanding of phenomena during combustion can be obtained. In multicylinder engines, situations such as cylinder-to-cylinder variations in fuel/air equivalence ratios exist which cause difficulty in interpreting the effects of dependent variables that govern engine output. Because of these difficulties, care should also be taken when translating single-cylinder engine data to results anticipated for multicylinder

engines (also discussed in Section 5).

Comparisons of maximum possible output power for methanol versus gasoline appear to be largely dependent upon effects of varying latent heats of vaporization. For an experimental set-up using a constant inlet temperature fuel-air mixing chamber, maximum power is approximately equal for methanol and isooctane (8). For a carburetor set up using a constant air temperature, uncontrolled inlet mixture temperature in a carburetor set up, an approximate 10% increase in maximum output power results for methanol compared with indolene at equal equivalence ratios (3, 9). Where inlet mixture temperatures are uncontrolled, greater depressions of the inlet charge temperatures for methanol (for one case 70°F with methanol versus 15°F with indolene) (9), result due to the higher latent heat of vaporization and mass flow rate of fuel. This results in a greater increase in inlet charge density and lower unburned gas temperatures during combustion; hence, volumetric efficiency and octane quality are improved (3,6,9,10,11,12). Slight reductions in compression work due to fuel droplets vaporized during compression (10) and energy conversion efficiency improvements due to faster flame propagation speeds could be additional factors explaining high output power with methanol.

Indicated specific fuel consumption (ISFC) for methanol is roughly twice as great as that for gasoline at comparable equivalence ratios and loads with MBT timing. This is in agreement with methanol's heat of combustion being roughly one half that of

gasoline's (Table 1). Indicated specific energy consumption (ISEC) or indicated thermal efficiency (η_T) shows improvement for methanol compared to isooctane (3, 12). Faster flame travel speeds for methanol would imply a more efficient energy conversion process. Also, reduced peak combustion temperatures for methanol (i.e., adiabatic flame temperature) could cause a decrease in the specific heat capacity of combustion products by suppressing dissociation, and a reduction in heat losses in the engine (3). It has been shown by Most and Wigg (13) and in this study that blends of methanol and gasoline (15-30%) do not result in an appreciable improvement in indicated thermal efficiency. Also, it has been shown in references (3, 12, 13) and in this study that blending water to methanol causes a reduction in indicated thermal efficiency.

Exhaust emissions levels are generally affected by equivalence ratio, load, inlet mixture temperature, compression ratio, and engine speed. Carbon Monoxide (CO) emissions at lean conditions ($\phi < 1.0$) for methanol are reported to be on the order of 0.9 - 1.5 times those of indolene; however, at lean conditions all CO levels are negligibly low for methanol fuels and indolene (8, 9, 12, 14). This is due to faster and more complete oxidation of CO in the presence of an abundance of oxygen. At rich conditions ($\phi > 1$), CO levels increased at a faster rate with gasoline than with methanol (8, 9, 14). A slower rise in CO concentrations for methanol is probably due to methanol's partially oxidized structure. At lean or rich conditions, overall CO levels for all fuels will be a function

of mixture preparation effects (12).

Comparisons of unburned fuel emissions (or hydrocarbons) will depend upon the definition of the emissions' composition and whether the relative levels are compared on a mole fraction (PPM) basis or an indicated specific (gm/IHP-HR) basis. By definition of emissions' composition, Aldehyde emissions are usually measured and compared separately with the unburned fuel emissions. Indicated specific Aldehyde emissions have been shown to be roughly 4 times greater for methanol compared tc gasoline at all equivalent ratios (8, 12). This is roughly 25-40% of the total unburned fuel emissions levels. In one study, the addition of water to methanol has shown to reduce Aldehyde emissions levels (14) (PPM basis) and in another study, the Aldehyde levels did not change appreciably (12) (indicated specific basis).

The level of unburned fuel emissions from methanol have been the subject of some debate. Reported values of unburned fuel emissions for methanol range from 0.1 to 3.0 times those of indolene or isooctane (8,9,12,15). Most of these differences are a result of measurement technique and analysis. The most believable results are those of Harrington and Pilot (9, 15) and Hilden and Parks (12) who report values for indicated specific unburned fuel emissions for methanol on the order of 1.0 to 3.0 times those of indolene. Blends of methanol and water tend to have higher unburned fuel emissions and Aldehyde emissions compared with methanol (12, 14).

Nitric Oxides (NO_x) levels for methanol are generally lower than those of isooctane and indolene at comparible equivalance ratios, loads, and spark advances (3,9,12,14,16). This is due to different burned temperature-time histories and lower overall peak combustion temperatures. Since lean operation with methanol is possible over a wide load range (8) at least an order of magnitude reduction in NO_x appears possible. The addition of water to methanol has shown to reduce the NO_x emissions levels significantly (3, 12, 14). The addition of methanol to indolene or gasoline (15-30%) has either no effect or slightly increases the NO_x levels in the exhaust.

Differences in lean combustion characteristics are important, since improved thermal efficiency and emissions quality (NO_x and CO) can result. A reduction in output power will also accompany lean operation; however, for steady cruise conditions lean operation will be favorable. Lean limits for methanol and blends of water with methanol are leaner than those for isooctane and indolene (8,9,12). Since wider load ranges are possible at lean conditions, significant efficiency advantages appear possible along with effective control of NO_x and CO emissions. Unburned fuel (UBF) emissions levels reach a minimum at slightly lean conditions ($\simeq \phi = .8 - .9$); however, levels start increasing rapidly as the lean limit is approached. The use of catalysts appear necessary to control UBF emissions when using methanol since no significant reductions appear possible at lean or rich operating conditions.

Significant octane quality advantages appear possible when using methanol, particularly when only small quantities of water are blended (3, 13). This is due to the higher latent heat of vaporization of methanol reducing the inlet mixture temperature and unburned gas temperature during combustion; hence, preflame reactions and knock are suppressed (10,11). One study has shown that by operation possible at leaner equivalence ratios and high compression ratios, without the need for inefficient pollution control devices for NO_x and CO, a 34-38% net energy economy advantage appears possible with a 5% water - 95% methanol blend (3, 13).

3. EXPERIMENTAL APPARATUS AND PROCEDURE

3.1 Experimental Apparatus

A Standard Cooperative Fuel Research (CFR) engine was used to study various combustion properties of methanol fuels. The CFR used was a valve-in-head, single cylinder, variable compression, spark ignition engine with three access ports on the side of the cylinder for instrumentation. Since the cylindrically shaped combustion chamber is normally quiescent in nature, a shrouded intake valve was installed to induce turbulence levels similar to those levels in modern day combustion chambers. Table 2 lists some specifications of the CFR. A complete overhaul of the engine was done before data was taken.

Figure 1 shows a schematic of the test stand. The CFR is coupled to a 16 HP G.E. DC dynamometer. The dynamometer acts as a power absorbing or driving device, and has a hydraulic load cell coupled with a torque arm on the housing for recording engine torque. A constant temperature mixing chamber was used to assure fuel/air mixture homogeneity, and to eliminate effects due to varying latent heats of vaporization of various fuels.The other auxiliary equipment included a standard breaker-type, high voltage ignition system, and external pumps and heat exchangers for the oil and coolant. The fuel supply system was a special high pressure-nitrogen propelled system with bleeding regulators and metering valves for controlling fuel flow rates. An ice bath was added in the fuel line just before the rotometer to keep the temperature constant (temperature changes

fluid viscosity; hence the calibration of the flow meter), and to cool the fuel to prevent cavitation. High pressure industrial burner nozzles were used to maintain a steady, small droplet-type flow of fuel into the mixing chamber.

Variables such as temperature and pressure of the oil, coolant, fuel, ambient air, and inlet mixture were measured using thermometers, manometers and pressure gauges. Air flow rate was measured by recording the pressure drop (inches of H_2O) across a standard design .515 inch I.D. ASME sharp-edged orifice. Fuel flow rate was measured by a rotometer recalibrated for each fuel at a constant temperature. Cylinder pressure was measured by an AVL 8QP500 ca piezoelectric pressure transducer mounted flush with the cylinder wall. Standard preparation and testing of the pressure transducer was done as described in reference (17). A TruRoto model #T-0360-DD-11-M-5D-5V rotary pulse generator (generates 360 + 5 volt pulses per revolution) and a specially designed electronic processor were used to measure crank angle degrees relative to top-dead-center (TDC) and to provide a trigger to the oscilloscope (see Appendix E). A Tecktronix Model 565 oscilloscope was used to display and record pressure versus crank angle records for each case and results were recorded on Polaroid film. Ignition angle, output from a magnetic pickup indicating TDC, and crank angle were measured and recorded on Polaroid film. Figures 2A and 2B show pressure-crank angle records and ignition angle-TDC marker-crank angle records for Case #40 (see Table 4). Engine speed was measured with a mechanical tachometer

and a strobe for fine adjustments.

Average exhaust emissions samples were taken in a mixing tank (see Figure 1), located roughly 10 ft downstream from the exhaust port. Nitric Oxides (NO_x) concentrations were measured via a chemi-luminescence technique with a Thermoelectron Model 10A NO_x analyzer. Both Carbon Dioxide (CO_2) and Carbon Monoxide (CO) concentrations were measured using Beckman non-dispersive infrared analyzers (Models # 315 A (S), and # 864). Oxygen (O_2) concentrations were measured with a Scott Model 150 paramagnetic oxygen analyzer. Unburned fuel (UBF) emissions (note this does not include Aldehyde emissions) were measured with a Scott Model #215 heated, total hydrocarbon analyzer. This yields a total PPM atomic carbon count for the unburned fuel component sampled.

Figure 3 shows a schematic of the gas analysis system used. Note that the sample line and filter are heated (400°F), UBF readings are measured wet, and NO_x, CO_2, CO, and O_2 are measured dry. Complete heating of the sample before the hydrocarbon analyzer (sample line and filter) and inside the analyzer is important to prevent condensation of water vapor and subsequent dissolving of methanol in the water before measurement. The calibration gases used for calibrating gas analysis equipment are listed in Table 3. Note that propane was used as a calibration gas for the hydrocarbon analyzer during experiments, and the methanol calibration gas was only used to check instrument response to oxygenated fuels (response is not 100%). A more detailed discussion on the interpretation of UBF

data is in Section 4.

3.2 Experimental Procedure

The fuels used in experiments were indolene clear as a base fuel for all comparisons, pure methanol, a 10% water-90% methanol blend, and a 15% methanol-85% indolene blend. Some important physical properties of these fuels are given in Table 1; also, the coefficients for calculation of thermodynamic properties are given in Table A-3 (Appendix A).

A baseline set of experiments were run to investigate various combustion and emissions characteristics of the four fuels. Variables held constant for the experiments were compression ratio (6.94:1), shaft speed (1600 RPM), indicated mean effective pressure (53.7 $\pm$ 1.5 psi IMEP), inlet mixture temperature (180 $\pm$ 2°F), oil temperature (145 + 8°F), and coolant temperature (185 ° 10°F). Spark timing was set at minimum advance for best torque (MBT) for all baseline results presented. For all MBT points, data $\pm$ 5 crank angle degrees relative to MBT was taken to assure proper choice for MBT. This was a useful aid for analysis at lean limits and analysis of all NO_x MBT data.

In addition to the MBT cases, data for a wide variation of spark timing was taken for one equivalence ratio in the lean region where significant energy conversion efficiency advantages and low NO_x and CO levels are anticipated.

The measurement and analysis of cylinder pressure - crank angle data requires careful attention for accurate results. Since

variations in cycle-to-cycle cylinder pressure exist in spark ignition engines, average pressure-crank angle histories must be defined. To define average pressure-crank angle histories, six random pressure cycles were photographed (done 1-3 times) from the oscilloscope display (pressure from -180° to +180° relative to TDC was recorded, see Figure 2A). Then, seventy consecutive pressure cycles were photographed to determine visually, a "statistically-representative" pressure cycle to analyze (see Figure 2C). An 8 x 10" enlargement of the best six overlayed pressure cycles was then made for digitizing (analog X-Y digitizer used) to transform picture coordinates to pressure-crank angle coordinates. To establish a reference point for the piezoelectric transducer output, it was assumed that cylinder pressure is equal to the inlet manifold pressure at 170° before TDC (i.e., immediately before the inlet valve closes). This was a reasonable assumption for defining high pressures during combustion because the reference pressure is at the end of the inlet process where little gas motion exists, and piston velocity is relatively small. Verification of accurate digitizing and accurate reference pressure choice was done by plotting log (Pressure) vs log (Volume) for all cases and $P\ V^{\alpha}$ for motored cases. Before pressure data was taken, an analysis similar to that presented in references (17, 18) was done to check pressure transducer performance, crank angle phasing, and the choice of clearance volume and reference pressure.

As an additional consistency check for measured pressure-crank angle data and measured torque from the dynamometer, IMEP calculated from measured pressure vs crank angle histories was compared with the IMEP calculated from the dynamometer BMEP. The integrated IMEP was calculated via the following definition (18)

$$\text{IMEP} \underset{\text{DEF.}}{=} \int_0^{720°} dV/V_d = \text{BMEP}_{fir} - \text{BMEP}_{mot} + \int_0^{720°} p_{mot}\, dV/V_d \qquad (1)$$

where indexes fir and mot refer to firing and motoring, P is pressure, V is volume, V_d is displacement volume, and BMEP is the brake mean effective pressure read from the dynamometer. The weakness of the above definition is the inherent assumption that friction during firing is equal to friction during motoring. Nevertheless, comparisons of integrated vs measured IMEP's showed a + .14% mean error with a standard deviation of the error being 3.0 for MBT cases.

To check the accuracy of fuel flow, air flow, and exhaust gas species concentration measurements, the equivalence ratio (ϕ) calculated from exhaust gas species concentrations was compared to that calculated from measured fuel and air flow rates. Appendix D gives equations and assumptions used to calculate ϕ for fuels containing oxygen and nitrogen. For all MBT cases, the comparisons of ϕ (measured) vs ϕ (calculated) had a mean error of - 1.1% with a standard deviation of the error 3.3.

For the baseline set of experiments the lean misfire limit was determined for each fuel. Holding load (IMEP) constant with MBT timing, and holding the remaining operating variables constant, the mixture was made progressively leaner to the point where lean misfire was observed. The point of lean misfire was defined when three to five misfires (pressure cycles equivalent to motoring cycles) per seventy consecutive cycles were observed. Figures 4A and 4B show six random pressure cycles (4A) and seventy consecutive pressure cycles (4B) at lean limit conditions for methanol. This definition of the lean limit was considered satisfactory since a slightly leaner mixture causes a rapid increase in misfire frequency, indicated specific fuel consumption, and unburned fuel emissions.

A second set of experiments were conducted increasing compression ratio to the point of incipient knock for the four fuels at a lean equivalence ratio (ϕ = .8), MBT timing, and a constant load (IMEP). Cylinder pressure vs crank angle was measured; however, only trade off relationships between indicated thermal efficiency, NO_x emissions, and UBF emissions were investigated. It should be mentioned that relative energy economy advantages could not be effectively studied for the four fuels since the varying latent heat of vaporization effects (which were eliminated by the constant temperature mixing chamber) on relative octane quality are important. Displaying the time derivative of cylinder pressure on the oscilloscope served as an aid in determining the point of incipient knock.

4. ANALYSIS AND INTERPRETATION OF RESULTS

Experimental results for combustion properties of methanol, 10% water-90% methanol, and 15% methanol-85% indolene will now be presented. Indolene clear is used as a base fuel for all comparisons.

The baseline data set where equivalence ratio (Ø) is varied out to the lean misfire limit holding load (IMEP), speed, compression ratio, inlet temperature, and oil and coolant temperature constant at MBT spark timing will first be discussed (Sections 4.1-4.4). Then, data describing some effects of spark advance and compression ratio, holding equivalence ratio and all other variables constant, will be discussed (Sections 4.5-4.6). Tables 4 and 5 give operating conditions for these data sets.

4.1 Combustion Properties of Methanol, 10% Water-90% Methanol, and 15% Methanol-85% Indolene Compared with Indolene

Appendix B describes the details of the thermodynamic model used to calculate burned and unburned gas properties during combustion. Appendix A describes what necessary modifications were made to an existing model developed for pure hydrocarbon fuels to account for oxygen and/or nitrogen in the fuel. Residual mole fractions were calculated from the equation of state for conditions at the time the exhaust valve closes. Exhaust temperatures were estimated from time resolved exhaust temperatures presented in reference (19) with adjustments made for varying fuel type.

The calculation used the most from the analysis is the energy release rate or mass fraction of the charge burned in the cylinder as a function of crank angle. Figures 5 through 8 show plots of mass fraction burned versus crank angle degrees after the spark for the four fuels studied at various equivalence ratios. These mass fraction burned curves, and the MBT data matrix in Table 4 are the basis for analyses to follow.

Kernel Development, Ignition Delay, and Combustion Duration

Three periods of combustion can be defined to provide quantitative description to average flame propagation characteristics during various phases of the combustion cycle. Based on the mass fraction burned versus crank angle calculations, the three periods are: a) kernel development period (Θ_k) is the time taken to burn 1% of the charge mass; b) ignition delay (Θ_I) is the time taken to burn 10% of the charge mass; c) combustion duration (Θ_c) is the time taken to burn 10% to 90% of the charge mass. Θ_k, Θ_I, Θ_c, and "time" refer to crank angle degrees. The addition of kernel development period along with ignition delay is done for completeness to provide more information to modelers of the combustion process. Also, values of 1%, 10%, and 90% of the mass fraction burned are normalized values with respect to the first peak value reached in the mass fraction burned calculations. Figure 9 shows definitions of these periods on a mass fraction burned versus crank angle diagram and a log (pressure) versus log (volume) diagram.

As an aid in understanding why Θ_k, Θ_I, and Θ_c change when certain dependent variables are varied, it is helpful to look at a physical description of turbulent flame propagation in the combustion chamber. First, it is understood that the intake process and piston motion generate eddies or small-scale turbulence that "persists" throughout the duration of the combustion cycle (20,21). At the time of the spark, the ignition process can be viewed as instant ignition of periphery regions of a few eddies (due to introduction of free radicals such as H, OH, and O) (20). These eddies then burn "as discrete microvolumes inwardly from peripheral ignition sites" throughout some critical volume called a flame kernal. Due to turbulent motion, subsequent ignition of entrained eddies surrounding the first burning eddies will follow, and combustion would proceed by the development of the flame kernel into a flame front which propagates with a finite thickness through the unburned mixture. The flame propagation rate and the flame front thickness are controlled by the eddy entrainment speed (proportional to turbulent intensity), the effective heat and mass transfer areas between adjacent eddies (eddy size or turbulent scale), and the characteristic reaction times for inward burning of individual eddies (proportional to ℓ/S_L where ℓ is the average eddy size and S_L is the laminar flame speed) (20,21).

During kernel development and ignition delay periods, the burning of the first few elements (or eddies) of charge ignited is the principal phenomena governing the heat release rate. Specifically, the proportionality has been shown to exist

$$\Theta_k/N \sim \ell/S_L \quad (2)$$

where Θ_k, ℓ, and S_L are as previously defined and N is the engine speed (22). Figure 10 shows the variation of kernel development period with fuel type and equivalence ratio. In comparison with indolene, the kernel development periods for methanol were significantly shorter at lean equivalence ratios (.65 times that of indolene @ ϕ = .80). With the exception of extreme lean (ϕ < .75) and extreme rich (ϕ > 1.05) conditions for 10% water-90% methanol, the other methanol fuels showed only slight reductions in kernel development times (Θ_k's for 10% water-90% methanol and 15% methanol-85% indolene are roughly .95 times those of indolene at ϕ = .8). An explanation of the shorter kernel development periods for methanol fuels can be centered around methanol's laminar flame speed being greater than that of indolene. The significant reductions of kernel development periods for methanol show this to be true.

During the ignition delay period the first few elements (or eddies) of charges are burned, and the small flame kernel begins to develop into a flame front of size characteristic of the dimensions (height) of the chamber. In Figure 11, ignition delay versus

equivalence ratio (Ø) is plotted. As anticipated, methanol and 10% water-90% methanol showed shorter ignition delay periods relative to indolene's(roughly .71 and .88 times those of indolene at Ø = .8, respectively). However, 15% methanol-85% indolene fuel had slightly higher ignition delay periods than indolene (about 1.1 times that of indolene at Ø = .8) except when approaching the lean limit.

For all cases, kernel development and ignition delay periods increased as the equivalence ratio was made leaner. The dilution of the unburned mixture with air tends to reduce the laminar flame speed; hence, the heat release rate is reduced.

By the time the combustion duration period begins, the flame front has developed to a size characteristic of the dimensions (height) of the chamber and begins propagating with a finite thickness through the unburned mixture. As shown in Figure 12, only moderate variations of combustion duration with fuel type and equivalence ratio (hence, characteristic reaction time) resulted. This is consistent with previous conclusions that flame propagation during the combustion duration period (fully developed turbulent flame propagation) is dominated by the turbulent intensity rather than turbulent scale and characteristic reaction times (21). The methanol fuels had combustion intervals slightly shorter than indolene's. At Ø = .8 for methanol, 10% water-90% methanol, and 15% methanol-85% indolene the combustion intervals were .87 and .91 lower than indolene's, respectively. The observed variations could be due to changes in the characteristic time for an eddy of size proportional to the

flame front thickness to burn. This is a function of the kinetics and the turbulence structure in the engine.

Turbulent Flame Speed and Flame Front Geometry

More quantitative information on relative heat release rates can be gained from calculations of turbulent flame speed from the reduced pressure-crank angle (time) data. Specifically, from calculations of the mass burning rate ($M\dot{x}$), the density of the unburned gases (ρ_u), and the cylinder volume, the turbulent flame speed (S_{u_T}) can be determined with assumptions of spherical flame geometry and negligible reaction zone thickness (20, 21). Appendix C outlines the method used to determine S_{u_T}.

Turbulent flame propagation properties were calculated for all cases in the baseline data set (refer to Table 4). Two cases for methanol at stoichiometric and lean limit conditions are examined in detail, followed by data describing some effects of equivalence ratio and fuel type on S_{u_T}.

Figures 13 and 14 show S_{u_T} plotted as a function of mass fraction burned (x) for Case #35 (ϕ=.57, methanol @ lean limit) and Case #40 (ϕ=.97, methanol). Figures 6 and 9 give additional information for these two cases. Figures 15 and 16 show S_{u_T} and x plotted as a function of R_T/D, where R_T is the calculated flame front radius and D is the diameter of the combustion chamber. Note that the spark plug is mounted on the upper edge of and flush with the chamber. The scatter of points for S_{u_T} vs x and R_T/D around the line drawn should be

be interpreted as error bounds for the calculations. The error bounds reflect the limitations of the pressure measuring techniques, and of the one statistically-representative pressure cycle opposed to on-line computer sampling and averaging of several pressure cycles. Nevertheless, one can see that throughout the combustion duration period, i.e., $.1 \leq x \leq .9$ (normalized), S_{u_T} does not change appreciably. Also, Figures 15 and 16 show that by the time 15-20% of the mass is burned, the flame front will have propagated at least (since $R_T < R_e$, see Appendix C) halfway across the chamber. This rapid expansion of flame radius (R_T) can be explained in part by increased area of the flame front (A_T) caused by expansion of the burned gas and distortion of the flame front by increasingly larger eddies (20,21). Unburned gas density also increases due to expansion of burned gases. It then follows that the mass entrainment rate of eddies into the flame front increases; hence, heat release rate increases (20). When the normalized radius ($R_{T/D}$) becomes sufficiently large, i.e., $R_{T/D} > .5$ in Figures 15 and 16 or $x > .2$ in Figures 13 and 14, $\dot{x}$ of equation (C-1) becomes relatively constant, and S_{u_T} is dominated by A_T and ρ_u which are both changing according to the change in cylinder volume and continuing heat release rate in the cylinder.

To obtain comparisons of turbulent flame speeds for the data from four fuels S_{u_T} versus ϕ at $x = .5$ is plotted (Figure 17). Flame speeds for methanol were higher than those for indolene, and higher than 10% methanol-90% water. Flame speeds for 15% methanol-

85% indolene are higher than those of indolene and even higher than methanol's for two cases. Results were not consistent with the combustion duration data in Figure 12, with the exception of methanol and indolene. However, results in Figure 17 are for one statistically-represented pressure cycle, and not an average of a number of cycles. This, coupled with limitations in pressure measuring techniques, could explain the inconsistencies observed. On-line computer sampling is now being developed for a better analysis of this type.

4.2 Lean Misfire Limits for Methanol Fuels

Operation at lean conditions is favorable for spark ignition engine combustion since energy conversion efficiency improves, and significant reductions in levels of Nitric Oxides and Carbon Monoxide can be attained (discussed further in Sections 4.3 and 4.4). Since lean misfire limits are functions of several dependent variables, the systematic technique described in Section 3.2 (constant speed and load, MBT timing) was used to determine relative lean misfire limits for the four fuels studied.

The results show (lean limits are indicated on all figures where equivalence ratio is varied) that the lean misfire limit for methanol (ϕ = .57) was significantly lower than that of indolene (ϕ=.68). The 10% water-90% methanol blend showed a slight reduction in

the lean limit (ϕ = .60) compared with methanol's (ϕ = .57), and the lean limit for 15% methanol-85% indolene (ϕ = .67) showed no noticeable extention from the lean limit of indolene (ϕ = .68).*

Lean inflammability limits are governed physically by the ratio of characteristic reaction rate (or heat release rate) and heat loss rates to the surroundings of the reaction zones (23, 24). Composition limits of inflammability exist (with decreasing temperature, reaction rate decreases more rapidly than heat loss rates), and convection dependent limits of inflammability exist (turbulent convection currents generated by the intake process and piston motion are capable of quencing flame kernel growth, or in engines, cause residual gas and fresh charge to not mix homogeneously (22, 23, 24). The flammability limits as defined by Coward and Jones ((see Table 1, physical properties) represent quiescent flammability limits, and appear to be beyond the individual lean misfire limits indicated from the CFR engine experiments. However, differences in lean misfire limits for varying fuel type have been reported implying both composition and turbulent convection were factors influencing the lean limits determined.

---

*At the lean limit, the IMEP and air flow rate for the 15% methanol-85% indolene blend were 53.0 psi and 227.2 grams/minute compared with 53.9 psi and 240.6 grams/minute for indolene (see Table 4). From a knowledge of lean limits being extended by an increase in IMEP (8) or an increase in intake generated kinetic energy (25) (air flow rate), one could conclude that the lean limit for 15% methanol-85% indolene compared with indolene's could be slighly leaner than indicated. Nevertheless, differences would still be small and would not imply that any significant extensions of the lean limit are possible.

For example, methanol's lean flammability limit @ STP in a quiescent atmosphere is at ϕ = .562 compared with ϕ = .57 determined by the systematic approach in Section 3.2. However, the engine lean misfire limit is for temperatures and pressures of the unburned gas at the time of the spark (from thermodynamic analysis P = 2.9 atm, $\bar{T}_u$ = 582°K, Case No. 35 for methanol) compared with STP conditions (P = 1 atm, T = 300°K). This increase in pressure will not affect the lean flammability limit (23); however, the increase in unburned gas temperature will extend the lean flammability limit by increasing the relative heat release rate (i.e., the heat release rate, proportional to EXP (-E/RT) increases much more rapidly than the heat loss rate, proportional at most to T^4) (26). Therefore the quiescent flammability limit from Table 1 for (ϕ = .562) would be lower than indicated for T_u = 582°K and P = 2.9 atm.

As previously discussed varying the fuel type from indolene to methanol resulted in a significant extension of the lean misfire limit (ϕ = .57 compared with ϕ = .68). Methanol's leaner misfire limit can be explained in part by its faster characterstic reaction rates (proportional to laminar flame speed, see Figures 10 and 11 for kernel development and ignition delay) and lower heat loss rates (due to lower burned gas temperatures). For an equivalent turbulent structure at the time of the spark (MBT spark advances and air flow rates are roughly equal), these factors appear consistent with the relative lean limits determined.

Variations in turbulent scale and intensity also appeared to play a dominant role at lean limit conditions for all fuels studied. Figure 4A shows an oscilloscope photograph taken of six random pressure cycles at lean limit conditions, and Figure 4B shows seventy consecutive cycles for the same case. Looking at Figure 4A, it appears that as composition limits of flammability are being approached, variations in turbulent scale and intensity appear to dominate the ignition process from cycle to cycle. Whether the effect is the variation of the eddy size initially ignited or variation of the homogeneity of residual gas and fresh charge, one cycle looks similar to a normal MBT pressure cycle before the lean limit is approached (see Figure 2A), and another cycle looks like corresponding pressure cycles for the spark either too advanced or too retarded*.

In summary, once stable ignition has been accomplished at lean misfire limits, combustion appears to proceed (however, moderately affected by reaction time; see Figure 12) as in normal conditions. It appears as if lean limits could be improved by a better understanding of factors influencing characteristic reaction rates and varying turbulent structure at the time of the spark.

---

*Calculation of characteristic turbulent diffusion times (27) versus residence time of fuel vapor and air in the mixing chamber show that variations in equivalence ratio of inducted mixture should be negligible.

4.3 Indicated Thermal Efficiency

Indicated thermal efficiency (η_{th}), for a fixed compression ratio and inlet temperature, is improved at lean conditions. Combustion at leaner conditions results in a decrease in peak flame temperature; subsequently, a decrease in specific heat capacity (c_{pb}), a suppression of dissociation in the combustion products, and a lowering of heat losses to the walls results (3). Of course there is a trade off when peak flame temperatures are significantly reduced because the thermal efficiency of the Otto cycle is lowered.

The results for the variation of indicated thermal efficiency (η_{th}) with equivalence ratio (ϕ) and fuel type are given in Figure 18 for the MBT data base (Table 4). In the rich region $\phi > 1.0$, the indicated thermal efficiency decreased rapidly for all fuels and no significant difference in values were observed. In the lean region, the indicated thermal efficiencies for methanol were higher than those of indolene, and for 15% methanol-85% indolene and 10% water-90% methanol, indicated thermal efficiencies were lower (i.e. at $\phi = .8$ η_{th} for methanol, 15% methanol-85% indolene, and 10% water-90% methanol were 1.02, .98, and .99 times that of indolene).

Although differences were small, some explanations can be given. One factor which appears to explain the differences most is the comparison of relative flame speeds or heat release rates. From Figures 10, 11, and 12 differences in the overall combustion intervals for the various fuels are consistent with the differences in thermal

efficiency observed. Shorter overall combustion intervals result in more net work delivered due to faster pressure rise rates (11) Another explanation for differences in thermal efficiency is the lower adiabatic flame temperature for methanol which can result in lower heat transfer rates to the walls. Also, the specific heats of the burned gases could vary with fuel type at equal equivalence ratios. From thermodynamic analysis these explanations were consistent with variations of η_{th} with ϕ; however, for the same ϕ's, variations of $\bar{T}_b$ (average burned gas temperature) and specific heats of burned gases (C_{pb}) were slightly noticeable from fuel to fuel. Figures 19 and 20 show variations of $\bar{T}_b$ and C_{pb} at peak pressures as a function of ϕ and fuel type. Note that lower peak temperatures result in lower specific heats.

Although the differences in thermal efficiency were small, the large gains in thermal efficiency anticipated for methanol are when small % volumes of water are blended (only 5% is necessary) (3, 13), and operation is possible at higher compression ratios. Trade offs do exist when compression ratio is increased since unburned fuel emissions, and in some cases, nitric oxide emissions tend to increase (discussed further in Section 4.6).

4.4 Exhaust Emissions

Determining relative exhaust emissions levels that result from the use of methanol, methanol-water blends, and gasoline-methanol blends is important for a final evaluation. In the section to follow, baseline results for MBT, constant speed, load (IMEP), and inlet temperature (Table 4) will be presented and all results will be compared with those of indolene.

Nitric Oxides (NO_x)

The Indicated Specific Nitric Oxide ($ISNO_x$) concentrations* measured for three methanol fuels is compared with those for indolene in Figure 21. The IS NO_x for methanol and 10% water-90% methanol were significantly lower than those for indolene at all equivalence ratios. IS NO_x levels for 15% methanol-85% indolene were nearly equal to the levels measured for indolene in the lean region ($\phi < .9$) and higher in the rich region ($\phi > .9$).

It is well accepted that Nitric Oxide (NO) forms mostly in the burned gases inside the engine cylinder, and the formation of NO is governed by the extended Zeldovich mechanism (22,28). Although kinetic calculations should be done to look at the effects of certain variables on measured NO_x levels, some qualitative insight can be gained by looking at the rate-limiting reaction in the extended Zeldovich mechanism for the formation of NO (22).

---

*NO_x implies that the NO_x converter was used during experiments to convert all NO_2 to NO; consequently, the total concentration of NO + NO_2 was recorded.

$$N_2 + O \rightarrow NO + N \quad (3)$$

The contribution to the rate of formation of NO from this reaction is

$$d\,[NO]/dt = k_1\,[O]\,[N_2] \quad (4)$$

where $k_1 = 1.4 \times 10^{14} \exp(-75{,}400\ IRT)\ cm^3\ mole^{-1}\ sec^{-1}$, and the units of [NO], [O], and $[N_2]$ are in moles (22). One can deduce from Equations (3) and (4) that peak values of NO will be formed at optimum combinations of temperature and oxygen availability (3). This is consistent with IS NO_x levels reaching peak values at slightly lean conditions (Figure 21) where high temperatures still exist and the dissociation of $O_2 \rightarrow 2O$ is important. When leaner conditions are approached, average burned gas temperatures are reduced (see Figure 19) due to dilution of the charge; consequently, chemical dissociation of $O_2 \rightarrow 2O$ is suppressed causing a reduction in specific heat capacity (Figure 20) (29). These two coupled effects both act to limit the rate of NO formation, and in turn the average NO_x levels measured in the exhaust gases. The same reasoning can be used to explain the reduction in NO_x levels for rich conditions except that the deficiency of oxygen (O_2) rather than the abundance acts to reduce average burned gas temperatures.

In the lean region ($\phi < .9$), the relative IS NO_x emissions measured for methanol fuels in comparison with indolenes can be explained in part by looking at average burned gas temperature histories $\bar{T}_b$ versus θ (time) that were calculated from the thermodynamic analysis of the combustion process (Appendices A and B).

Figure 22 shows average burned gas temperature histories in the lean region (at $\phi \lesssim .8$) for three fuels studied. The shapes of the curves are similar; however, the differences in temperature due to varying fuel type for the different $\bar{T}_b$ versus θ profiles are consistent with measured $ISNO_x$ trends (Figure 21) and the predicted temperature dependence on d[NO]/dt in Equations (3) and (4).

In the rich region ($\phi > .9$), similar trends of decreased $ISNO_x$ explained by lower relative $\bar{T}_b$ versus θ histories (see Figure 23) were only true for methanol and 10% water-90% methanol in comparison to each other, and in comparison to indolene and 15% methanol-85% indolene. Histories of $\bar{T}_b$ as a function of θ have similar shapes and nearly equal values for indolene and 15% methanol-85% indolene (Figure 23). This appears to imply that the indolene-methanol blend containing methanol, a partially oxidized substance, caused an increase in oxygen atom concentration [O]; hence, for a slightly varying temperature ($\bar{T}_b$), d[NO]d/t is increased in Equation (4). A recent reaction mechanism presented by Bowman (30) for the combustion of methanol shows that the initiation step of the reaction mechanism is accomplished mainly by thermal decomposition of methanol

$$CH_3\ OH \rightarrow CH_3 + OH \qquad (5)$$

A relatively high OH radical concentration could cause a high O atom concentration in the burned gases. To support these ideas, an investigation of the kinetics should be done to verify measured NO_x vs predicted NO_x from measured pressure-time histories (done in a later report).

Unburned Fuel Emissions

Studies have indicated (4, 12, 14) that the major portion of hydrocarbon components (roughly 80-90%, ppm basis) measured in the exhaust gas of methanol fueled engines is unburned methanol. Total aldehydes represent the major portion of the hydrocarbon components that are not in the form of unburned methanol (roughly 10-20%, ppm basis) (4). Since aldehyde emissions are not detected by the FID total hydrocarbon analyzer (12), and since unburned methanol is not really a pure hydrocarbon substance, the nomenclature of "unburned fuel (UBF)" emissions was used to represent exhaust gas concentrations of unburned methanol and all other hydrocarbons excluding aldehydes. Also, since results were presented on an indicated specific basis (IS UBF), and since a propane-calibrated FID is not 100% responsive to unburned methanol concentrations (12,15) a special section was added (Appendix E) explaining the method used in computing IS UBF emissions from ppm measurements.

Experimental IS UBF emissions level measurements for the three methanol fuels in comparison with results for indolene are presented in Figure 22 for the baseline data matrix (Table 4). Measurements indicate that in the lean region for $\phi < .9$, all IS UBF emissions levels for the methanol fuels were higher than those for indolene (i.e., at $\phi = .8$ IS UBF levels for 10% water-90% methanol, methanol, and 15% methanol-85% indolene were 2.4, 2.1, and 1.4 times those of indolene respectively).

For $\phi > .9$ and rich conditions, all IS UBF emissions increased steadily, and IS UBF emissions for indolene appeared to increase at a more rapid rate than those of the methanol fuels; however, IS UBF levels were nearly the same value for all fuels (see Figure 22). IS UBF results do not include total aldehydes. Levels of total aldehydes have been measured to be higher from methanol fueled engines (12, 14) and the addition of water to methanol could possibly reduce the total aldehyde levels (14).

A discussion of measured trends of unburned fuel emissions can involve a diversity of phenomena during the combustion cycle (31). In general quench layers and crevices at the cylinder walls are the source of unburned fuel emissions. During combustion the flame first propagates up to the wall, but due to heat transfer and free radical destruction in the unburned mixture to the cool cylinder walls and piston face, flame quenching occurs. When the exhaust valve opens a portion of the head and cylinder wall quench layers near the exhaust valve are entrained during blowdown. Then a vortex is formed as the piston scrapes the UBF-rich boundary layer off the cylinder wall, and at the end of the exhaust stroke a major part of this vortex exits the cylinder (19). Since many variables were held constant during experiments such as speed, load, compression ratio, coolant temperature, and engine configuration, only variations in UBF quench region formation, post-quench oxidation in the combustion chamber, and oxidation in the exhaust system appear to be sources of the different UBF emissions levels measured (31).

Since mass fractions of methanol fuels in the unburned mixture are higher than indolene's at equal equivalence ratios (over twice as large for methanol and 10% water-90% methanol, see Table 2, $\phi = 1$ fuel/air ratio), variations in unbured fuel quench regions appears to be a first explanation for the difference in experimental UBF emissions measurements. In addition to the fact that mass fractions of fuel in the unburned mixture vary, quench distance will also vary, and the physics of the quenching process should be investigated. Recent calculations done by Ferguson (32) show that quench distance in an engine scales with laminar quench distance. The Peclet number (P_e) based on quench distance (D), laminar flame speed (S_u°), unburned gas density (ρ_u), frozen specific heat of burned gas (Cp_b) and frozen thermal conductivity of the unburned gas at the adiabatic flame temperature (K) is correlated by

$$P_e = \frac{\rho_u S_u^\circ \, Cp_b D}{K} = F\left[\frac{T_{b_L}^\circ}{T_b^\circ} \quad \frac{T_b^\circ - T_u}{T_b^\circ}\right] \tag{6}$$

where

$T_{b_L}^\circ$ = lean limit adiabatic flame temperature

T_b° = adiabatic flame temperature

T_u = temperature of the unburned gas at the time of quench

and

F = a constant determined by the type of quenching.

Rewriting Equation (6), the quench distance in the engine is of the order

$$D \sim \frac{K}{\rho_u S_u^\circ C_{p_b}} F\left[\frac{T_{b_L}^\circ}{T_b^\circ} \quad \frac{T_b^\circ - T_u}{T_b^\circ}\right] \tag{7}$$

From the standpoint of methanol's adiabatic flame temperature being lower and its lean limit being leaner than indolene's, it can be shown that the quantity $\left[\frac{T_{b_L}^\circ}{T_b^\circ} \quad \frac{T_b^\circ - T_u}{T_b^\circ}\right]$ is smaller for methanol. The effect of T_u being slightly lower for methanol would oppose this trend (see Figure 23). Also, from thermodynamic analysis of the combustion process ($\rho_u C_{p_b}$ for methanol is greater than $\rho_u C_{p_b}$ for indolene), accounting for K being a weak function of fuel type*, and from insight that methanol's laminar flame speed is greater than indolene's (see Figures 10 and 11), the quantity $K/\rho_u S_u^\circ C_{p_b}$ is smaller for methanol. These results imply that methanol's quench distances are smaller than those for indolene's; however, the mass fraction of methanol in the unburned mixture being roughly 2.2 times that of indolene's still appears to be the most important reason for higher experimentally measured UBF emissions.

---

*Supported for methanol by calculations done by methods described in reference (42).

Rewriting Equation (6), the quench distance in the engine is of the order

$$D \sim \frac{K}{\rho_u S_u^\circ C_{p_b}} \; F\left[\frac{T_{b_L}^\circ}{T_b^\circ} \quad \frac{T_b^\circ - T_u}{T_b^\circ}\right] \tag{7}$$

From the standpoint of methanol's adiabatic flame temperature being lower and its lean limit being leaner than indolene's, it can be shown that the quantity $\left[\frac{T_{b_L}^\circ}{T_b^\circ} \quad \frac{T_b^\circ - T_u}{T_b^\circ}\right]$ is smaller for methanol. The effect of T_u being slightly lower for methanol would oppose this trend (see Figure 23). Also, from thermodynamic analysis of the combustion process ($\rho_u C_{p_b}$ for methanol is greater than $\rho_u C_{p_b}$ for indolene), accounting for K being a weak function of fuel type*, and from insight that methanol's laminar flame speed is greater than indolene's (see Figures 10 and 11), the quantity $K/\rho_u S_u^\circ C_{p_b}$ is smaller for methanol. These results imply that methanol's quench distances are smaller than those for indolene's; however, the mass fraction of methanol in the unburned mixture being roughly 2.2 times that of indolene's still appears to be the most important reason for higher experimentally measured UBF emissions.

---

*Supported for methanol by calculations done by methods described in reference (42).

Calculations of S_u° for methanol and indolene would be required for a more quantitative comparison.

Higher IS UBF emissions for methanol and methanol fuels can also be explained in part by lower overall combustion temperatures reducing effectiveness in post-quench oxidation in the combustion chamber, and oxidation in the exhaust system.

Carbon Monoxide Emissions

Carbon monoxide (CO) emissions from spark ignition engines are controlled primarily by the equivalence ratio. Figure 24 shows results of indicated specific CO (IS CO) emissions for baseline, MBT data. In the lean region, for $\phi < 1$, all IS CO levels were low. IS CO for methanol was lowest, followed by indolene, 10% water-90% methanol, and 15% methanol-85% indolene. As rich conditions were approached, $\phi > 1$, IS CO concentrations increased steadily with increasing ϕ for all fuels. Since the data base was designed to focus on lean operation, no relative trends could be established for rich conditions. Other experimental results indicate CO emissions for methanol are slightly lower at rich conditions; however, their results show higher CO levels at lean conditions (9, 15). Nevertheless, CO emissions at lean operating conditions ($\phi < 1$) are significantly low for all fuel types, and steadily increase with ϕ when $\phi > 1$. For the same reasons that the partially oxidized nature of methanol affects N_2 and NO oxidation, this can also account for the slighly lower CO levels for methanol at rich conditions.

4.5 Spark Advance versus Indicated Thermal Efficiency and Emissions

The effect of spark advance on indicated thermal efficiency (η_{th}) IS NO_x, and IS UBF is presented in Figures 25-28. These figures show that η_{th} and IS NO_x are the most sensitive to spark advance relative to the MBT point.* Also shown in the figures is the method used to determine IS NO_x at MBT.

4.6 Increased Compression Ratio versus Indicated Thermal Efficiency and Emissions

The effect of increasing compression ratio on indicated thermal efficiency (η_{th}), IS NO_x, and IS UBF is presented in Figures 29-32 for the four fuels. For a constant equivalence ratio (ϕ = .8), load (IMEP) and MBT timing, compression ratio was increased to the point of incipient knock. No octane quality differences could be established since the constant temperature mixing chamber minimized the important latent heat of vaporization effects.

η_{th} and ISUBF emissions increased with compression ratio for all four fuels; however, IS NO_x follows no particular pattern.* To establish realistic tradeoffs between η_{th}, IS NO_x and IS UBF and compression ratio, studies such as those done in references (3,13,16). should be carried out using carburetor set-up where the full octane and emissions potential can be realized (varying latent heat of vaporization effects become important in this type of study).

*See Table 5 for operating conditions.

5. ON METHANOL'S POTENTIAL FOR COMMERCIAL APPLICATION AS A MOTOR FUEL

If policy decisions involved with the use of various synthetic fuels are to be made in a rational as well as scientific manner, practicalities and economics should be investigated in addition to examining combustion properties. Specifically, it is essential to seek an accurate overall perspective of the development of these fuels from acquisition of the natural resource, to final end-use in the vehicle. Focusing only on certain aspects of the complete picture could result in a misconception of the actual source-to-end-use economics, the environmental impact, and the performance of the fuel in the vehicle. In the sections to follow, a qualitative as well as quantitative discussion on methanol's potential for automotive application is presented to help put into perspective the systems nature of converting to synthetic fuels.

5.1 Resource Supply/Demand

Increased interest has arisen in the use of synthetic fuels because of the increased demand for petroleum and gradual exhaustion of domestic and global petroleum resources. For automotive application, where petroleum-derived gasoline would be replaced, synthetic gasoline and methanol produced from shale rock and/or coal appear to be the most practical alternatives. Sizes of U.S. domestic coal and shale rock reserves are roughly 2.5 times the size of the U.S. petroleum reserves (33) and shale reserves are roughly 2.0 times the size of Middle-East oil reserves (1).

Development times and environmental constraints on resources are also important since the development of alternate fuels are generally more limited by these two factors rather than the actual size of the particular resource base (7). Domestic coal reserves are scattered over many different regions (34). For example, the potential of developing western coals is much larger than indicated by the magnitude of the resource base since a large portion is recoverable by strip mining at high stripping ratios. The shale rock resource base is slightly larger than coal's (roughly 1.1 times as large) (33); however, unlike domestic coal reserves, domestic shale rock reserves are centrally located in the Rocky Mountain region. From a resource standpoint, the better of the two will depend upon relative development times and environmental constraints involved (7).

5.2 Production

Methanol can be produced from essentially any carbonaceous substance such as coal, natural gas, petroleum, shale rock, and municipal and agricultural refuse (photo synthesis is also another source) (35). The most practical resource available for large-scale production of methanol would be coal due to the enormous size of the resource base and large scale availability.

Production of methanol is generally accomplished by first forming synthesis gas ($CO + H_2$), followed by synthesis of methanol via the following step

$$CO + 2H_2 \rightleftarrows CH_3OH \qquad (2)$$

As an example, overall steps involved with one promising method of production described in reference (7) would be: (1) coal preparation for the particular gasification process used; (2) gasification of coal via a standard, commercially available technique to a low BTU gas (with low methane yield); (3) shift of the H_2/CO ratio for methanol synthesis (Equation (2)) and removal of CO_2 and H_2S; (4) methanation of remaining CO, CO_2, H_2 to Methane (CH_4) and Water (H_2O); (5) compression before methanol conversion; (6) Methanol synthesis at high pressure (50-300 atm, 200-250°C) from CO and H_2 over a catalyst using existing technology; and (7) purification to remove dissolved gases and small amounts of dimethyl ether. Specific needs for developing technology would be a high pressure gasifier to avoid the subsequent compression step, and a more active catalyst for methanol synthesis capable of low temperature operation to relieve the heat removal limitations of the strongly exothermic synthesis process.

5.3 Distribution and Storage

Since methanol is a liquid fuel, distribution and storage would be in many ways similar to that of distributing gasoline. Major differences would be: 1) direct distribution from the Methanol synthesis plant to the consumer since no refining or upgrading is required; 2) the size of Methanol's distribution system would be roughly 2.0 times the size of gasoline's for an equivalent energy capacity (see heat of combustion, Table 1); 3) a special distribution system would be required when methanol is first introduced.

Methanol could be introduced in fleet programs (as a blend or as pure methanol) for commercial vehicles in large cities, or as a blend with gasoline in fuel supplies to the general public. The use of a gasoline/methanol blend would require a completely dry distribution and storage system due to phase separation problems with gasoline/methanol blends in the presence of small quantities of water (5, 6, 7). This is reported to involve a 40% cost penalty to portions of the "dry" system concerned with equipment and operating procedures (7). Fuel stability problems will still exist once such a blend is stored in the vehicle (5, 7). If introduction was first done in fleet programs (as of today a more probable approach), methanol would be initially shipped from the plant via railroad cars to bulk terminals near major population centers. As market requirements and availability grow, pipelines would be constructed (7).

5.4 Economic Evaluation

Relative costs of supplying energy to the consumer, and the capital intensity involved will be major criteria in a final evaluation of an alternate synthetic fuel. In addition to these criteria, looking at questions of relative overall efficiency, availability of appropriate end-use equipment, availability of supplies in appropriate volume to meet the demand, and environmental impact will be important for a complete economic analysis (3, 7, 13).

A current price of methanol from conventional sources is now roughly $.38/gal. or $6.64/M BTU. The current U.S. average refining price of regular grade gasoline (excluding taxes and dealer margins

is roughly $.37/gal. or $3.35/M BTU (13). Since this investigation is on synthetic fuels to replace present-day use of gasoline, future cost projections for methanol will be centered around those for synthetic gasoline from coal and shale rock.

A detailed cost analysis was done in an EPA report (7) for the 1982-2000 year time period for projected costs, at the pump, of various synthetic fuels for automotive application. Relative projected costs for manufacture and distribution of methanol (equivalent BTU basis) were calculated to be roughly 1.45 - 1.25 times costs for synthetic gasoline from shale rock, and roughly 1.15 - 1.02 times costs for synthetic gasoline from coal. Relative magnitudes of capital intensity for production and refining* of methanol were roughly 1.35 times costs for synthetic gasoline produced from shale rock, and roughly .83 times costs for synthetic gasoline derived from coal**.

Methanol appears to be more costly to the consumer if compared to synthetic gasoline produced from coal and especially shale rock. As mentioned previously, other questions must also be answered before a complete economic evaluation can be made. A discussion of the economic sensitivity to these questions will follow.

---

*Refining of crude oil from shale rock via conventional techniques and no refining required for methanol.

**In general, cost estimates for synthetic fuels accounted for the following (see Reference (7) for greater detail): 1) escalated raw material costs and improving mining technology; 2) use of existing and improving methods in production technology; 3) special considerations for immediate and future distribution and storage; 4) exclusion of inflationary factors and tax at the pump; 5) roughly a $\pm$ 10% accuracy expected for all cost projections.

End-use efficiency of methanol in a spark ignition engine along with effective control of the undesirable exhaust emissions appears significantly better than an engine operated on gasoline. A more detailed discussion of vehicle performance is in the next section; however, a recent study has indicated that a 34-38% energy economy advantage appears possible when using methanol (13).

Availability of appropriate end-use equipment would entail redesign and increased costs of present day automobiles if methanol is used. Specifically, the carburetion system, intake manifold, and "cold start" technology would require modifications; hence, vehicle costs could possibly be higher.

Availability of supplies to meet the potential demand is an important question to address. Since limited supplies would be available initially*, a practical and economical approach would be to have a gradual transition from use of 100% gasoline to use of 100% methanol. This would allow the transition to depend upon normal market factors such as cost and availability (3, 7, 35). Two approaches for introduction of methanol were mentioned: use in fleet vehicles in large cities, or use as a blend with gasoline by the public. Use in fleet vehicles would limit usage of methanol to 5% of the total automotive fuel demand; however, many of the "bugs" of using methanol could be worked out before introduction to the general public (7). Use of gasoline/methanol blends would

*Current U.S. methanol production capacity is the order of 3.5 M gal/day (2 M gal/day on a gasoline energy equivalent basis), and current gasoline consumption rate is roughly 300 M gal/day (13).

allow from 5 to 7.5% (based on a 15% methanol-gasoline blend) of the total automotive fuel demand (total BTU) to be replaced by methanol, and introduction would be a more continuous process. The hurdle with a gasoline/methanol blend is that in spite of the 40% cost penalty that can be taken to maintain dry distribution and storage systems, phase separation in the vehicle can still occur.

Economic sensitivity to environmental constraints would arise in mining of the natural resource, manufacture and distribution, and final end-use in the vehicle. In general, costs arising from environmental constraints in mining, manufacture, and distribution are similar for methanol and synthetic gasolines. The potential of western shale rock reserves may be more restrained because of the centralized location in the Rocky Mountain region. However, for processing of shale rock or coal, water availability will be a key factor along with the economic success of desalination of brackish water (7). As mentioned in the next section, methanol's use in a spark ignition engine, with the exception of Unburned Fuel and Aldehyde emissions, should result in cleaner and more efficient operation than with a gasoline powered engine. As a result, signifant energy economy advantages appear possible.

5.5 Performance of a Methanol-Fueled Automobile

Performance aspects of methanol, methanol/water blends and gasoline/methanol blends in a spark ignition engine were described in detail in Sections II and IV for single cylinder engines. In general significant efficiency emissions quality advantages (with the

exception of UBF and Aldehyde emissions) are possible when using Methanol, especially when small quantities of water are blended with methanol. For gasoline/methanol blends, no significant efficiency or emissions quality advantages appeared possible. A slight increase in octane quality is possible by blending methanol with gasoline (16). Operation at higher compression ratios would most likely increase NO_x emissions since NO_x levels were equal to or slightly greater than those for gasoline at equal compression ratios (13, 16, this study).

Care should be taken in translating single cylinder engine results to results anticipated in multicylinder engines and a full-sized vehicle. Two studies (12,13) have shown how sensitive NO_x, UBF, and Aldehyde emissions are to inlet mixture preparation (i.e., cylinder-to-cylinder mixture variations). For a better evaluation, more studies similar to those performed in references (4, 36) should be carried out testing methanol fuels in full sized vehicles.

5.6 Engineering Development

New technology would be necessary for the distribution and storage of gasoline/methanol blends. Also, new carburetion systems for the use of methanol would have to be developed.

Economics and practical aspects would improve if methanol could be introduced as a blend without the need for a dry distribution and storage system. Additives (Benzol, Benzene, Acetone, and Butyl Alcohol) or emulsification have been suggested to increase the water tolerance; however, none have been proven as practical (5, 6, 7).

From an engineering development point of view, an advantage of initial introduction in fleet programs would be the allowance of time for auto designers to remove "bugs" before introduction to the general public. For example, increased solvency and corrosion properties arise when using methanol fuels. If gasoline/methanol blends were used, the fuel system would need to be redesigned to handle the increased vapor pressure of the fuel.

Carburetion systems for methanol would have to be redesigned for different fuel/air stoichiometry (roughly a 2:1 difference), more manifold heating (roughly 8:1), and cold start situations. Additional heating could be accomplished by exhaust gas heating of the intake manifold, or engine coolant heating if necessary. Ideally, the methanol manifold should allow for the following (4).

1) 100% vaporization at idle and low speed conditions where power is unimportant and good distribution is critical for lean operating conditions
2) partial vaporization at part throttle and wide open throttle where both power and distribution is desired (proper proportions yet undetermined).

Due to methanol's high latent heat of vaporization (roughly 3 1/3 times that of gasoline) and single boiling point, performance

in cold start situation is the remaining hurdle*. Possible solutions have been examined such as blending a volatile component(s) to methanol, prevaporization of the fuel (fuel injection), or use of a starting fuel system. Blending volatile components required excessively large quantities for good results, and recondensing of prevaporized fuel can occur. The most practical solution appears to be starting fuel system since only small quantities would be required. The starting fuel could be gasoline or another fuel such as dimethyl ether (4).

5.7 Environmental Impact

Use of synthetic fuels would have an impact on the environment during mining of the natural resource, manufacture and distribution, and final end-use in the vehicle.

As mentioned previously, mining of coal and shale rock involve similar environmental constraints. Specifically for coal mining, the resource used for large-scale methanol production, land reclamation, waste disposal, and water availability will be major environmental concerns. Effects of federal mining legislation and the reaction to the influx of large numbers of people into sparsely populated areas will also be important. Environmental restrictions

---

*Without a starting fuel system for ambient conditions below 50°F, cold starts were nearly impossible (4).

on mining shale rock are similar to those for mining coal. A more centralized location of shale rock reserves opposed to scattered location of coal reserves, could impose a few additional constraints (7).

Manufacture and distribution of the synthetic fuels also involve overlapping environmental concerns. Effluents from manufacturing plants must be controlled; leaks and spills in the distribution system must be prevented. When methanol is distributed in tankers, a methanol spill would differ from an oil spill by dissolving in the water rather than floating on the surface. Which type of spill would biodegrade more quickly should be determined. Toxicity hazards with spills or human and animal contact should also be mentioned. Oral injestion of methanol is hazardous because blindness could result. Oral injestion of gasoline is generally not as hazardous if properly taken care of; however, aspiration is extremely hazardous and could be fatal. Other risks such as skin penetration, inhalation, nose, eye and throat contact are generally low for both methanol and gasoline (7).

As discussed previously, the use of methanol as a motor fuel, with the exception of UBF and Aldehyde emissions, will result in significant emissions quality advantage. Existing oxidation catalyst technology could be used as a last resort for UBF and Aldehyde emissions. Equal levels of exhaust emissions can be attained with gasoline fueled engines; however, a reduction in efficiency would result.

6. CONCLUSIONS

The following conclusions can be drawn on the basis of the single-cylinder engine data presented.

• Overall combustion intervals (particularly in the lean region) were shortest with methanol, followed by 10% water-90% methanol, and slight differences for 15% methanol-85% indolene and indolene. Only combustion duration periods for 15% methanol-85% indolene were shorter than indolene's.

• From calculations of mass fraction burned vs crank angle (time), turbulent flame speeds were calculated for MBT data assuming spherical flame geometry and thin flame front. Results indicated that turbulent flame speed does not vary appreciably during the combustion duration period (fully developed flame propagation). Flame speed increased and decreased accordingly during initial and final stages of combustion (final period analysis limited by thin flame front assumption). Results for turbulent flame speed (at $x = .5$) vs equivalence ratio for the four fuels studied were generally consistent with results from the average overall combustion intervals.

• Lean misfire limits were leanest for methanol, followed by 10% water-90% methanol, and slight differences for 15% methanol-85% indolene and indolene.

• Differences in constant IMEP, and MBT indicated thermal efficiencies were small; however, at lean conditions ($\phi < .9$), highest indicated thermal efficiencies resulted for methanol, followed by

indolene, 15% methanol-85% indolene, and 10% water-90% methanol.

• At MBT - constant IMEP conditions, indicated specific nitric oxide (IS NO_x) levels were highest for 15% methanol-85% indolene, followed by indolene, methanol, and 10% water-90% methanol.

• In the lean region ($\phi < .9$), indicated specific unburned fuel (IS UBR) emissions levels were highest for 10% water-90% methanol, followed by methanol, 15% methanol-85% indolene, and indolene. For richer conditions ($\phi > .9$) differences were small with the exception of indolene whose levels rose more rapidly than the methanol fuels.

• In the lean region ($\phi < .9$), indicated specific carbon monoxide (IS CO) emissions levels were all significantly low and were highest for 15% methanol-85% indolene, followed by 10% water-90% methanol, indolene, and methanol. All IS CO levels increased steadily as equivalence ratio was increased past $\phi = 1$.

• As spark advance is retarded relative to the MBT point lower IS NO_x levels, lower indicated thermal efficiencies, and small differences in IS UBF levels resulted.

• As compression ratio is increased to the point of incipient knock (at $\phi = .8$) indicated thermal efficiency increases, IS UBF levels increase, and IS NO_x levels either increase, decrease, or remain the same.

The following conclusions can be drawn on methanol's potential for commercial applications as a motor fuel.

- Enormous domestic supplies of coal are available for methanol production.
- The production of methanol would probably be accomplished by gasification of coal to a low BTU gas followed by existing technology for methanol synthesis.
- A separate distribution and storage system roughly 2.0 times the volume of an equivalent gasoline system would be required.
- Relative projected costs of methanol to the consumer, compared with synthetic gasoline from shale rock or coal, are higher per BTU contained; however, other factors such as end-use efficiency, availability of appropriate end-use equipment, availability of supplies to meet the demand, and environmental constraints, will be important.
- Engineering development problems are involved with converting present day automobiles to run on methanol. Carburetion systems would have to be redesigned for different fuel/air stoichiometry, manifold heating, and cold start requirements. Also, more experiments in multicylinder engines are needed before scaling up from single-cylinder engine data can be accomplished.
- Impact on the environment from use of all synthetic fuels appears to be similar for production and use of methanol as well as synthetic gasoline. Although methanol generally burns cleaner in a spark ignition engine, emissions standards would require emissions from all

vehicles to be low. The final question will rest on the final source-to-end use economics and practicalities involved.

REFERENCES

1. H.C. Hottle, and J.B. Howard, New Energy Technology - Some Facts and Assessments, MIT Press, Cambridge, Mass. 1971.

2. L. Linden, Personal Communication, MIT Energy Laboratory, June, 1976.

3. W.J. Most and J.P. Longwell, "Single-Cylinder Engine Evaluation of Methanol - Improved Energy Economy and Reduced NO_x," SAE Paper No. 750119, 1975.

4. H.G. Adelman, D.G. Andrews, and R.S. Devoto, "Exhaust Emissions from a Methanol-Fueld Automobile," SAE Paper No. 720693, 1972.

5. E.E. Wigg, "Methanol as a Gasoline Extender: A Critique," Science, Vol. 186, No. 4166, 29 November 1974.

6. J.A. Bolt, "A Survey of Alcohol as a Motor Fuel," SAE Special Publication No. SP-254, 1964.

7. F.H. Kant, R.P. Cahn, A.R. Cunningham, M.H. Farmer, W. Herbst and E.H. Manny, "Feasibility Study of Alternate Fuels for Automotive Transportation," Vols. II and III, EPA Report #EPA-460/3-74-009-b, June 1974.

8. G.D. Ebersole and F.S. Manning, "Engine Performance and Exhaust Emissions: Methanol vs. Isooctane," SAE Paper No. 720692, August 1972.

9. J.A. Harrington and R.M. Pilot, "Combustion and Emissions Characteristics of Methanol," SAE Paper No. 680401, May 1968.

10. E.S. Starkman, H.J. Newhall, and R.D. Sutton, "Comparative Performance of Alcohol and Hydrocarbon Fuels," SAE Special Publication No. SP-254, 1964.

11. E.F. Obert, Internal Combustion Engines and Air Pollution, Intext Educational Publishers, New York, N.Y., 1973.

12. D.L. Hilden and F.B. Parks, "A Single-Cylinder Engine Study of Methanol Fuel-Emphasis on Organic Emissions," SAE Paper No. 760368, February 1976.

13. W.J. Most and E.E. Wigg, "Methanol and Methanol - Gasoline Blends as Automotive Fuels," presented at The Combustion Institute, Central States Section, Spring Meeting April 5-6, 1976, Columbus, Ohio.

14. W.E. Bernhardt and W. Lee, "Combustion of Methyl Alcohol in Spark Ignition Engines," the 15th Symposium on Combustion, The Combustion Institute, 1974.

15. J.A. Harrington, "Application of a New Combustion Analysis Method in the Study of Alternate Fuel Combustion and Emissions Characteristics," paper presented at Symposium on Future Automotive Fuels, sponsored and held at General Motors Research Laboratories, Warren, Michigan, October 1975.

16. R.T. Johnson and R.K. Riley, "Single Cylinder Spark Ignition of Octane, Emissions, and Fuel Economy Characteristics of Methanol-Gasoline Blends," SAE Paper No. 760377, February 1976.

17. D.R. Lancaster, R.B. Krieger and J.H. Lienesch, "Measurement and Analysis of Engine Pressure Data," SAE Paper No. 7500026, presented at the Automotive Engineering Congress, Detroit, Michigan, February 1975.

18. G.A. Danielli, "A Performance Model of a Wankel Engine, Including the Effects of Burning Rates, etc." Ph.D. Thesis, Department of Mechanical Engineering, MIT, January 1976.

19. R.J. Tabaczynski, "Time-Resolved Measurements of Hydrocarbon Mass Flowrate in the Exhaust of a Spark-Ignition Engine," SAE Paper No. 720112, 1972.

20. N.C. Blizard and J.C. Keck, "Theoretical and Experimental Investigation of a Burning Model for Spark-Ignition Engines," SAE Paper No. 740191, 1974.

21. D.R. Lancaster, R.B. Krieger, S.C. Sorenson and W.L. Hull, "Effects of Turbulence on Spark-Ignition Engine Combustion," SAE Paper No. 760160, February 1976.

22. K. Komiyama and J.B. Heywood, "Predicting NO_x Emissions and Effects of Exhaust Gas Recirculation in Spark Ignition Engines," SAE Paper No. 730475, 1973.

23. B. Lewis and G. Von Elbe, Combustion, Flames and Explosions of Gas, Second Edition, Cambridge University Press, 19

24. F.A. Williams, Combustion Theory, Addison-Wesley, Reading, Mass., 1965.

25. G.G. Desoete, "The Influence of Isotropic Turbulence on the Critical Ignition Energy," 13th Symposium (International) on Combustion, The Combustion Institute, 1973, p. 735.

26. A.M. Mellor and I. Glassman, Basic Combustion Phenomena, Course Notes, Mechanical Engineering Department, Purdue University, 1970.

27. J.J. Evangelista, R. Shinnar and S. Katz, "The Effect of Imperfect Mixing on Stirred Combustion Reactors," 12th Symposium on Combustion.

28. G.A. Lavoie, J.B. Heywood and J.C. Keck, "Experimental and Theoretical Study of Nitric Oxide Formation in Internal Combustion Engines," Combustion Science and Technology, Vol. 1, 1970, p. 313.

29. M.K. Martin and J.B. Heywood, "Approximate Relationships for the Thermodyanmic Properties of Hydrocarbon-Air Combustion Products,"

30. C.T. Bowman, "Shock-Tube Investigation of the High Temperature Oxidation of Methanol," Combustion and Flame, Vo. 25, No. 3, December 1975.

31. J.B. Heywood, "Pollutant Formation and Control in Spark Ignition Engines," paper presented at the 15th Symposium (International) on Combustion, Tokyo, Japan, 1974.

32. C.R. Ferguson and J.C. Keck, "On Laminar Flame Quenching and its Applications to Engine Combustion,

33. J.C. Mingee, "The Future Need for Rocky Mountain Energy Supplies," paper presented at Annual Meeting, Society of Petroleum Engineers, Dallas, Texas, February 1974.

34. A.L. Hammond, W.D. Metz and T.H. Maugh, Energy and the Future, American Association for the Advancement of Science, Washington, D.C., 1973.

35. T.B. Reed and R.M. Lerner, "Methanol: A Versatile Fuel for Immediate Use," Science, Vol. 182, No. 4119, 28 December 1973.

36. R.M. Lerner, T.B. Reed, E.D. Hinkely and R.E. Fahey, "Improved Performance of Internal Combustion Engines using 5-20% Methanol," Lincoln Laboratory, MIT, 1974.

37. C.R. Ferguson, "Calculation of Unburned Mixture Properties," and "Turbulent Flame Geometry and Flame Speed Calculations," Sloan Laboratory Internal Reports, MIT, 1976.

38. S.D. Hires, A. Ekchian, J.B. Heywood, R.J. Tabaczynski and J.C. Wall, "Performance and NO_x Modeling of a Jet Ignition Prechamber Stratified Charge Engine," SAE Paper No. 760161, February 1976.

39. M.K. Martin, "Photographic Study of Stratified Combustion using a Rapid Compression Machine," S.M. Thesis, Department of Mechanical Engineering, MIT, January 1975.

40. J.A. LoRusso, "C_p Curve Fit Polynomials (Avco Everett version)," Sloan Laboratory Internal Report, February 1976.

41. D.R. Stull, E.F. Westrum Jr. and G.C. Sinke, "The Chemical Thermodynamics of Organic Compounds," John Wiley & Sons, Inc., New York, N.Y., 1969.

42. F.D. Rossini, K.S. Pitzer, R.L. Arnett, R.M. Braunn and G.C. Pimentel, Selected Values of Physical and Thermodynamic Properties of Hydrocarbons and Related Compounds, Carnegie Press, Pittsburgh, Pa., 1953.

43. Janof Thermochemical Tables, Second Edition, National Bureau of Standards Publication, NSRDS-NBS 37, 1971.

44. S. Gordon, et al., "Computer Program for Calculation of Complex Chemical Equilibrium Compositions...," National Technical Information Service, Report No. N71-37775, 1971.

45. O. Oforah, "Effect of Valve Lift on Dynamic Pressure and Flame Propagation in a Spark Ignition Engine," S.M. Thesis, Department of Mechanical Engineering, MIT, June, 1976.

46. C.R. Ferguson, "Time Resolved Exhaust Emissions of a Wankel Engine," SAE Paper No. 750024, February 1975.

47. R.S. Spindt, "Air-Fuel Ratios from Exhaust Gas Analysis," SAE Paper No. 650507, 1965.

Table 1

Some Physical Properties of Indolene, Methanol, 10% Water-90% Methanol, and 15% Methanol-85% Indolene

Property	Indolene	Methanol	10% Water-90% Methanol	15% Methanol-85% Indolene
Average Molecular Formula	$C_{7.261}H_{13.87}$	CH_3OH	$C_{.777}H_{3.554}O_{.9891}$	$C_{5.218}H_{1}).65O_{.3409}$
Average Molecular Weight	101	32	28.7	78.72
Specific Gravity @ 60°F	.743[b]	.796	a	a
Stoichiometric				
- fuel/air ratio	.06828	.15472	.17779	.07405
- air/fuel ratio	14.67	6.463	5.625	13.504
Heat of Combustion (lower) BTU/lb_m	18493	8644	7442	17062
Vapor Pressure, 100°F, psia	9.1	4.55	a	~ 12.0
Flammability Limits				
- Volume % in air @ STP	1.1-6.0[c]	7.3-3.6[d]	a	a
- Equivalence ratio @ STP	.661-3.8	.562-4.0	a	a
Heat of Vaporization @ Boiling Point & 1 atm, BTU/lb_m	150[e]	473	a	a
Boiling Point (B.P.), °F @ 1 atm	86-391[f]	148	212/148[g]	86-391
Octane Ratings - Motor	83.6	87.4[d]	92.8[d]	a
- Research	90.8	109.6[d]	114.0[d]	a

a - values not calculated
b - reference (9)
c - approximated by using isooctane's properties
d - reference (13)
e - estimated average for gasoline
f - initial B.P. @ 86°F, 50% off @ 122°F, 90% off @ 304°F, Max. @ 391°F
g - 212°F is the boiling point of water @ 1 atm; 148°F is the B.P. of methanol @ 1 atm

Table 2

CFR Engine Specifications

Parameter			Value
Base (cm)			8.255
Stroke (cm)			11.43
Connecting Rod Length (cm)			25.4
Clearance Volume $(cm)^3$ @ C.R. = 6.937:1			103.04
Clearance Height (cm) @ C.R. = 6.937:1			1.80
Radius from Cylinder Centerline to Spark Plug (cm)			4.125
Intake Valve	-	opens	10 deg a.t.d.c.
	-	closes	34 deg a.b.d.c.
Exhaust Valve	-	opens	40 deg b.b.d.c.
		closes	15 deg a.t.d.c.
Spark Gap (cm)			.124 (.049 in)

Table 3

Calibration Gases for Exhaust Gas Analysis System

	Species %					
	CO_2	O_2	CO	NO_x	C_3H_8	CH_3OH
Gas 1*	-	-	-	205×10^{-6}	-	-
Gas 2*	8.1	4.3	.125	-	-	-
Gas 3*	11.2	9.1	.184	-	-	-
Gas 4*	-	-	-	-	.00996	-
Gas 5*	4.2	.97	.066	-	-	-
Test Gas**	-	-	-	-	-	790×10^{-6}

*N_2 balance

**Methanol calibration gas (N_2 balance) used to determine propane calibration sensitivity to methanol.

Sensitivity ≃ .9

Table 4 Operating Conditions for the Baseline Data Matrix (1600 RMP, C.R. = 6.937:1. MBT Spark Timing, Exhaust Pressure ≈ 1.0 atm)

Fuel Type	Case No.	Ø	Air Flow (gm/min)	Spark Advance (D.A.T.D.C.)	Inlet Pressure (atm)	Inlet Temperature (°R)	Exhaust Temperature* (°R)	IMEP (psi)
Indolene	1	1.13	172.1	-24	.466	639	990*	52.2
	6	.94	175.5	-26	.475	642	1015	52.2
	8	1.01	169.8	-29	.465	637	1020	54.3
	10	.80	201.4	-32	.530	636	960	53.3
	17	.69	237.8	-48	.615	642	915	55.2
	20	.68	240.6	-46	.618	642	920	53.9
	115	.80	192.2	-33	.523	641	960	51.8
Methanol	23	.72	200.7	-26	.570	641	890*	53.5
	26	.77	185.7	-25	.533	644	900	53.3
	32	.58	245.9	-46	.665	641	825	54.3
	35	.57	251.8	-47	.672	642	825	52.6
	40	.97	163.9	-21	.491	641	925	54.3
	43	1.12	161.1	-18	.496	642	940	53.9
10% Water-90% Methanol	51	.91	174.4	-23	.530	643	940*	52.2
	54	1.06	156.1	-20	.494	643	940	52.2
	57	1.22	155.0	-18	.470	639	885	52.4
	63	.60	248.1	-40	.676	640	840	53.9
	124	.80	182.11	-26	.545	639	880	52.6
15% Methanol-85% Indolene	75	.67	227.2	-41	.593	640	880*	53.0
	79	.73	218.4	-38	.575	641	910	54.7
	83	.78	202.5	-38	.541	642	935	52.4
	88	.99	173.7	-29	.478	642	990	53.3
	91	1.11	169.8	-24	.474	642	970	54.3

*Exhaust temperatures estimated (see Section 4)

Table 5 Operating Conditions for Spark Advance Study

(1600 RPM, C.R. = 6.937:1, Exhaust Pressure ≈ 1.0 atm)

Fuel Type	Case No.	Spark Advance (D.A.T.D.C.)	Inlet Temperature (°R)	IMEP (psi)
Indolene	10	-32	636	53.3
MBT spark = -32°	11	-37	637	53.0
Ø = .80	14	-27	637	53.8
Air Flow = 201.4 gm/min	15	-22	637	52.2
Methanol	26	-25	644	53.3
MBT spark = -23°	27	-30	644	52.8
Ø = .77	28	-20	644	53.3
Air Flow = 185.7 gm/min	29	-10	644	50.7
	30	0	644	43.5
10% Water-	57	-18	639	52.4
90% Methanol	58	-24	637	52.0
MBT spark = - 18°	59	-34	637	49.7
Ø = 1.22	60	-13	638	51.3
Air Flow = 155.0 gm/min	61	-5	639	50.1
15% Methanol-	83	-38	640	52.4
85% Indolene	84	-43	641	51.8
MBT spark = -36°	85	-33	641	52.8
Ø = .78	86	-23	641	50.9
Air Flow = 202.5 gm/min	87	-13	641	44.8

Table 6 Operating Conditions for Compression Ratio Study

(1600 RPM, MBT Spark Timing, Exhaust Pressure ≈ 1.0 atm)

Fuel Type	Case No.	Compression Ratio	MBT Spark Advance (D.A.T.D.C.)	Inlet Temperature °R	IMEP (psi)
Indolene Ø = .80	111	9.572	-17	638	56.0
	112	8.143	-25	640	53.7
	115	6.937	-33	641	51.8
Methanol Ø = .81	102	9.400	-13	640	55.8
	105	8.143	-20	639	54.7
	127	6.937	-25	640	53.3
10% Water- 90% Methanol	118	10.22	-9	637	55.2
	121	8.143	-20	639	53.0
	124	6.937	-26	639	52.6
15% Methanol- 85% Indolene	96	9.540	-21	640	55.8
	99	8.143	-27	642	55.0
	128	6.937	-36	640	52.4

Figure 1

EXPERIMENTAL C.F.R. ENGINE SETUP

SLOAN LABORATORY MAY,1976

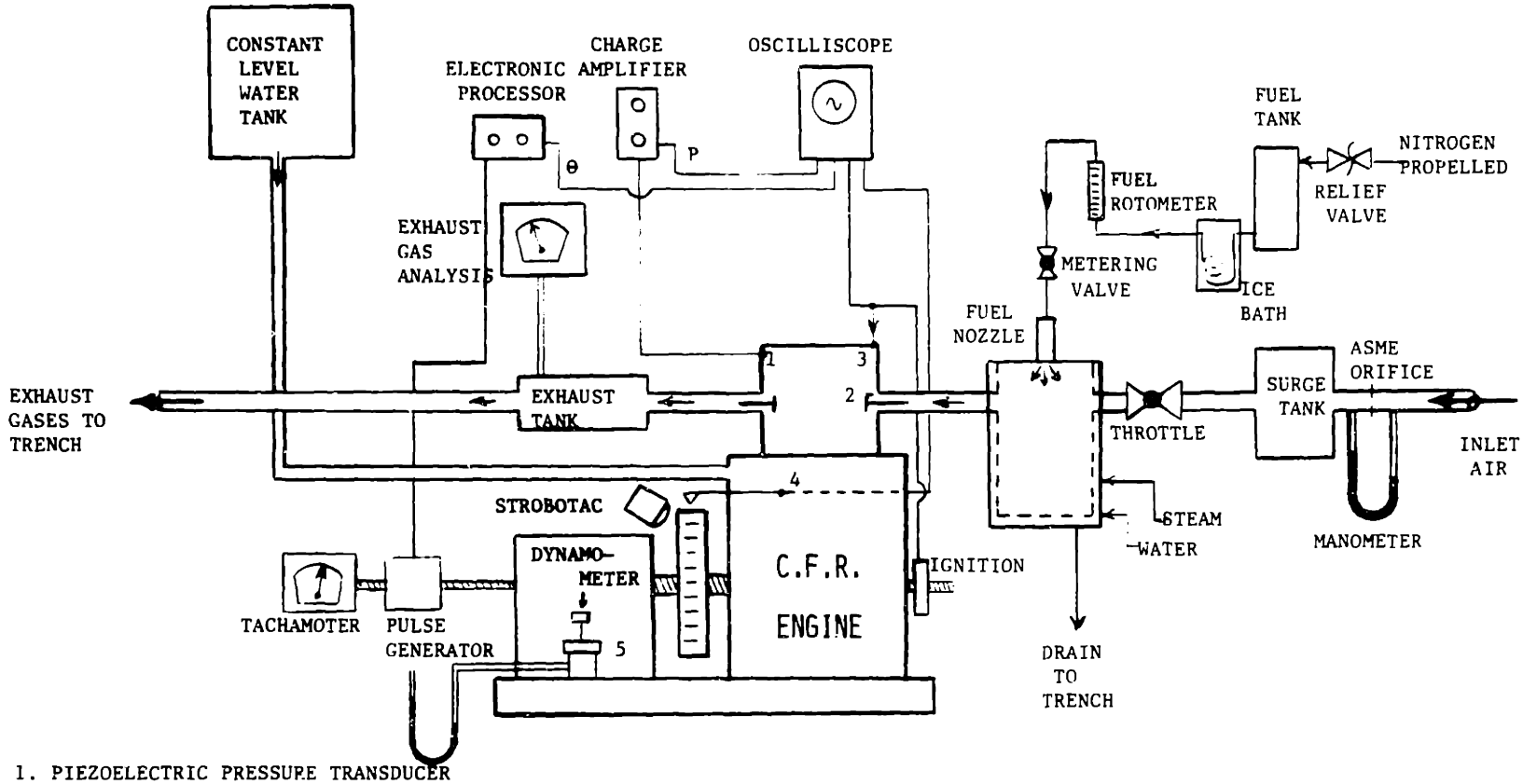

1. PIEZOELECTRIC PRESSURE TRANSDUCER
2. SHROUDED INTAKE VALVE
3. SPARK PLUG(MOUNTED ON UPPER EDGE OF CHAMBER)
4. MAGNETIC PICK-UP(TDC MARKER)
5. HYDRAULIC LOAD CELL(TORQUE)

FIGURE 2A.

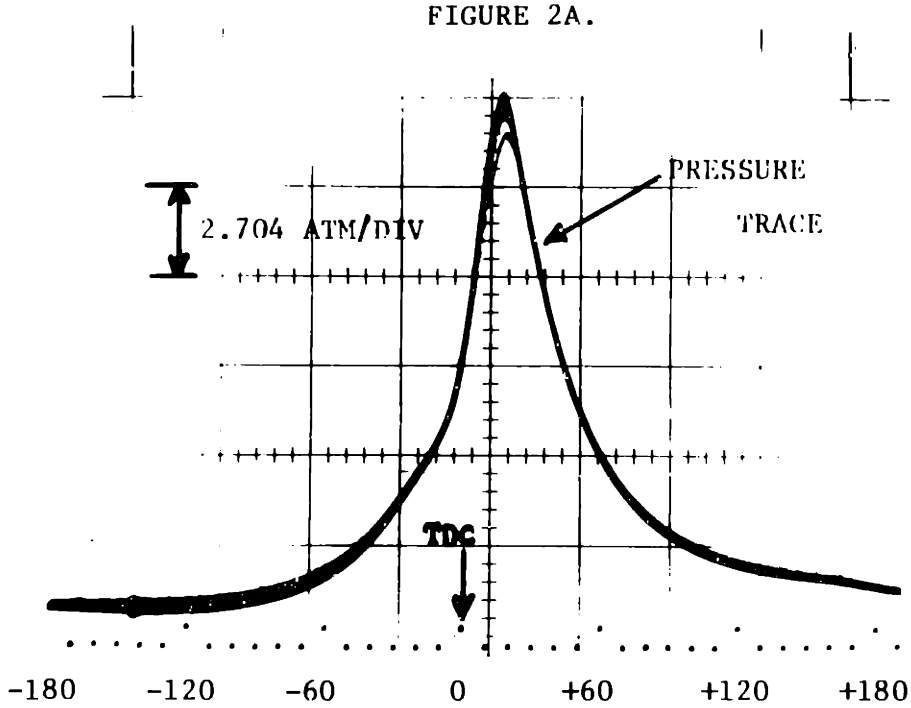

FIGURE 2B.

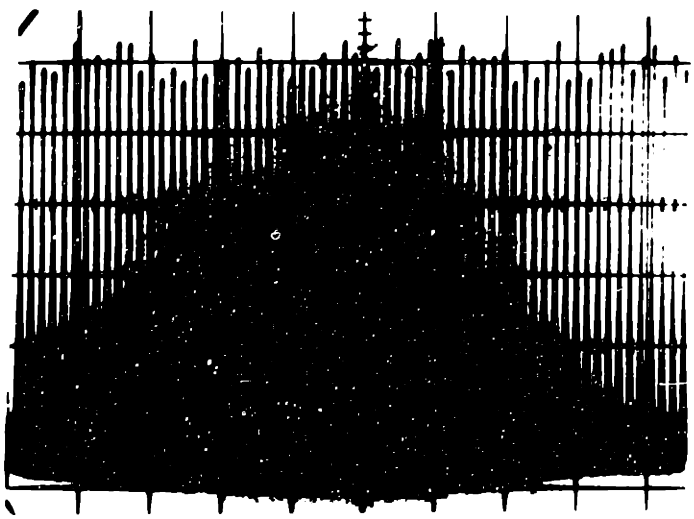

FIGURE 2C.

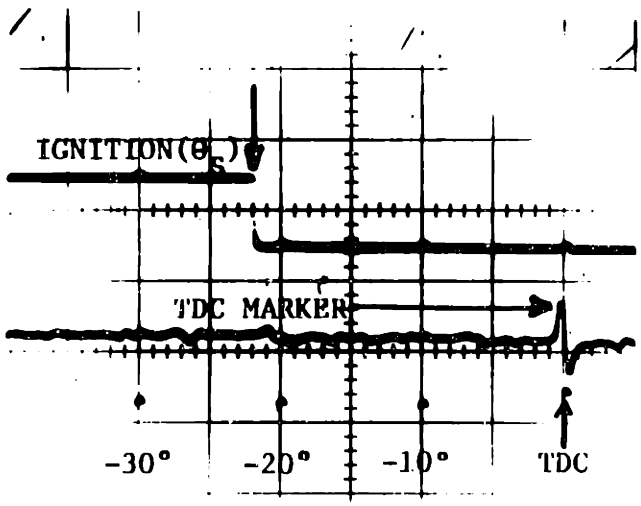

Figure 2 - (2A) Pressure transducer output vs crank angle degrees (six cycles) for case # 40;
(2B) Ignition angle (θ_s), TDC marker pulse, crank angle degrees for case # 40;
(2C) 70 consecutive pressure cycles for case # 40

Figure 3

EXHAUST GAS ANALYSIS SYSTEM

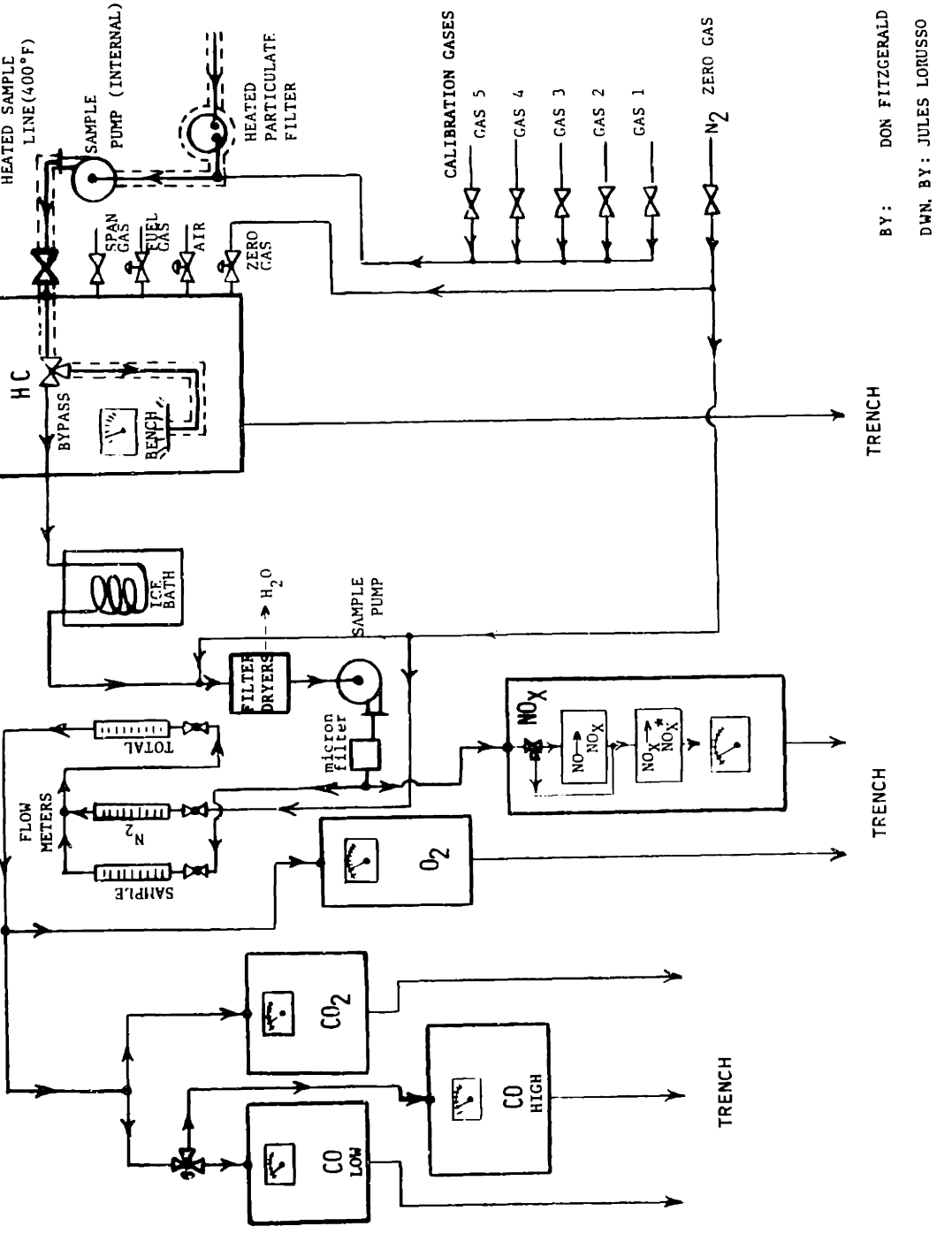

FIGURE 4A.

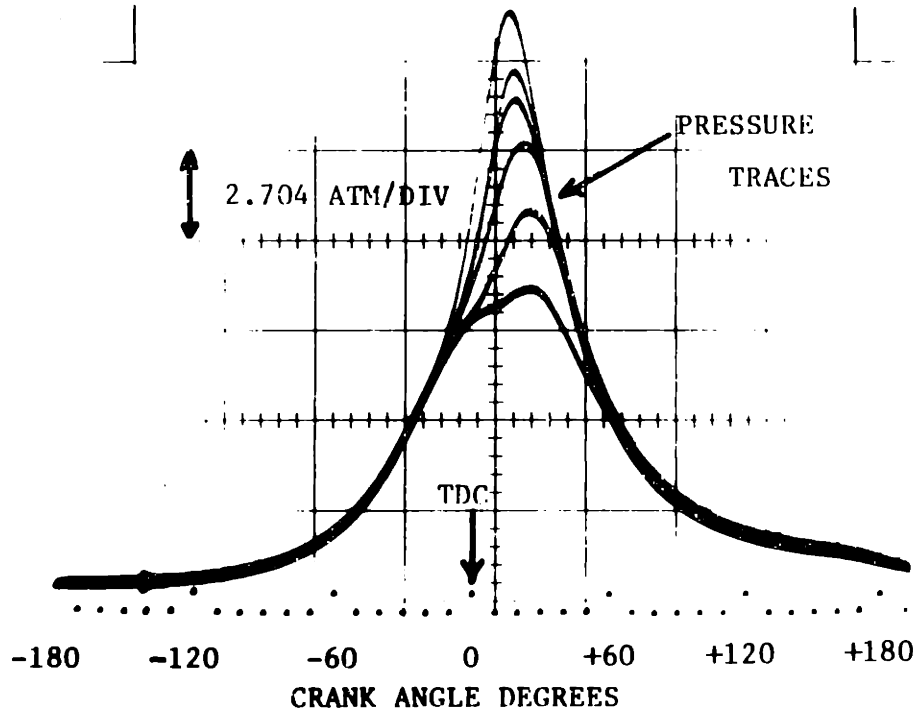

FIGURE 4B.

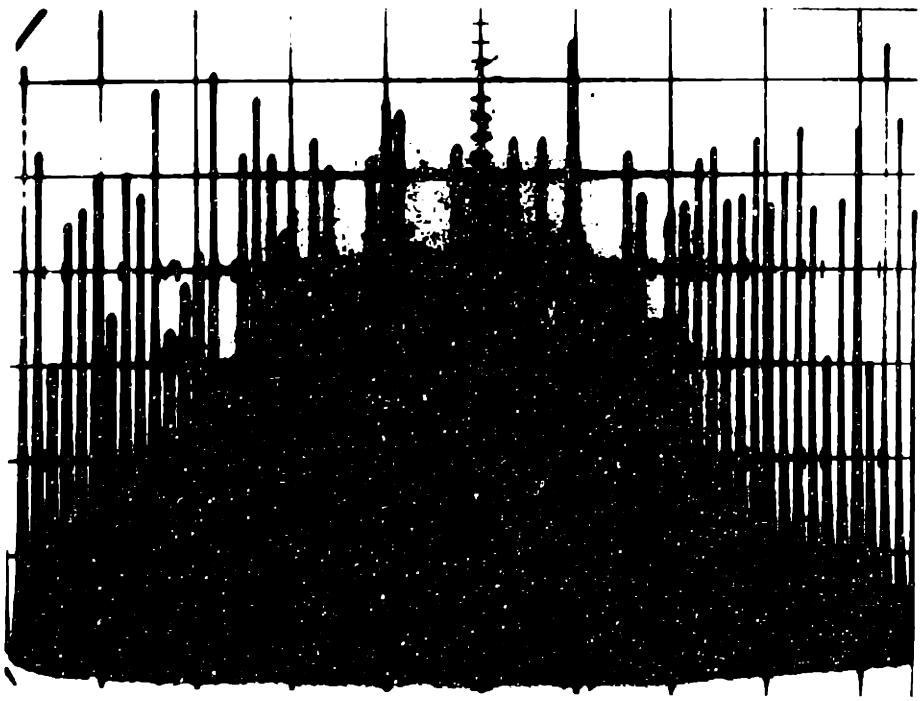

Figure 4 - (4A) Six random pressure cycles at lean misfire conditions;
(4B) 70 consecutive pressure cycles for lean misfire conditions

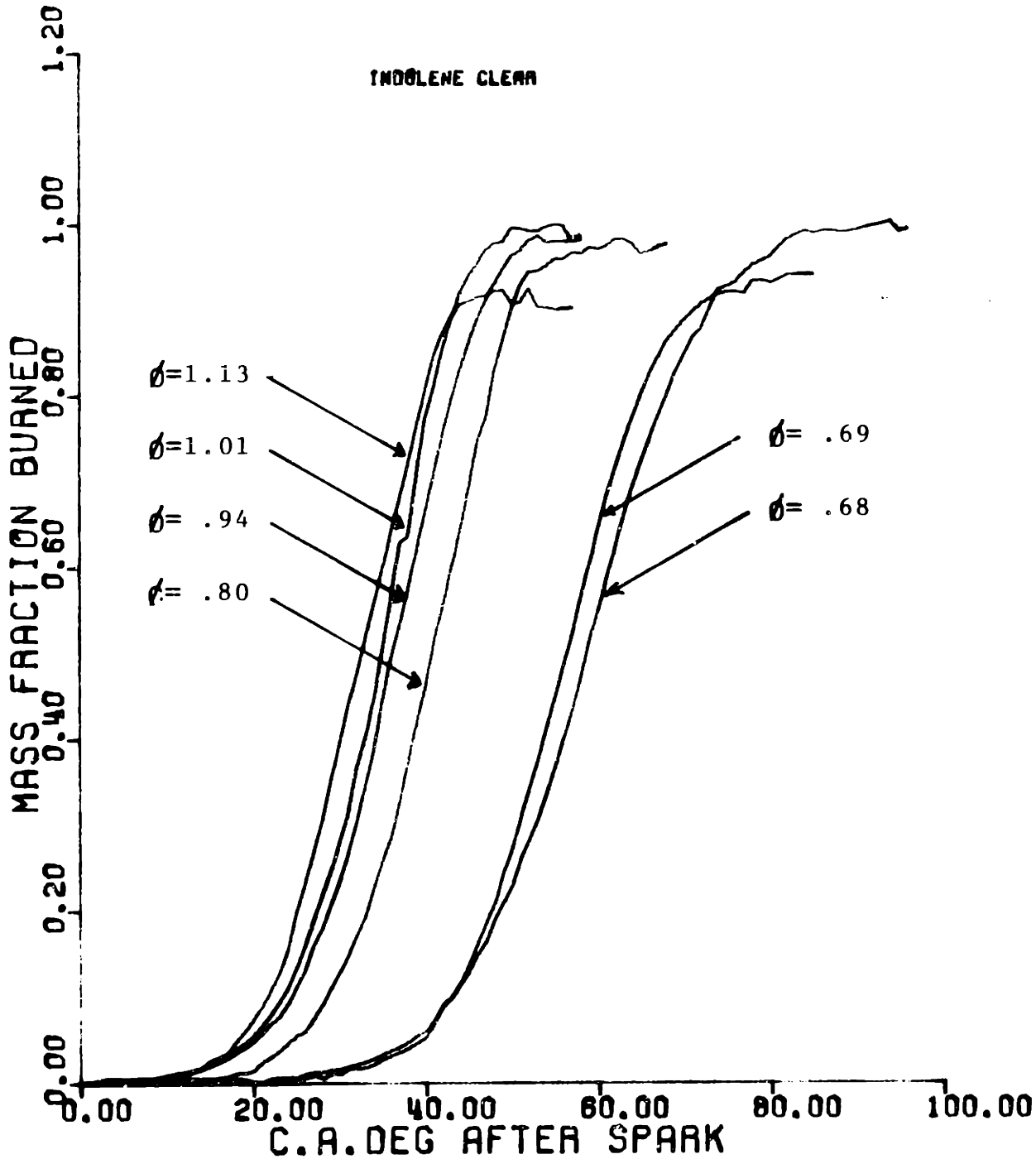

Figure 5 Mass fraction burned (x) vs. crank angle degrees (Θ) and equivalence ratio (Ø) for indolene at baseline conditions (Table 4)

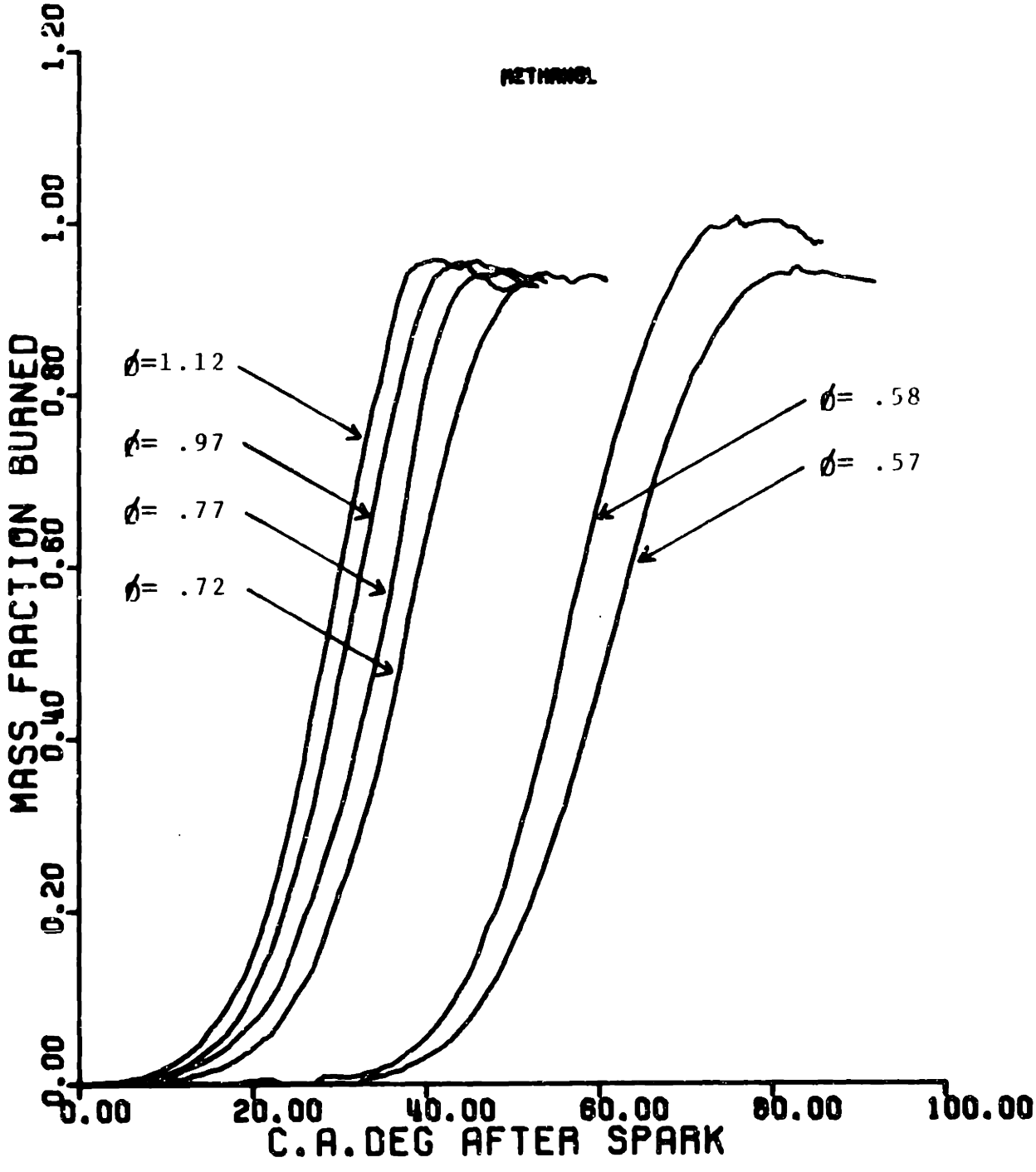

Figure 6 Mass fraction burned (x) vs. crank angle degrees (θ) and equivalence ratio (Ø) for methanol at baseline conditions (Table 4)

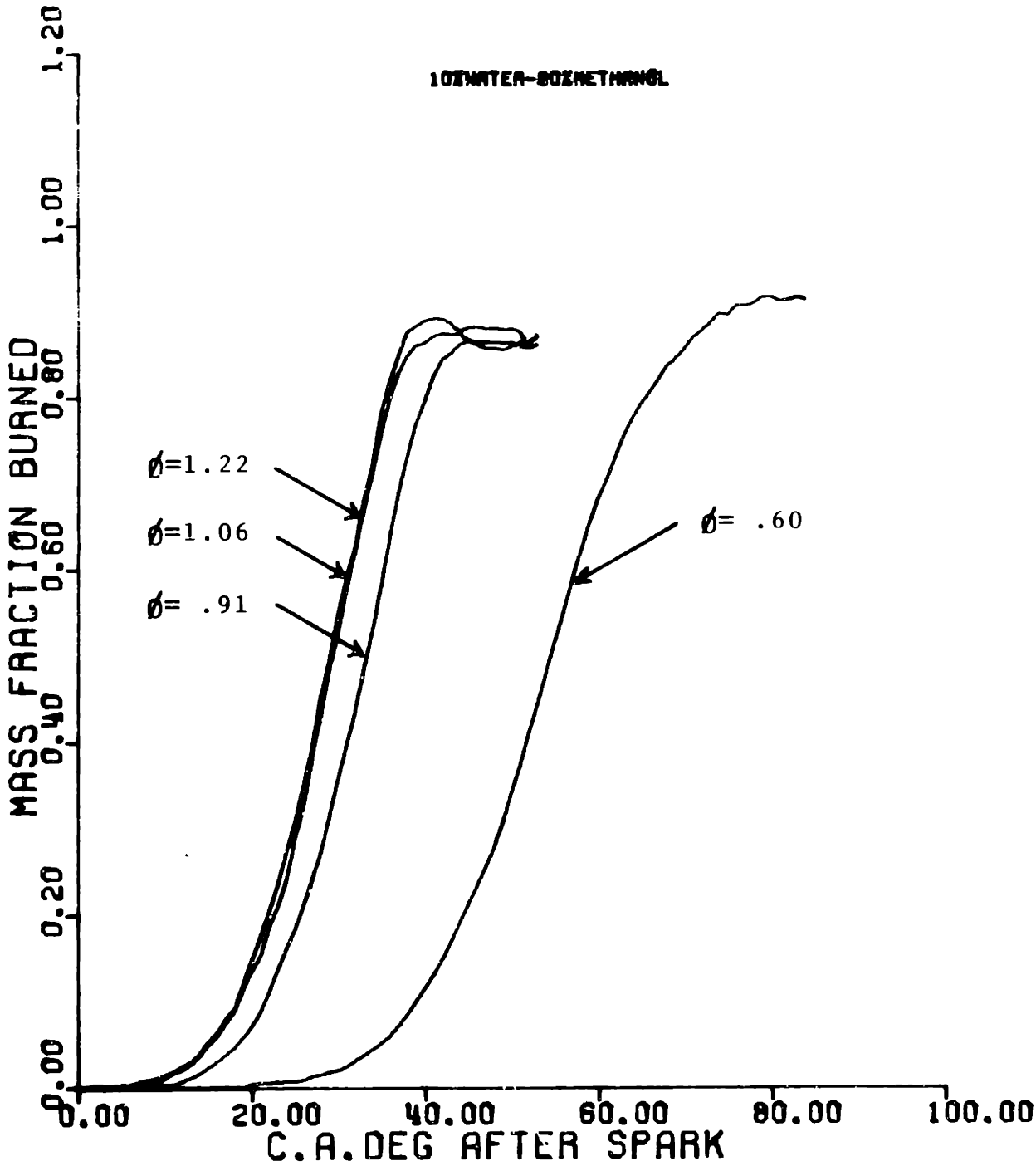

Figure 7 Mass fraction burned (x) vs. crank angle degrees (θ) and equivalence ratio (Ø) for 10% water-90% methanol at baseline conditions (Table 4)

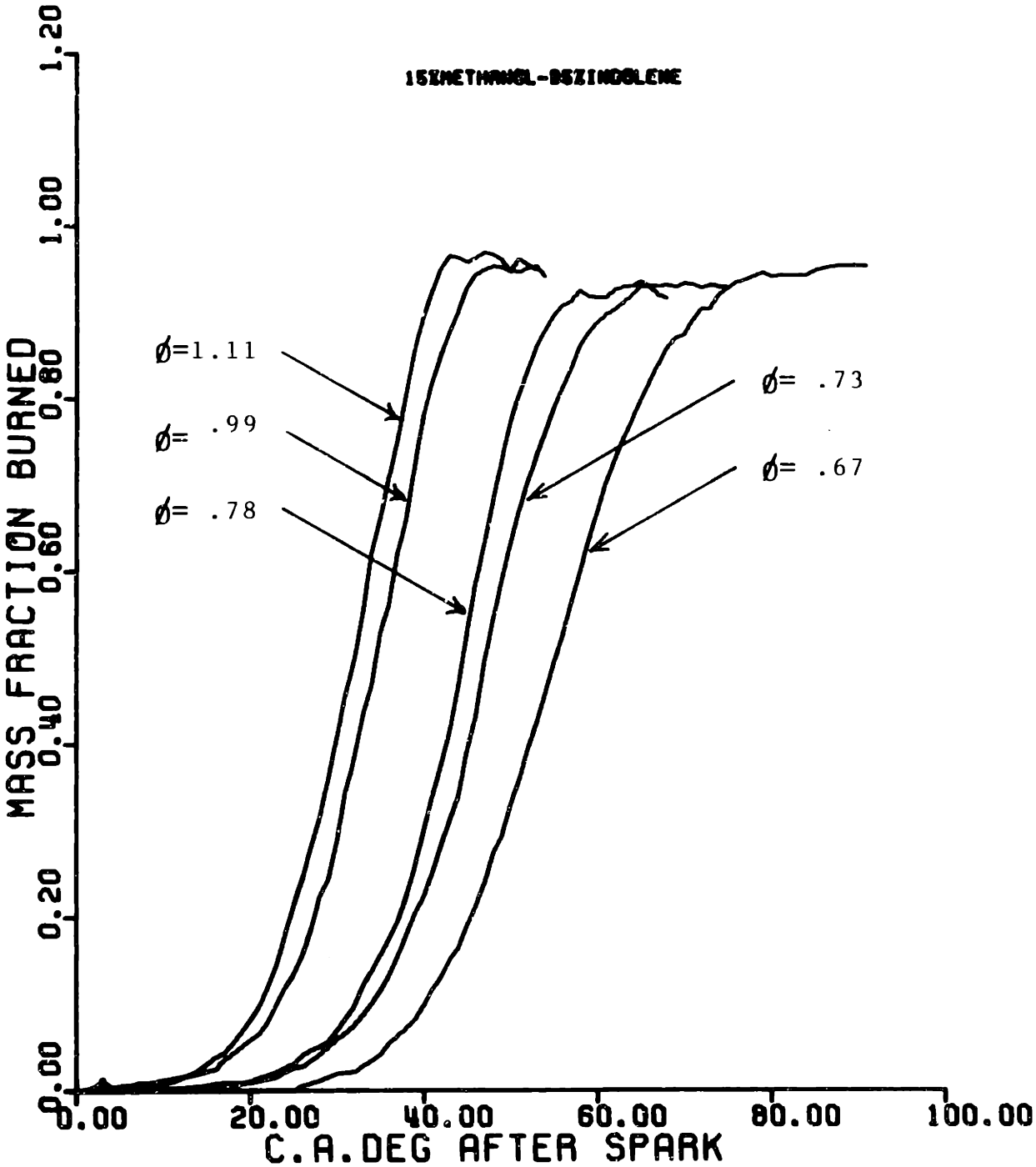

Figure 8 Mass fraction burned (x) vs. crank angle degrees (θ) and equivalence ratio (Ø) for 15% indolene-85% methanol at baseline conditions

Figure 9A.

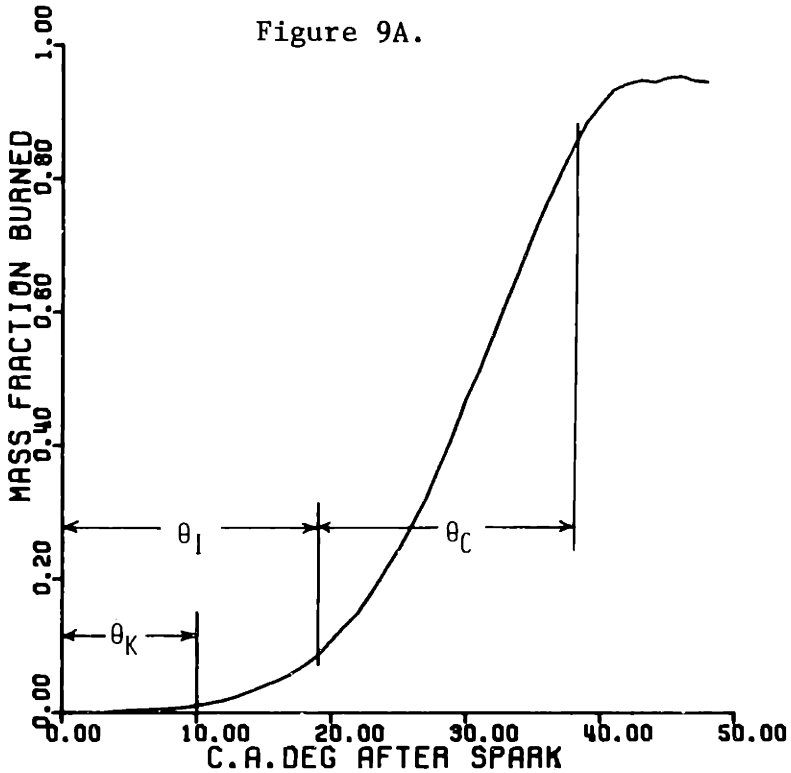

Figure 9B.

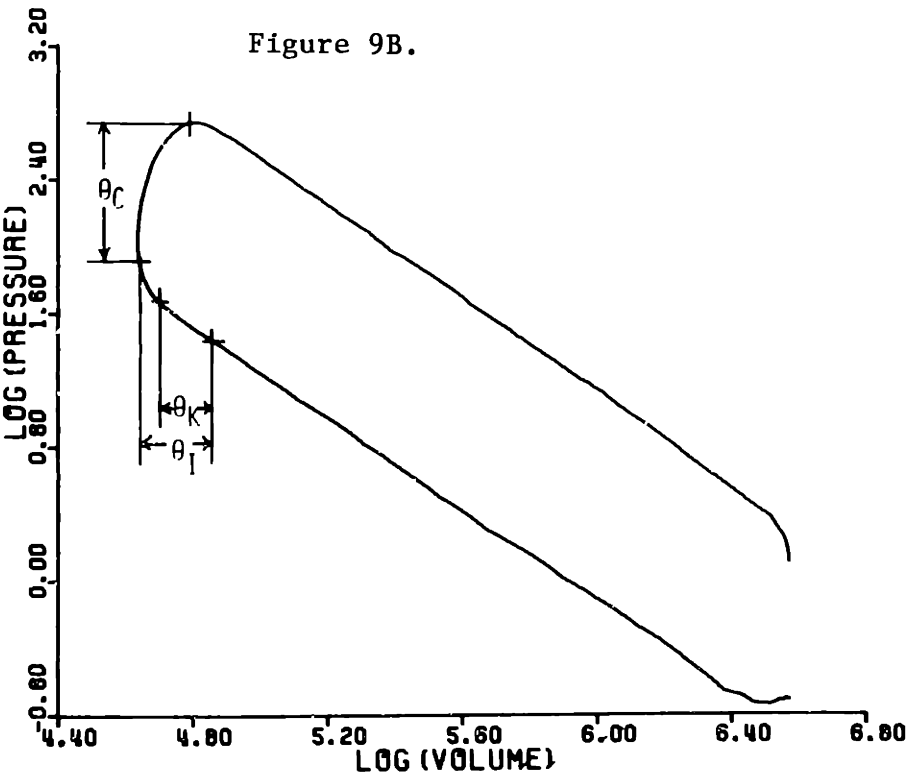

Figure 9 Definitions of kernel development (θ_k), ignition delay (θ_I), and combustion duration intervals (θ_c) on mass fraction burned (x) vs. crank angle (θ) and log (Pressure) vs. log (Volume) diagrams: (9A and 9B) Case #40, ϕ = .97, methanol

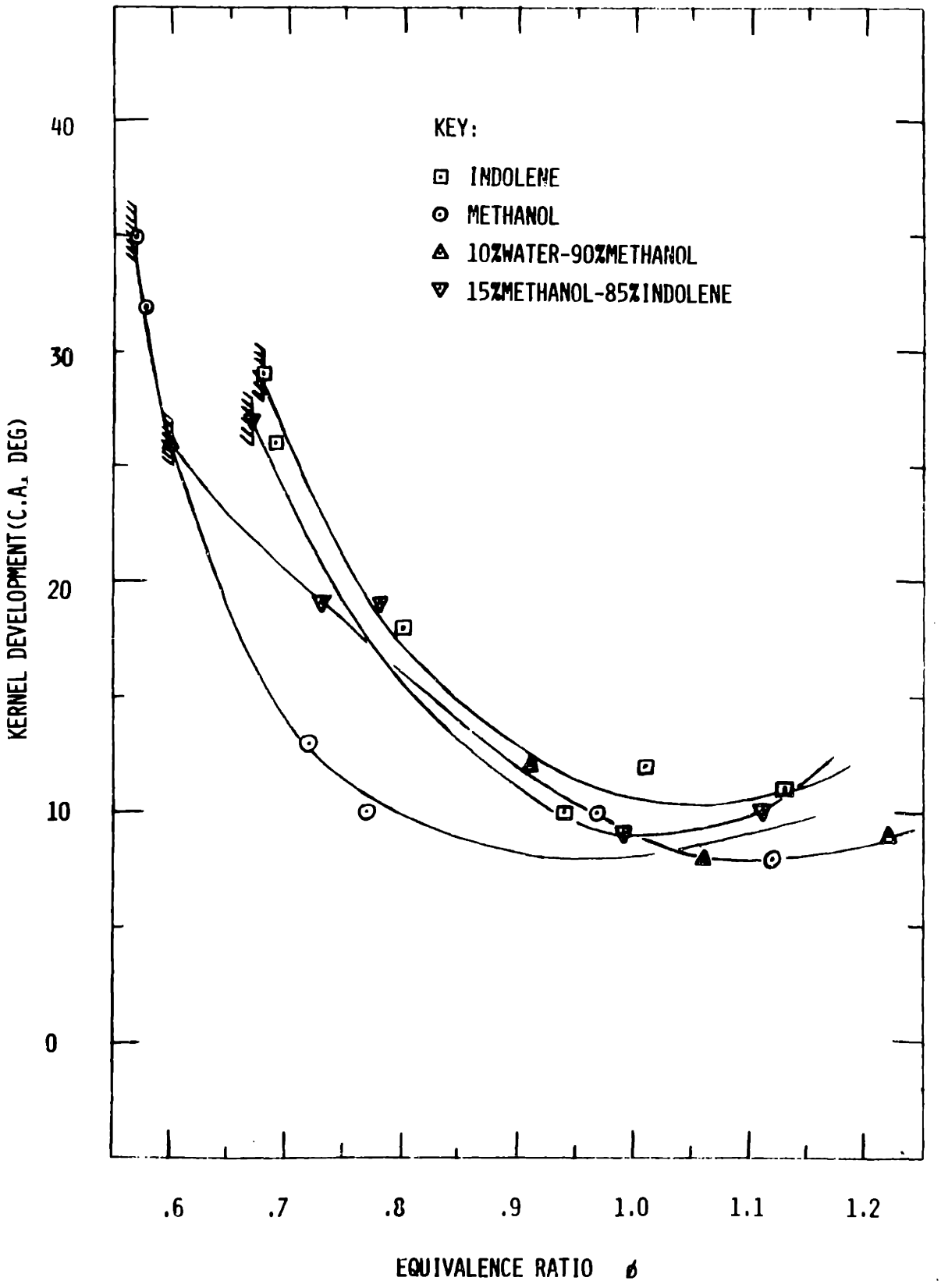

Figure 10 Kernel development interval (θ_k) vs. equivalence ratio (ø) and fuel type at baseline conditions (Table 4)

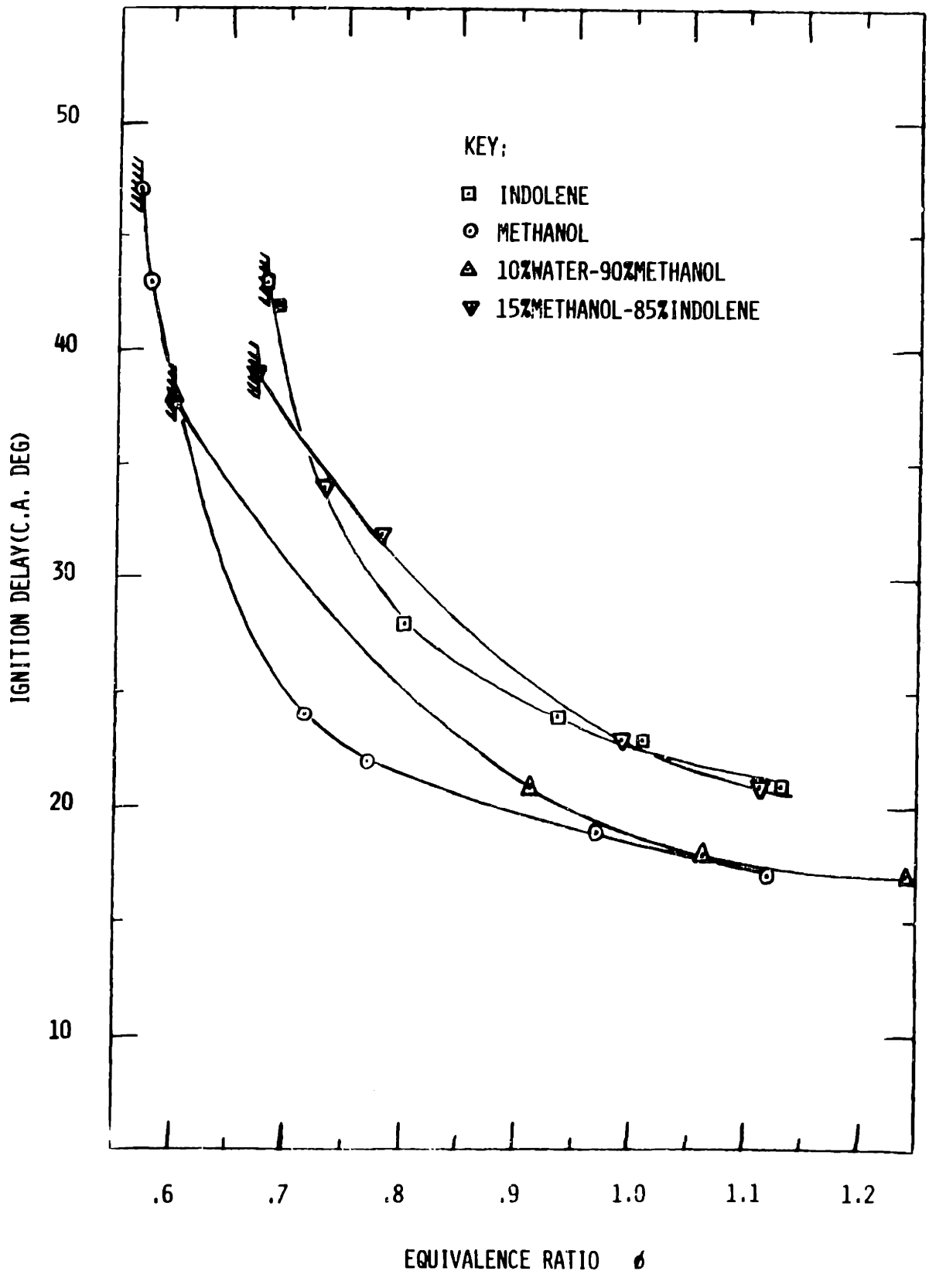

Figure 11 Ignition delay interval (θ_I) vs. equivalence ratio (ϕ) and fuel type at baseline conditions (Table 4)

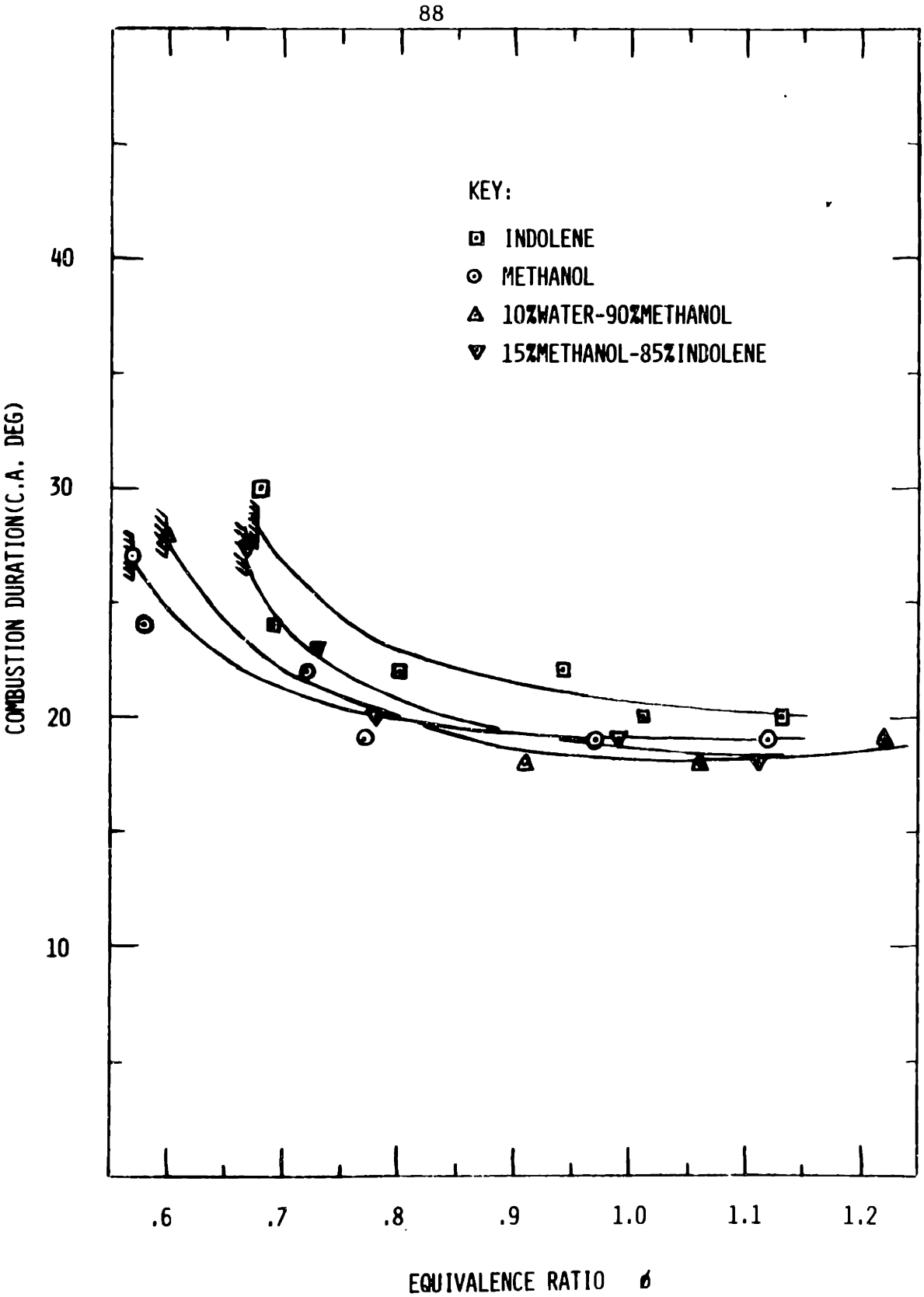

Figure 12 Combustion duration interval (Θ_c) vs. equivalence ratio (ϕ) and fuel type at baseline conditions (Table 4)

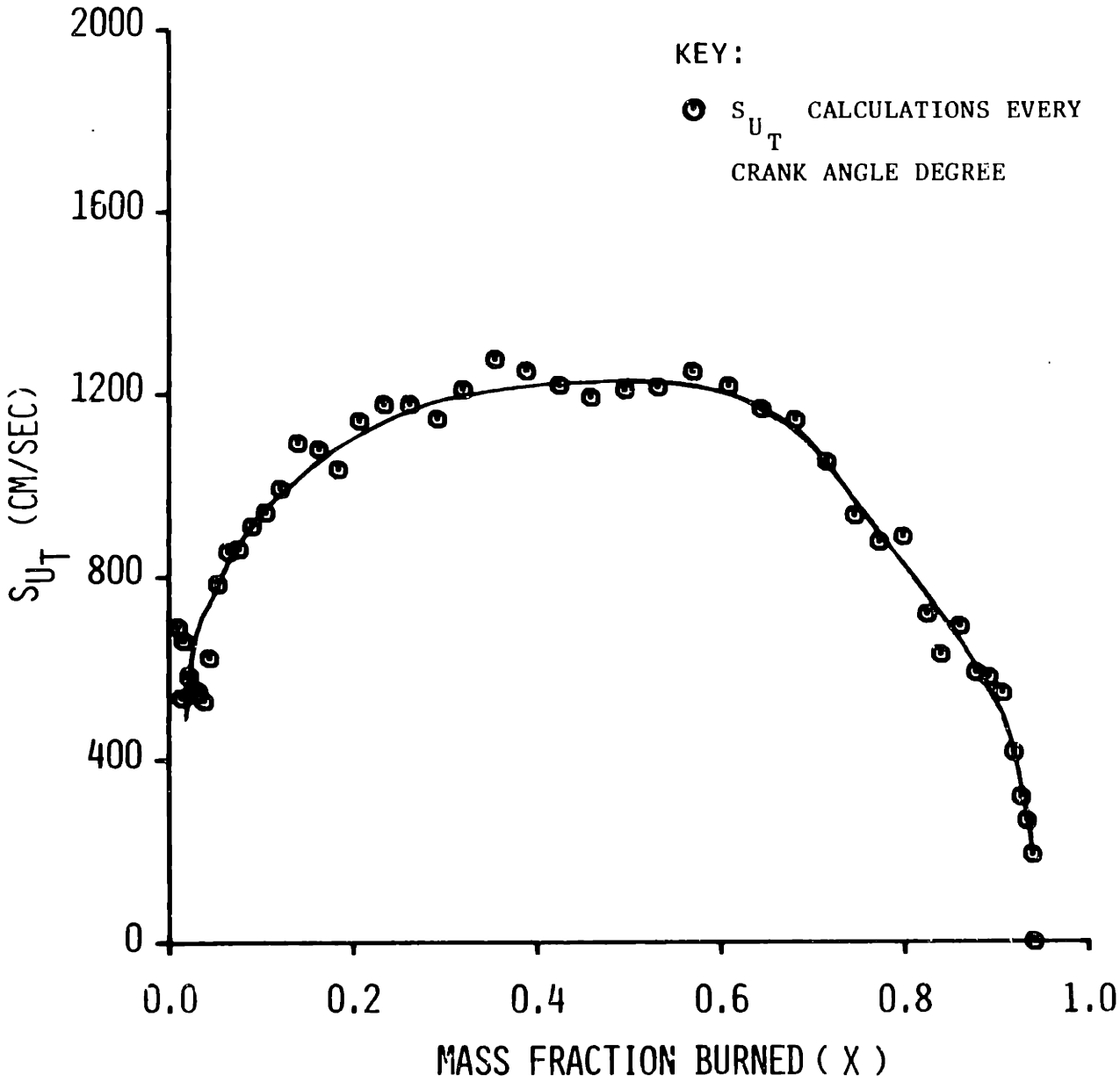

Figure 13 Turbulent flame speed (S_{u_T}) vs. mass fraction burned (x) for case # 35, methanol, ϕ = .57, methanol, lean limit, baseline conditions

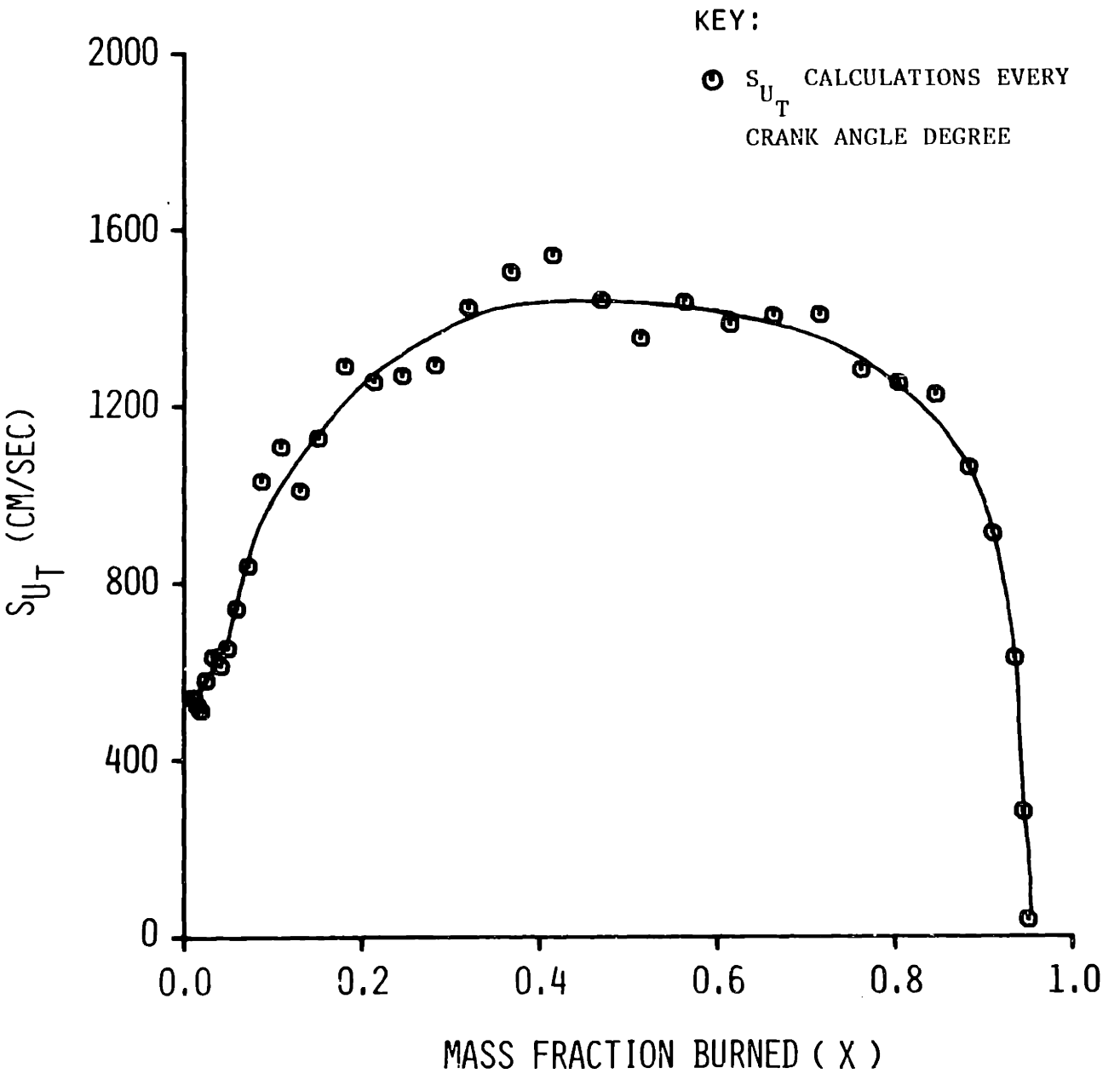

Figure 14 Turbulent flame speed (S_{u_T}) vs. mass fraction burned (x) for case # 40, Ø = .97, methanol, baseline conditions

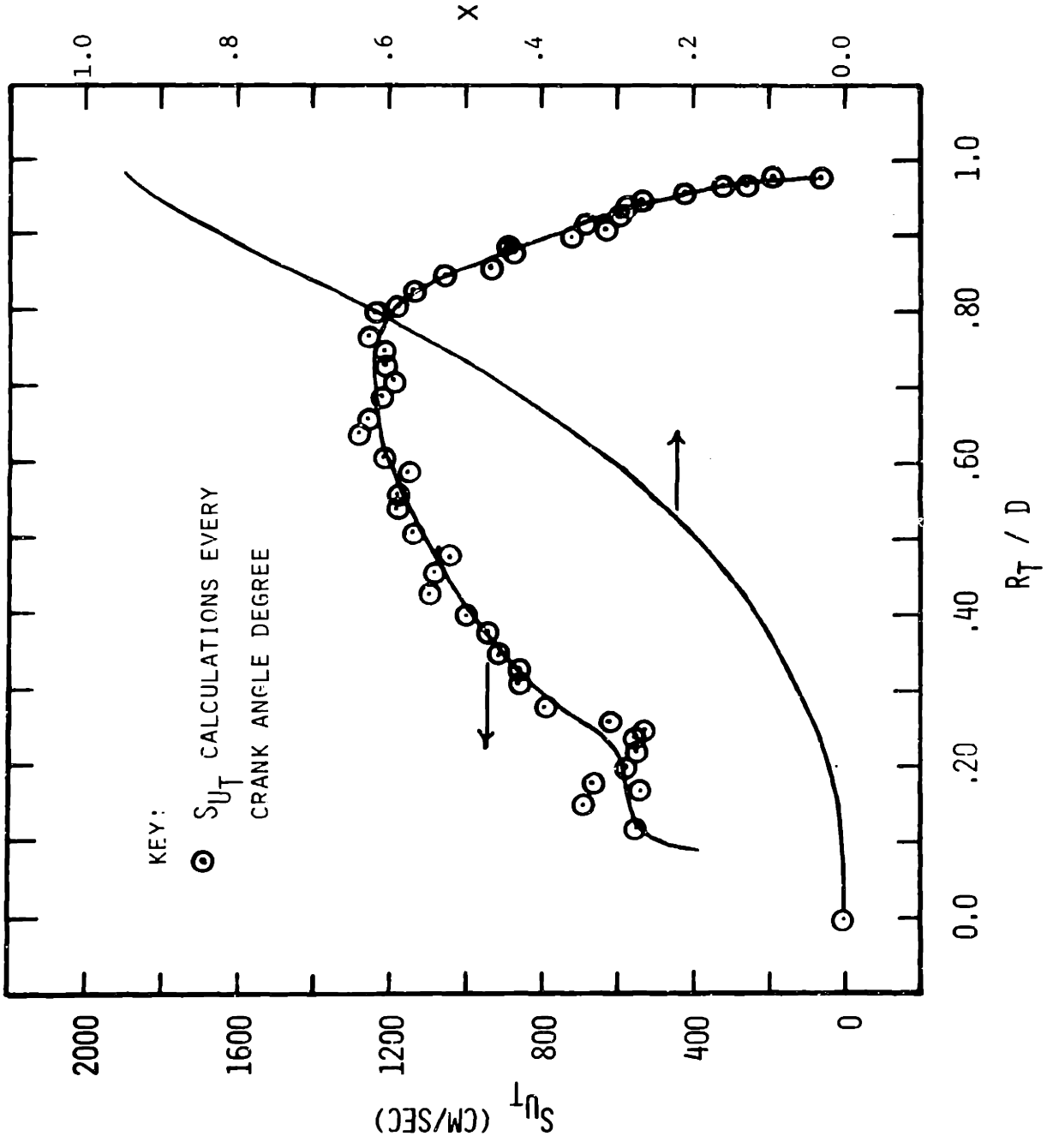

Figure 15 Turbulent flame speed (S_{u_T}) and mass fraction burned (x) vs. normalized flame radius (R_T/D) for case # 35, ϕ = .57, methanol, lean limit, baseline conditions

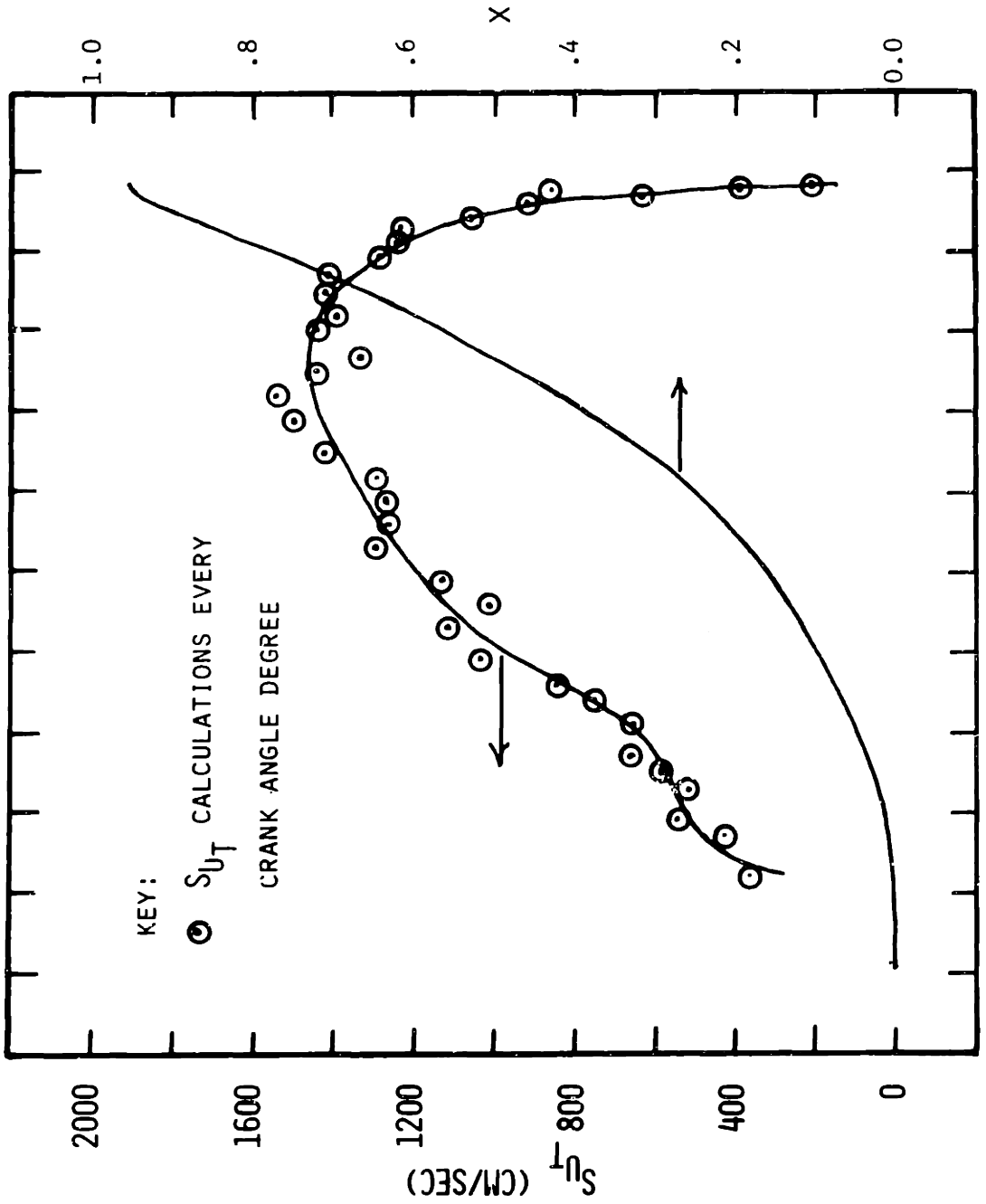

Figure 16 Turbulent flame speed (S_{u_T}) and mass fraction burned (x) vs. normalized flame radius (R_T/D) for case # 40, ϕ = .97, methanol, baseline conditions

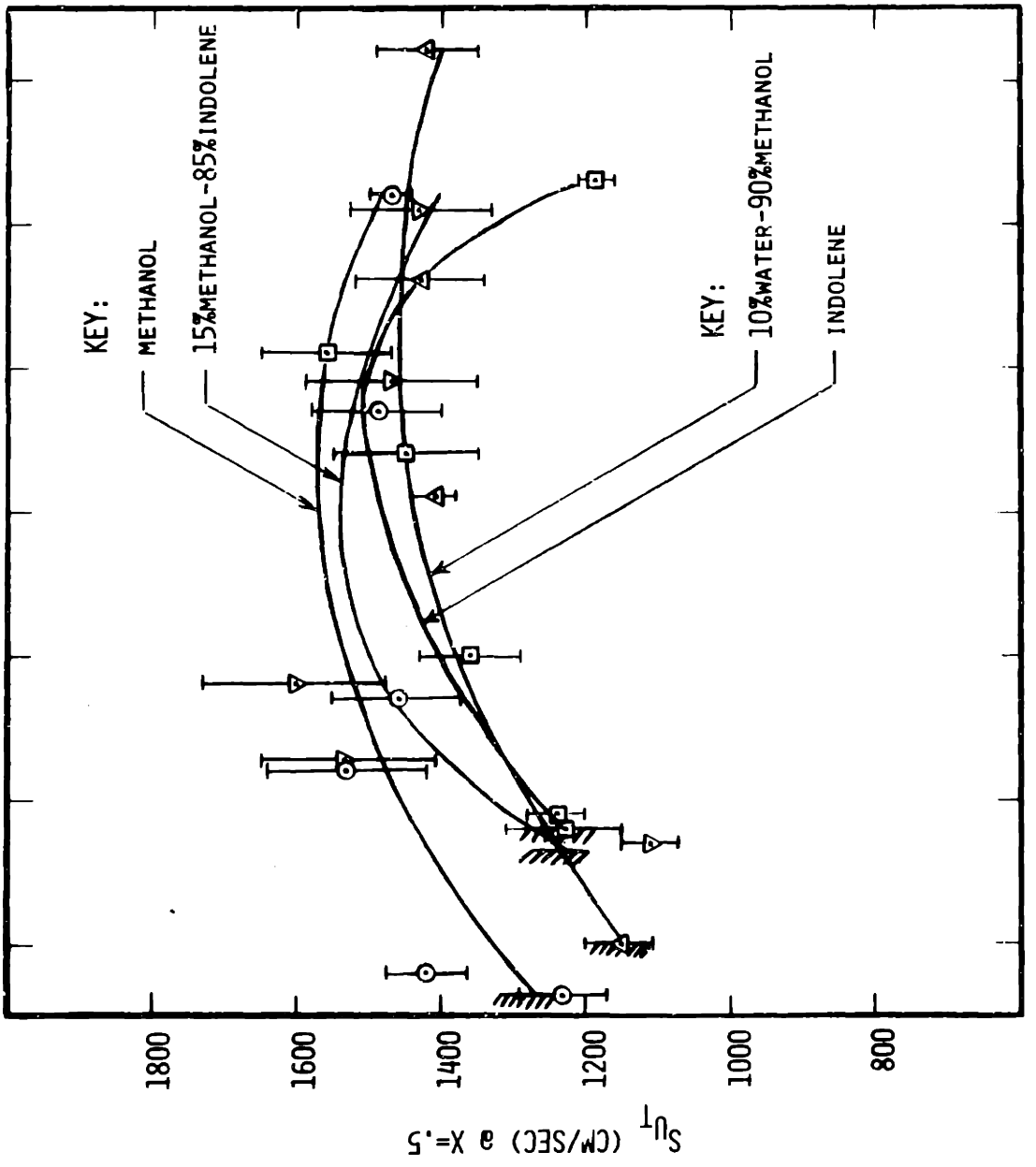

Figure 17 Turbulent flame speed (S_{u_T}) at x = .5 vs. equivalence ratio (ϕ) and fuel type at baseline conditions (Table 4)

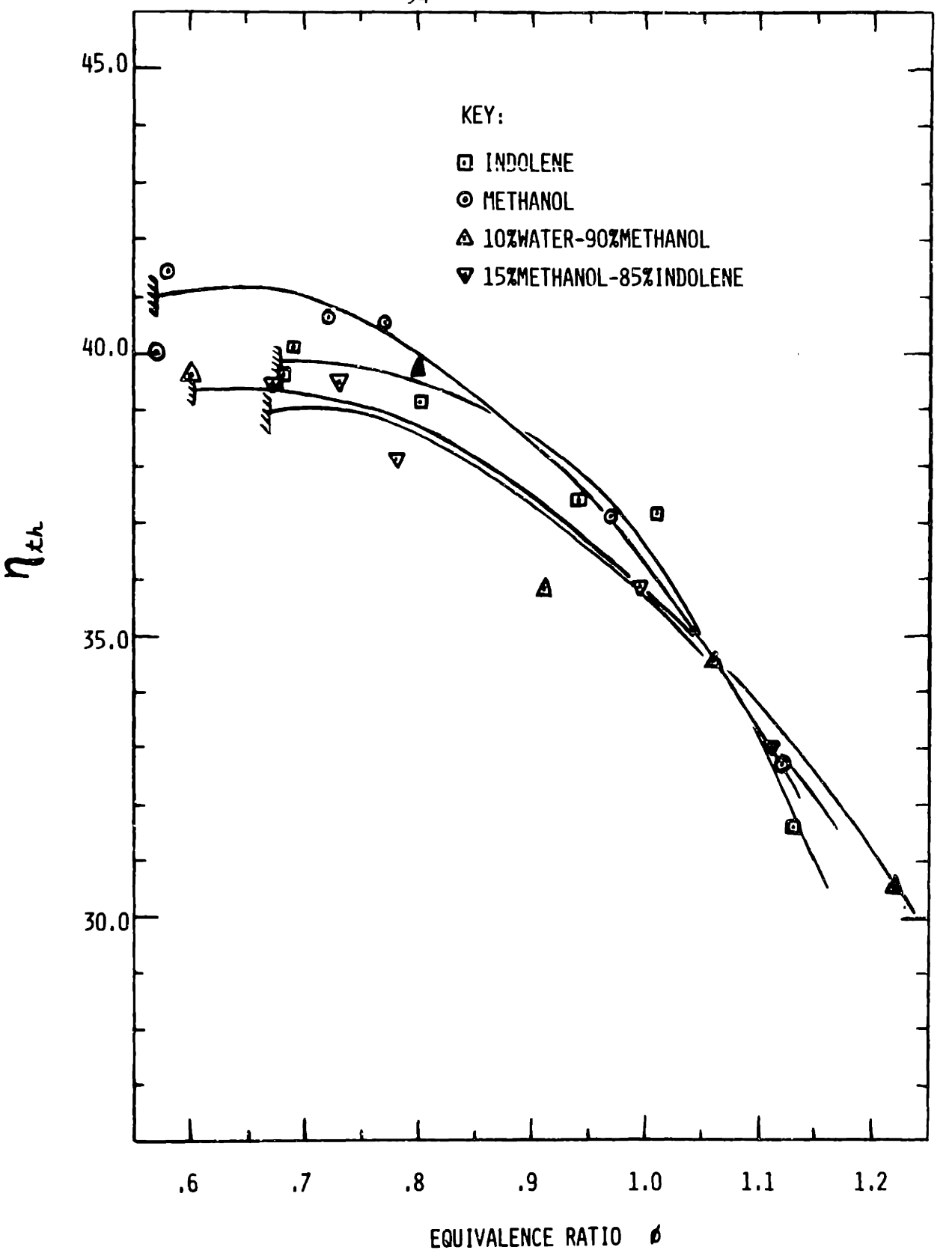

Figure 18 Variation of indicated thermal efficiency (η_{th}) with equivalence ratio (ø) and fuel type at baseline conditions (Table 4)

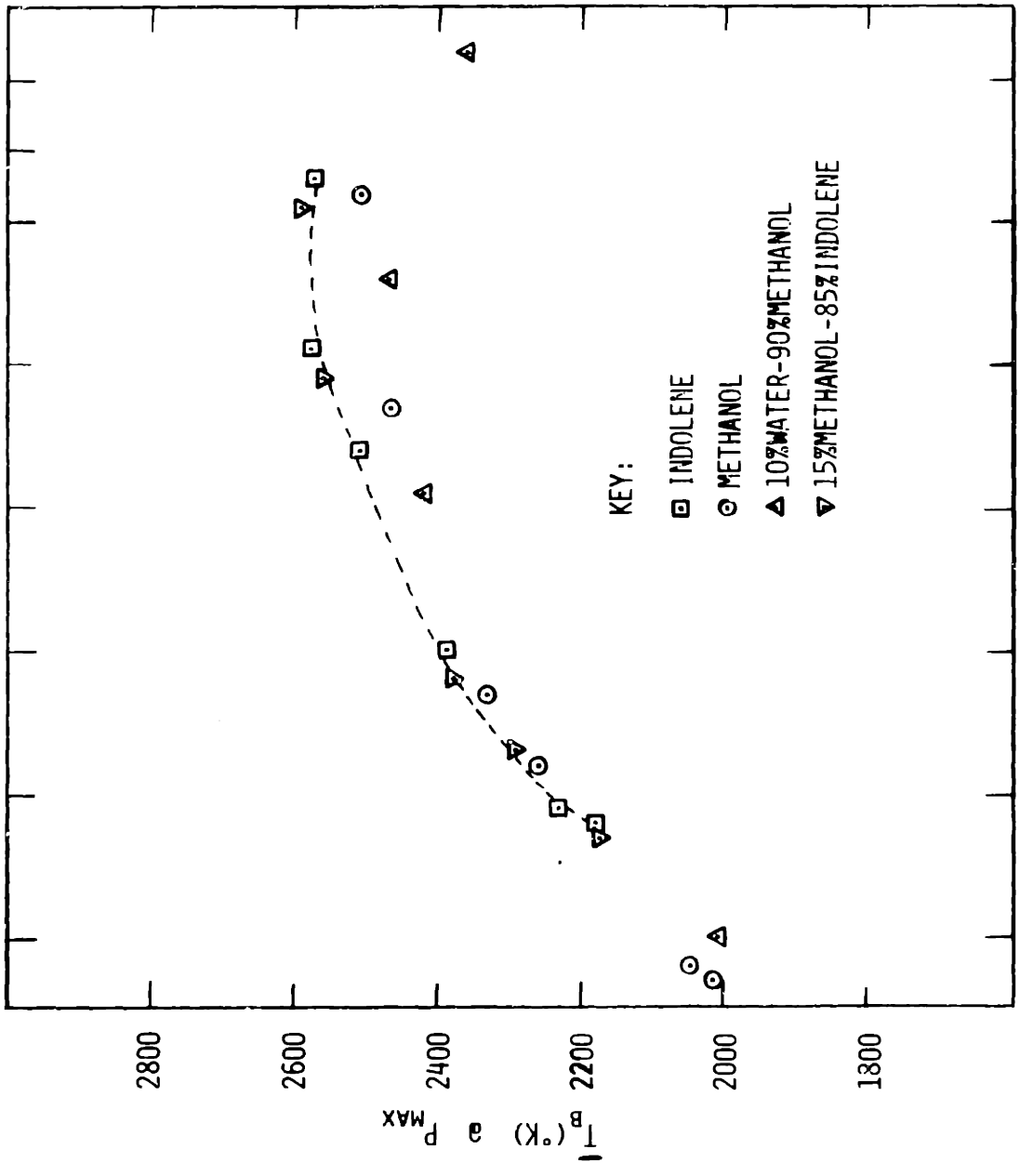

Figure 19 Average burned gas temperature ($\bar{T}_b$) at peak pressure vs. equivalence ratio (ϕ) and fuel type at baseline conditions (Table 4)

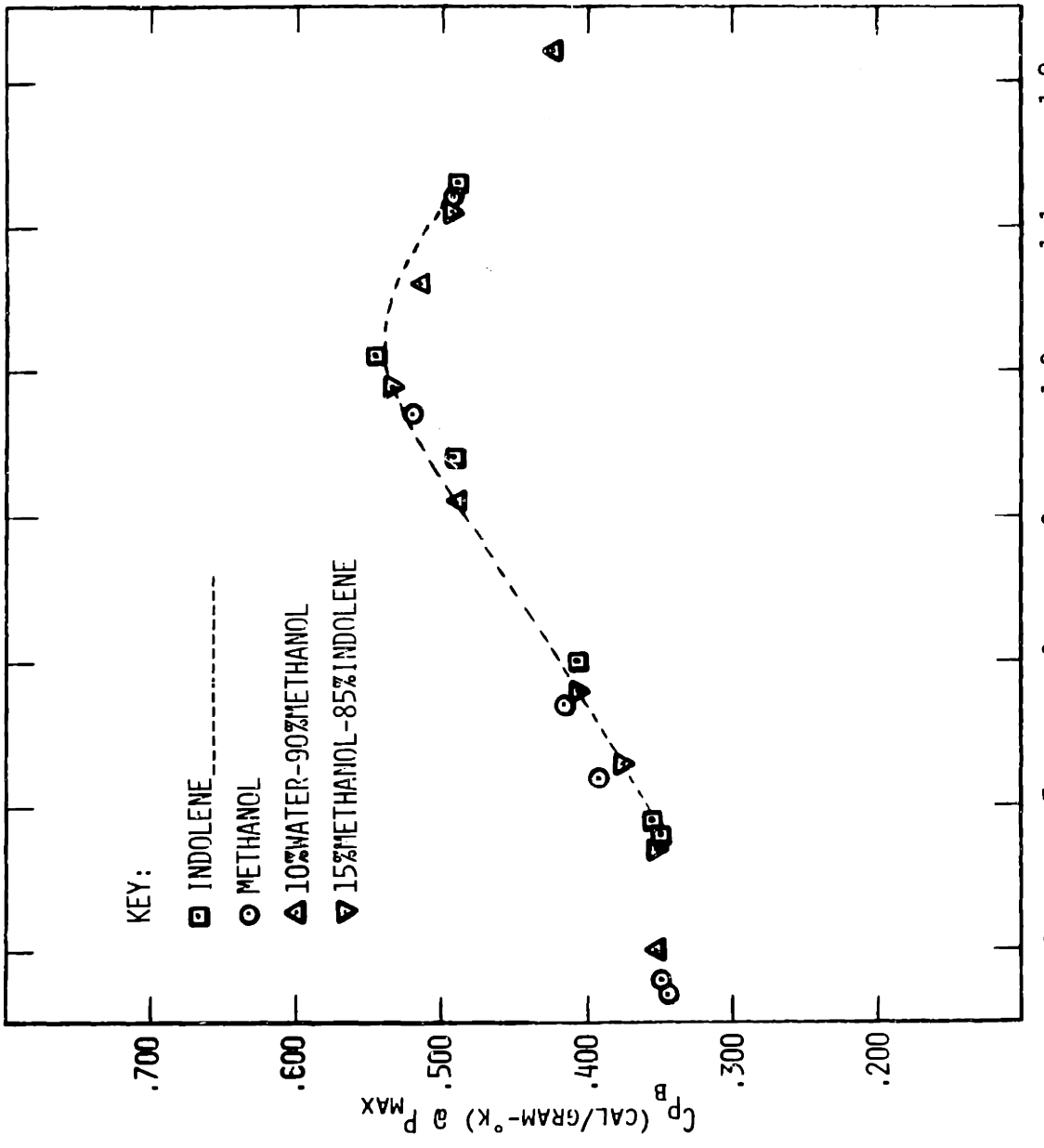

Figure 20 Specific heat at constant pressure of burned gases (C_{p_b}) at peak pressure vs equivalence ratio (ϕ) and fuel type at baseline conditions (Table 4)

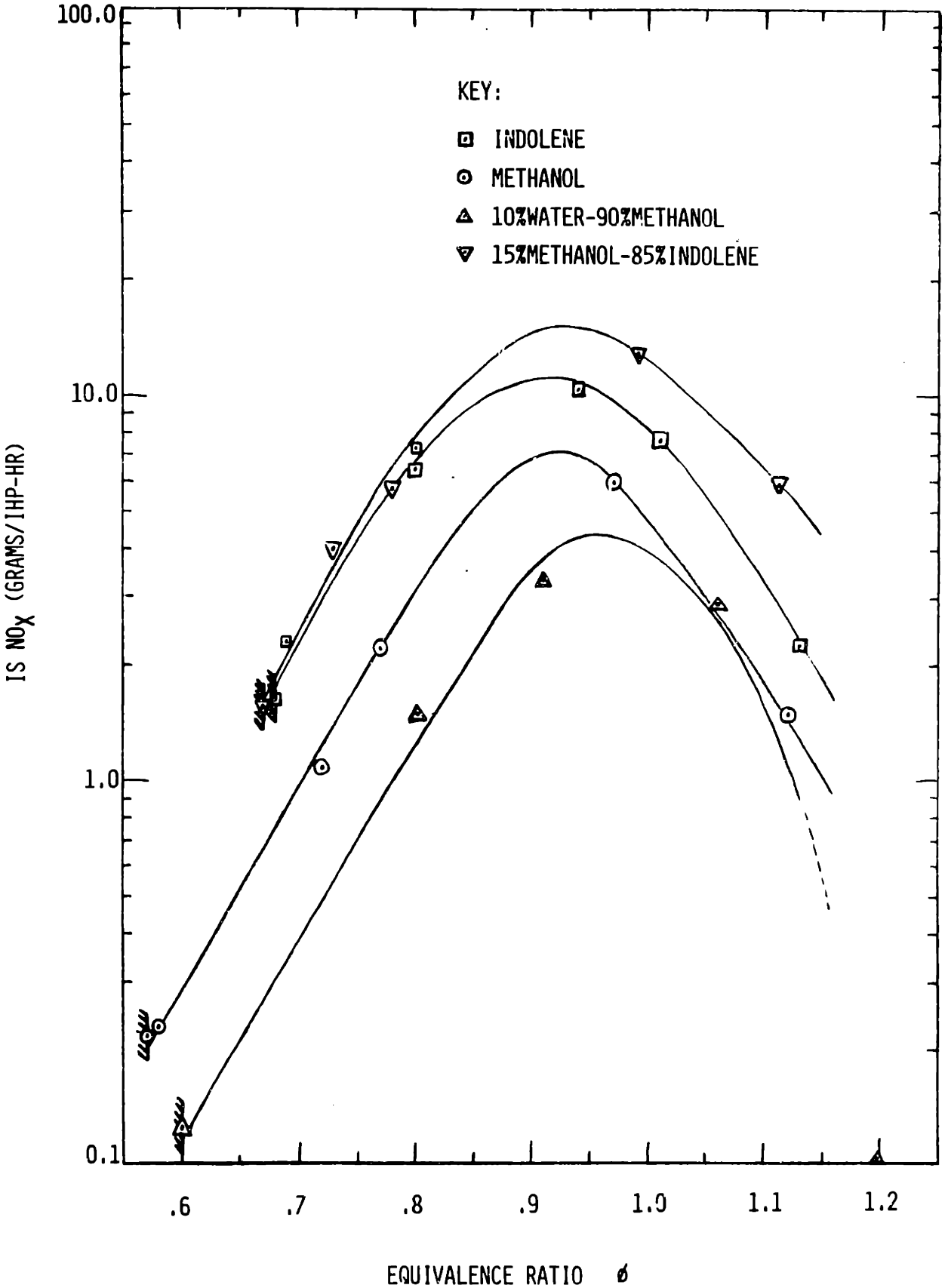

Figure 21 Indicated specific nitroc oxide (IS NO_x) vs. equivalence ratio (Ø) and fuel type at baseline conditions (Table 4)

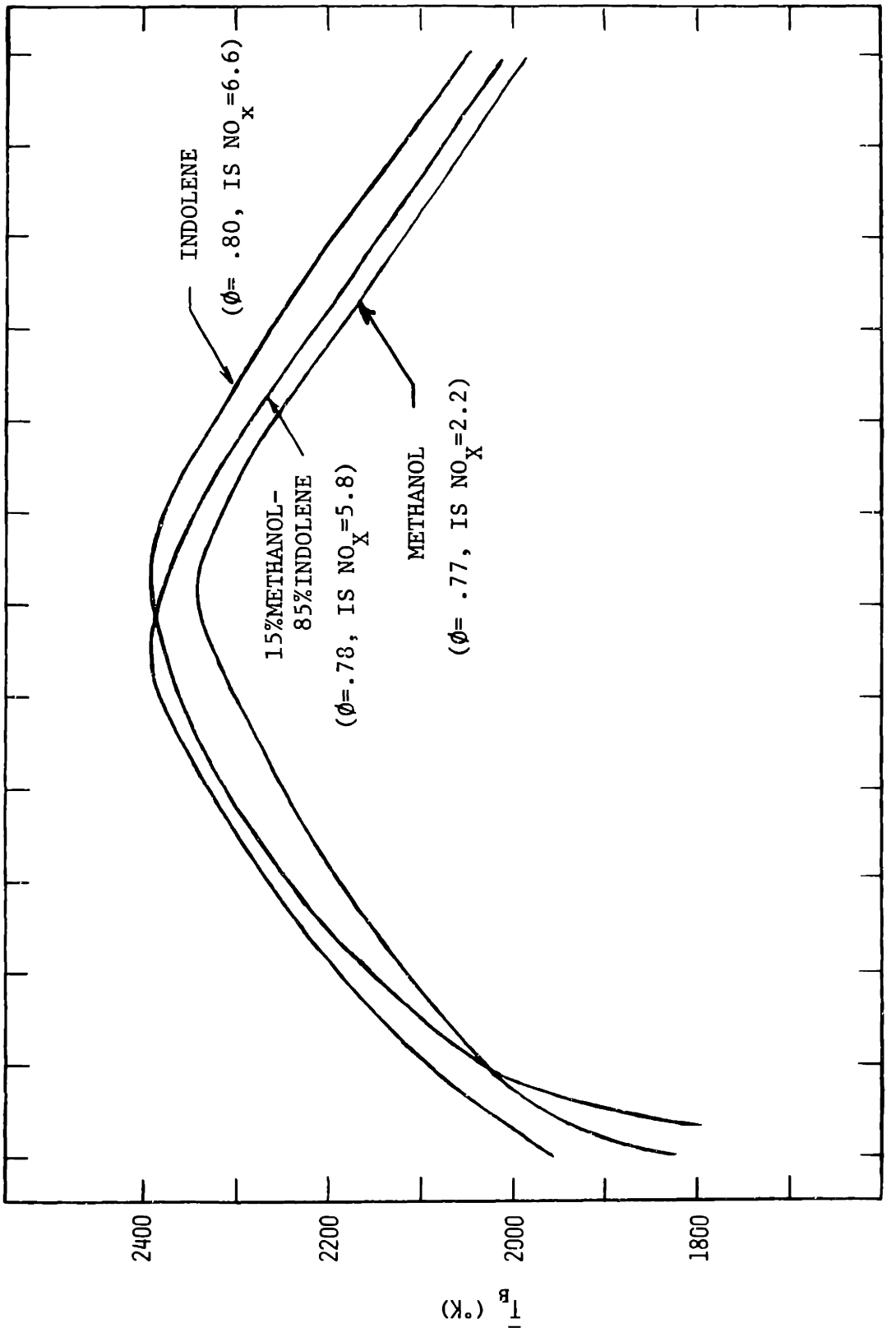

Figure 22 Average burned gas temperature ($\bar{T}_b$) vs. crank angle (θ) histories for varying fuel type at lean base - ^{b}line conditions

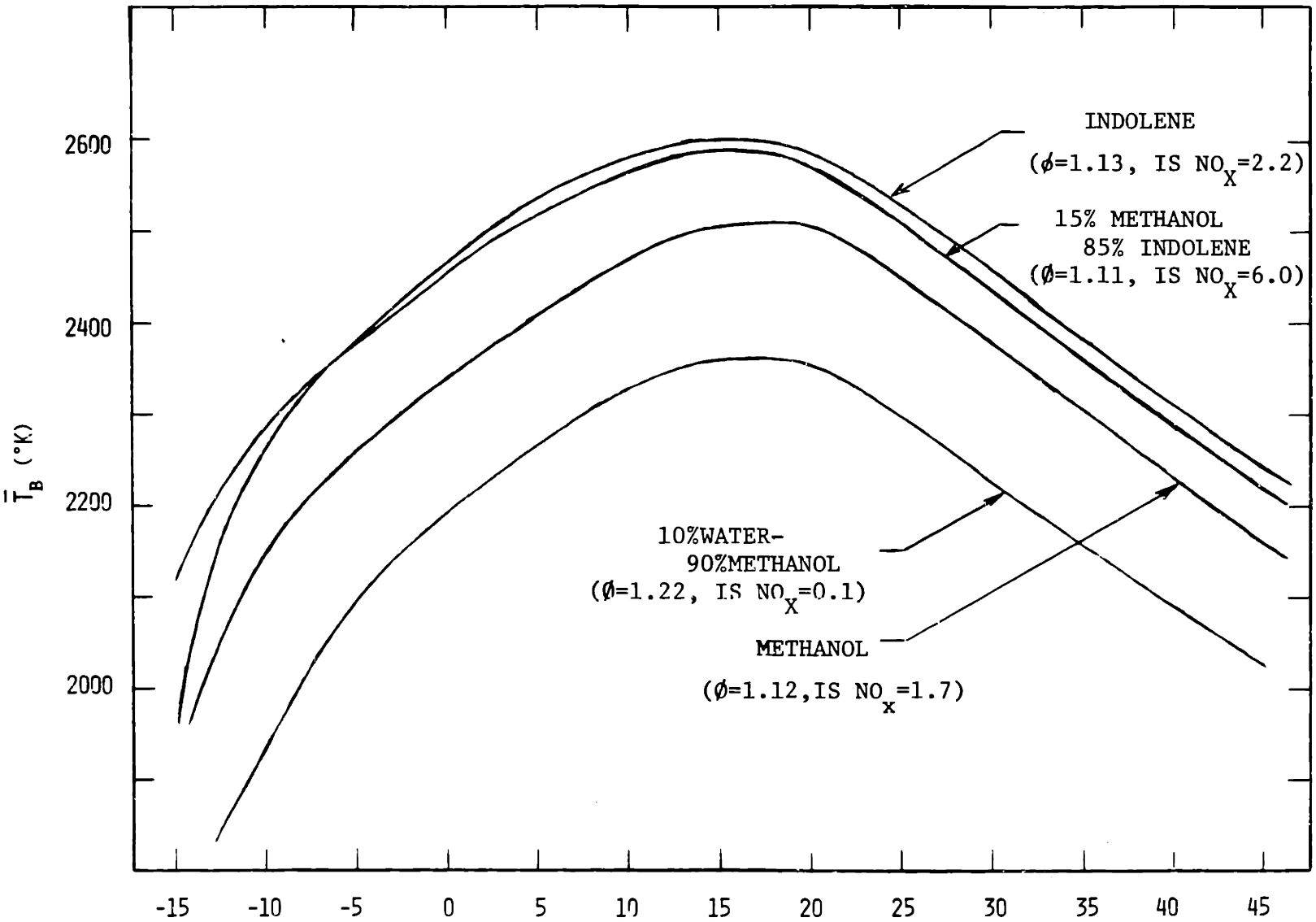

Figure 23 Average burned gas temperature ($\bar{T}_b$) vs. crank angle (Θ) histories for varying fuel type at rich base - line conditions

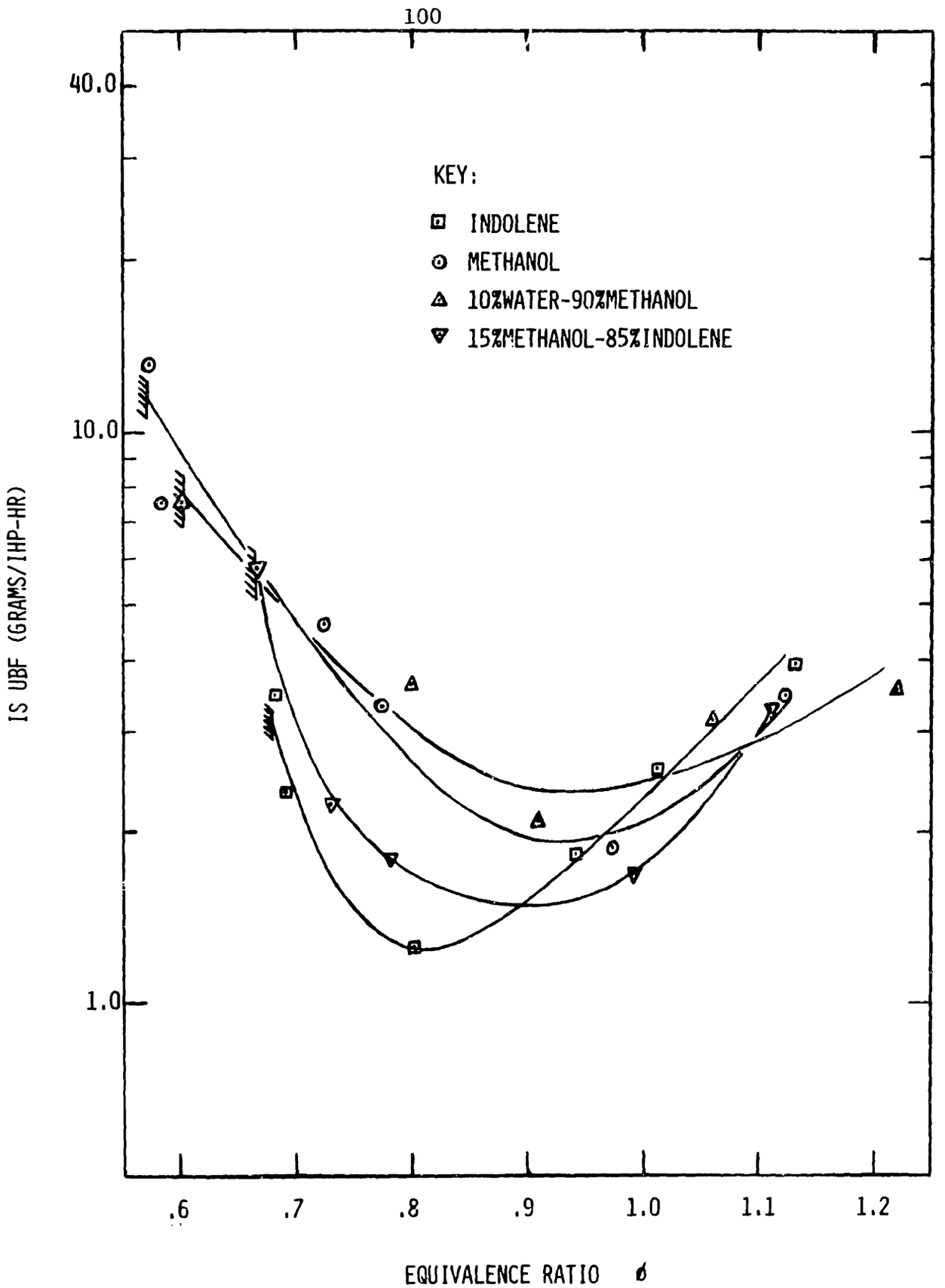

Figure 24 Indicated specific unburned fuel emissions (IS UBF) vs. equivalence ratio (ø) and fuel type at baseline conditions (Table 4)

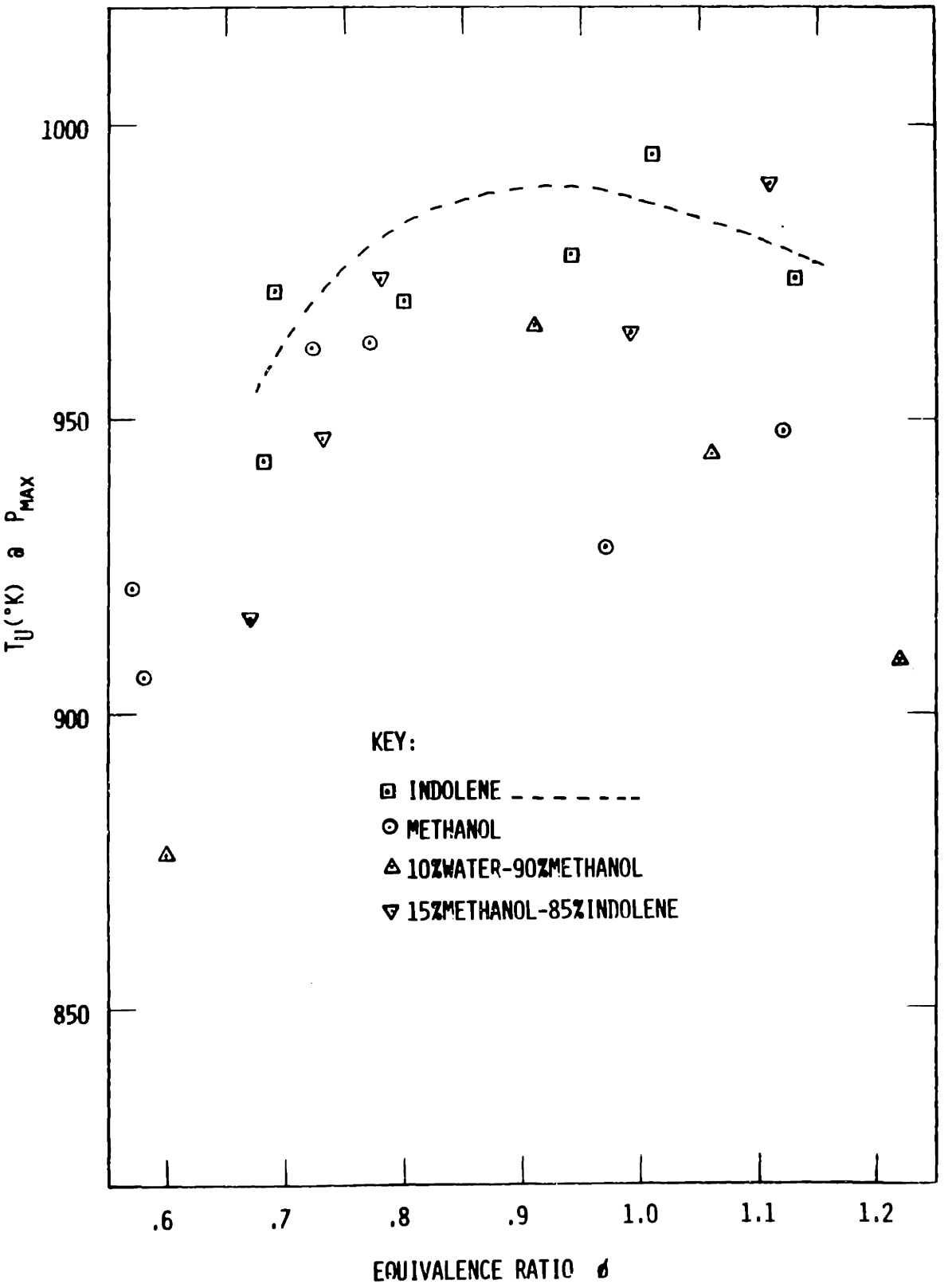

Figure 25 Unburned mixture temperature (T_u) at peak pressure vs. equivalence ratio (ϕ) and fuel type at baseline conditions

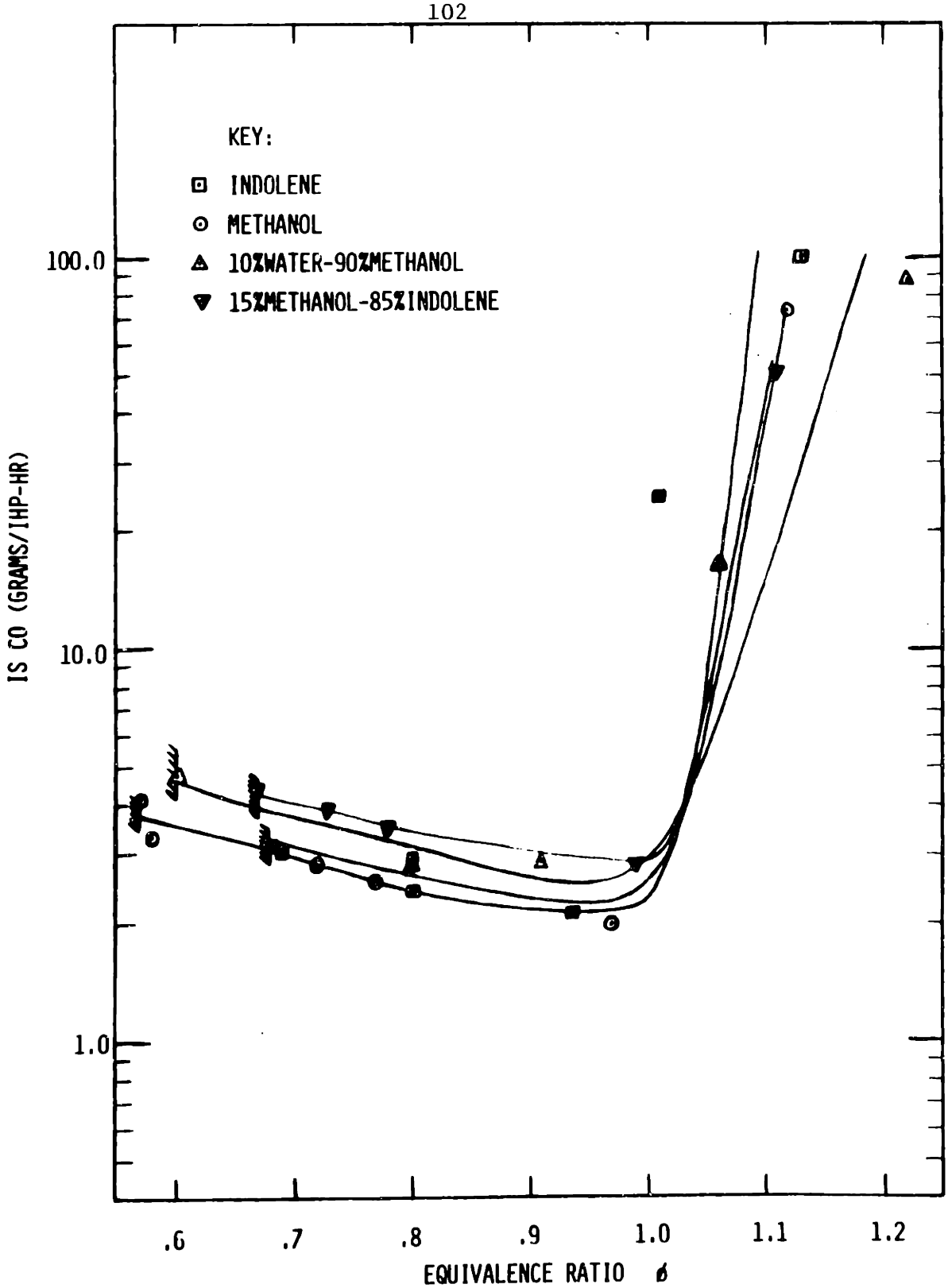

Figure 26 Indicated specific carbon monoxide emissions (IS CO) vs. equivalence ratio (ϕ) and fuel type at baseline conditions

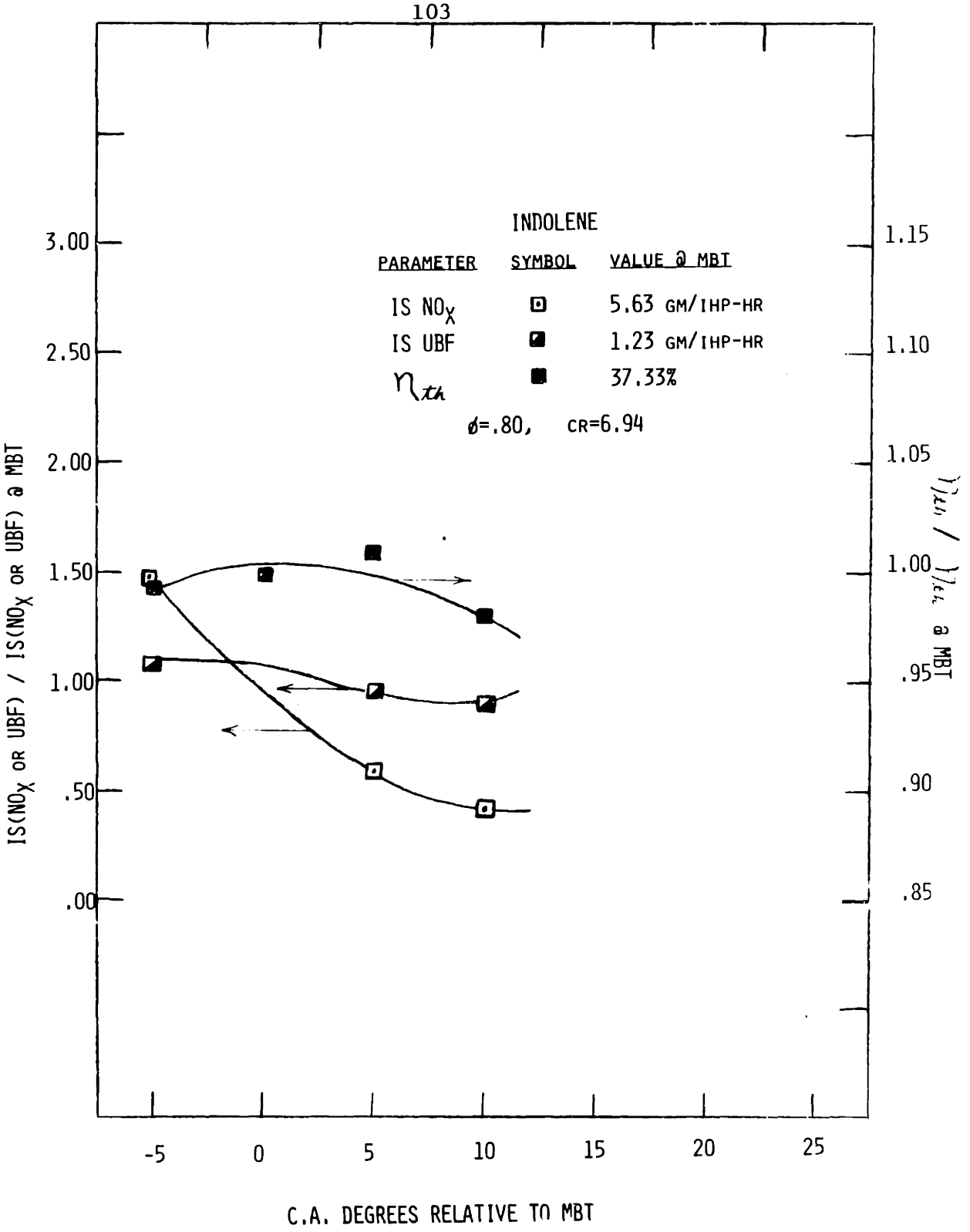

Figure 27 η_{th}, IS NO_x emissions, and IS UBF emissions vs. spark advance relative to MBT for indolene

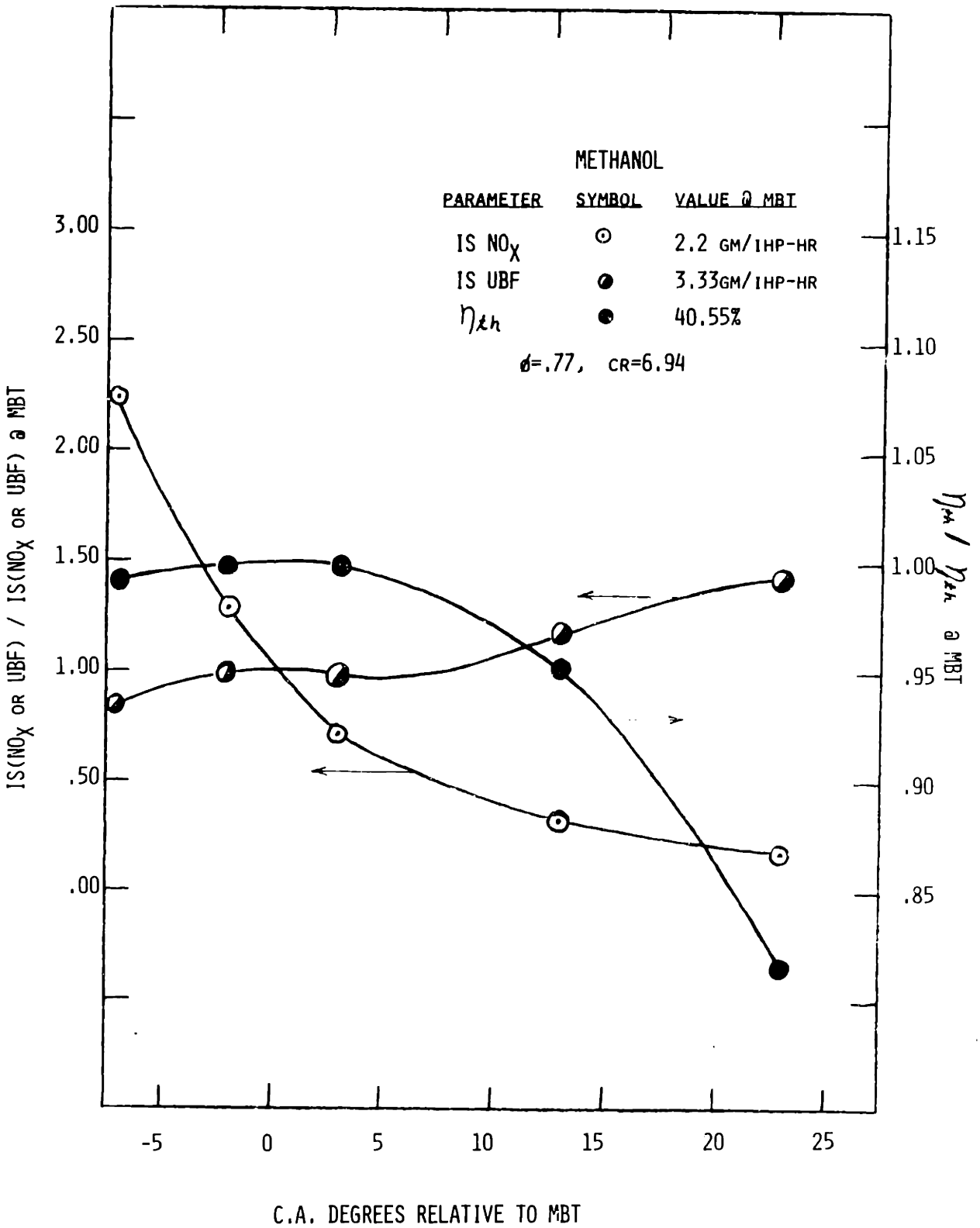

Figure 28 η_{th}, IS NO_x emissions, and IS UBF emissions vs. spark advance relative to MBT for methanol

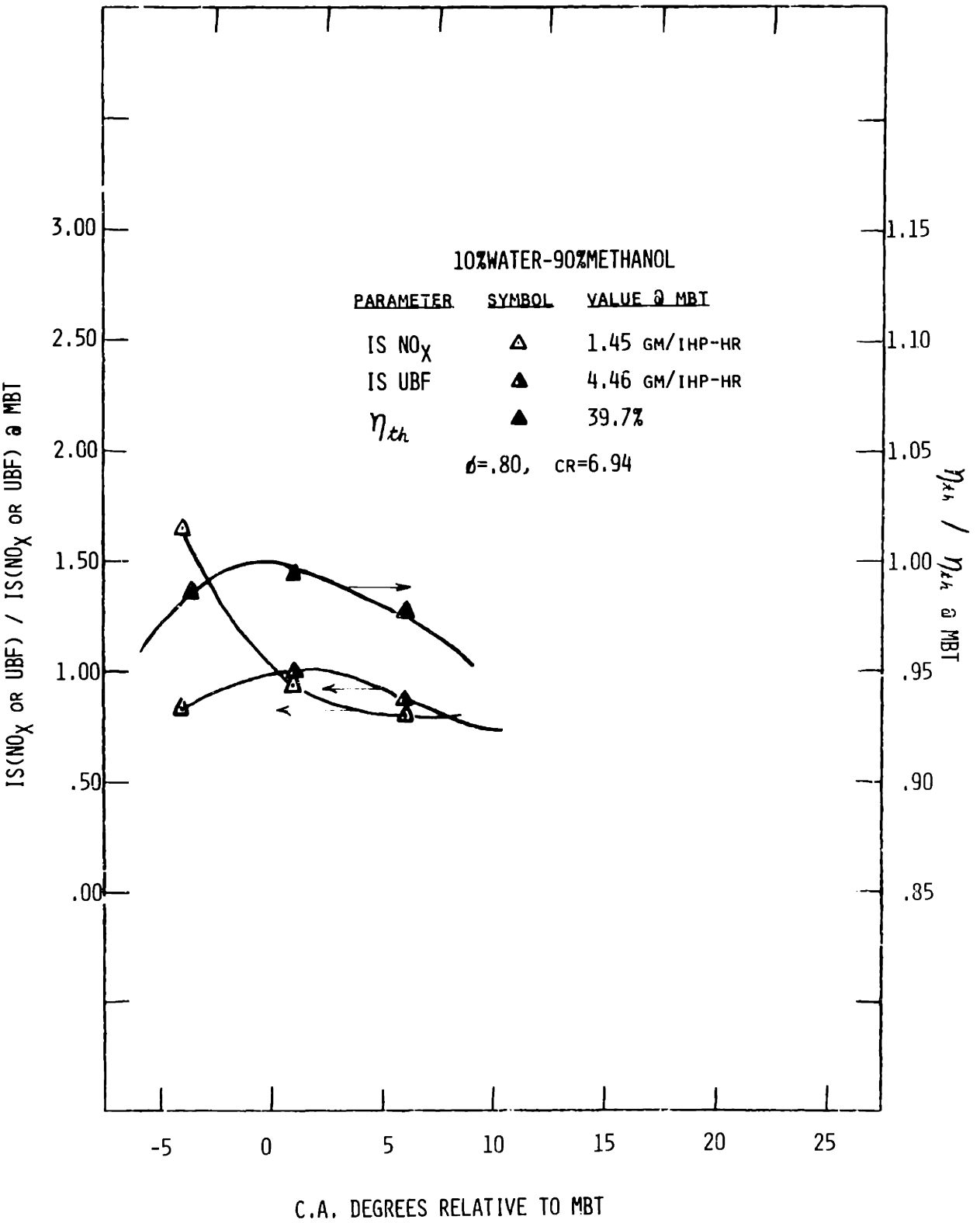

Figure 29 η_{th}, IS NO_x emissions, and IS UBF emissions vs. spark advance relative to MBT for 10% water-90% methanol

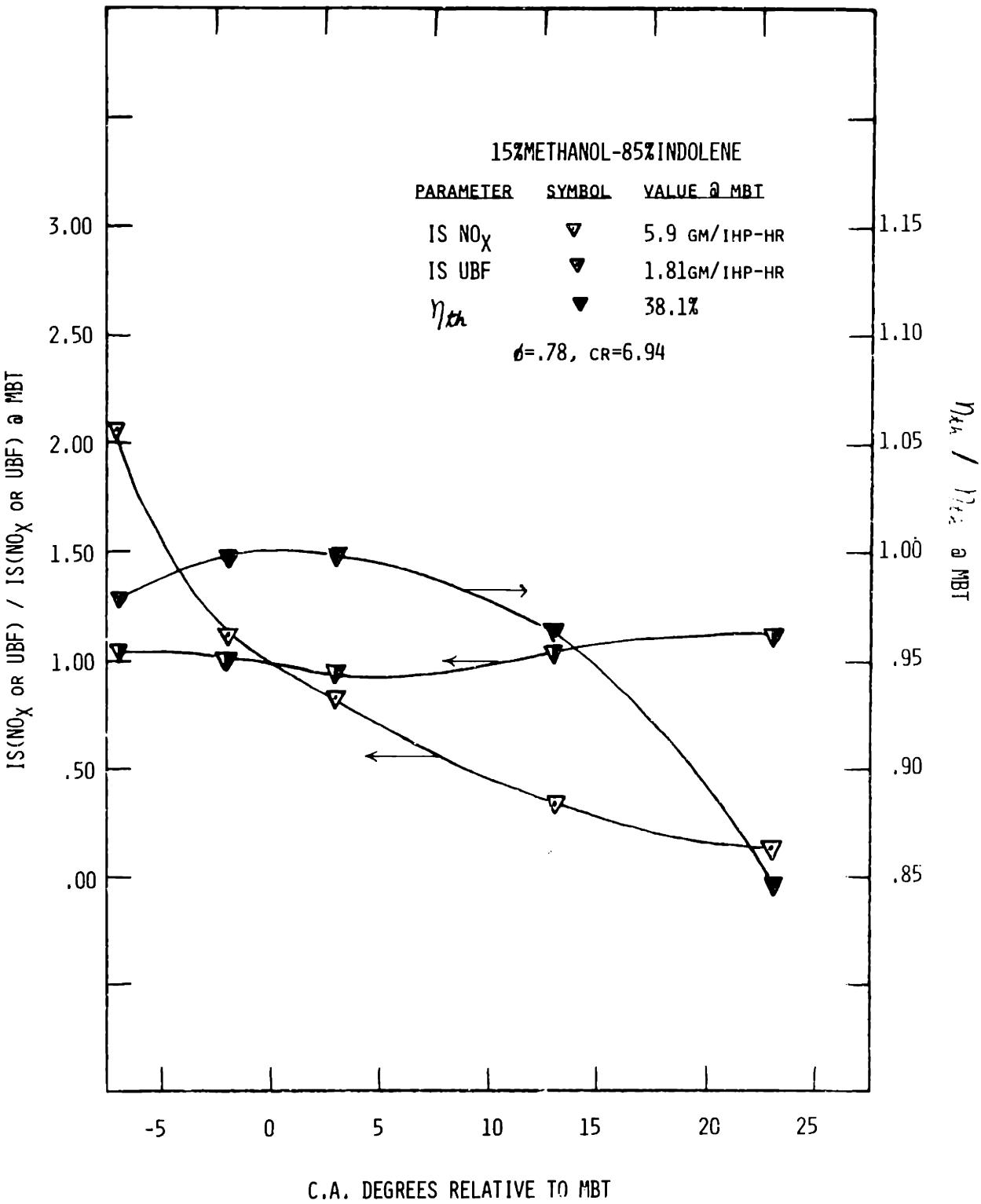

Figure 30 η_{th}, IS NO_x emissions, and IS UBF emissions vs. spark advance relative to MBT for 15% methanol-85% indolene

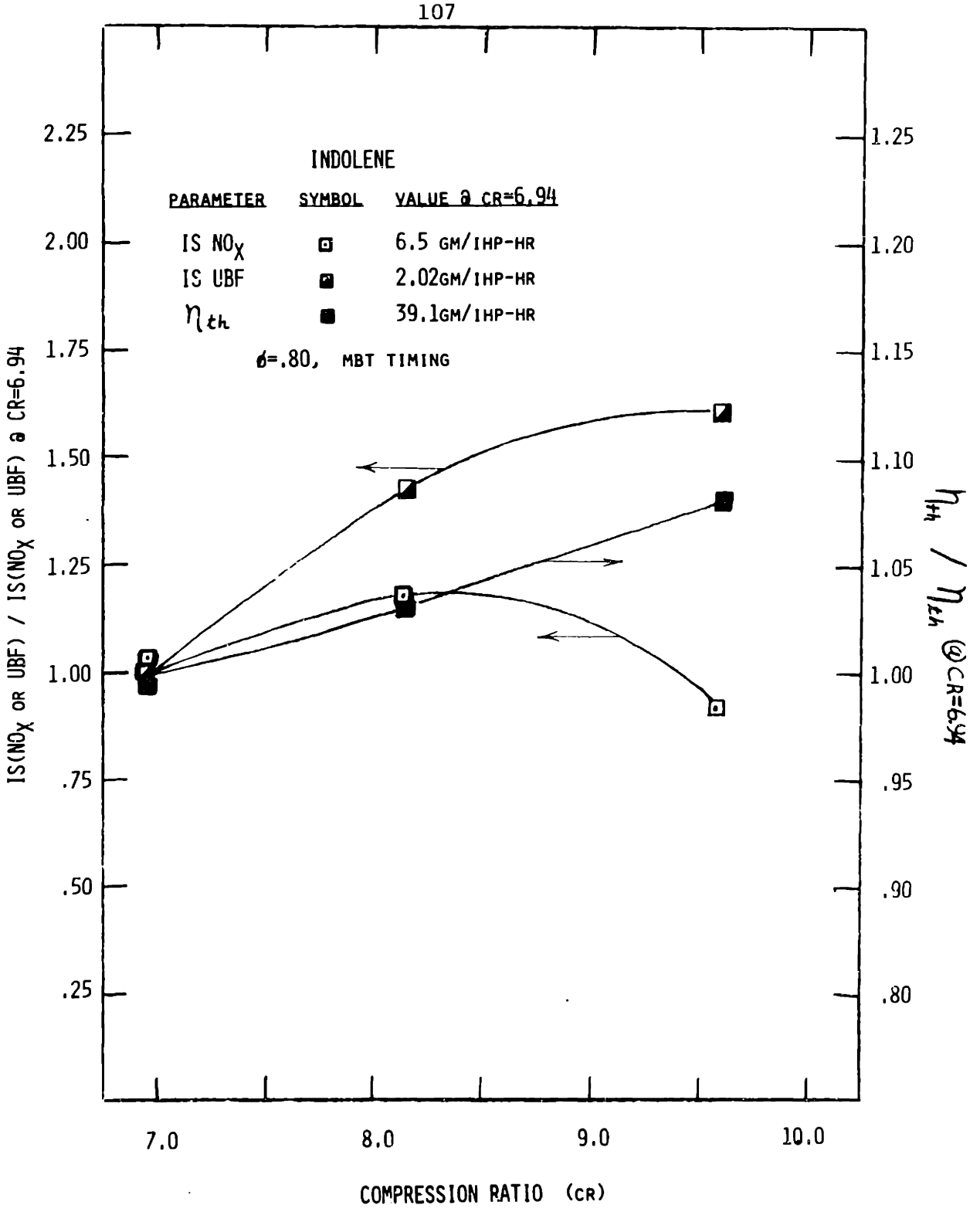

Figure 31 η_{th}, IS NO_x emissions, and IS UBF emissions vs. compression ratio (C.R.) for indolene

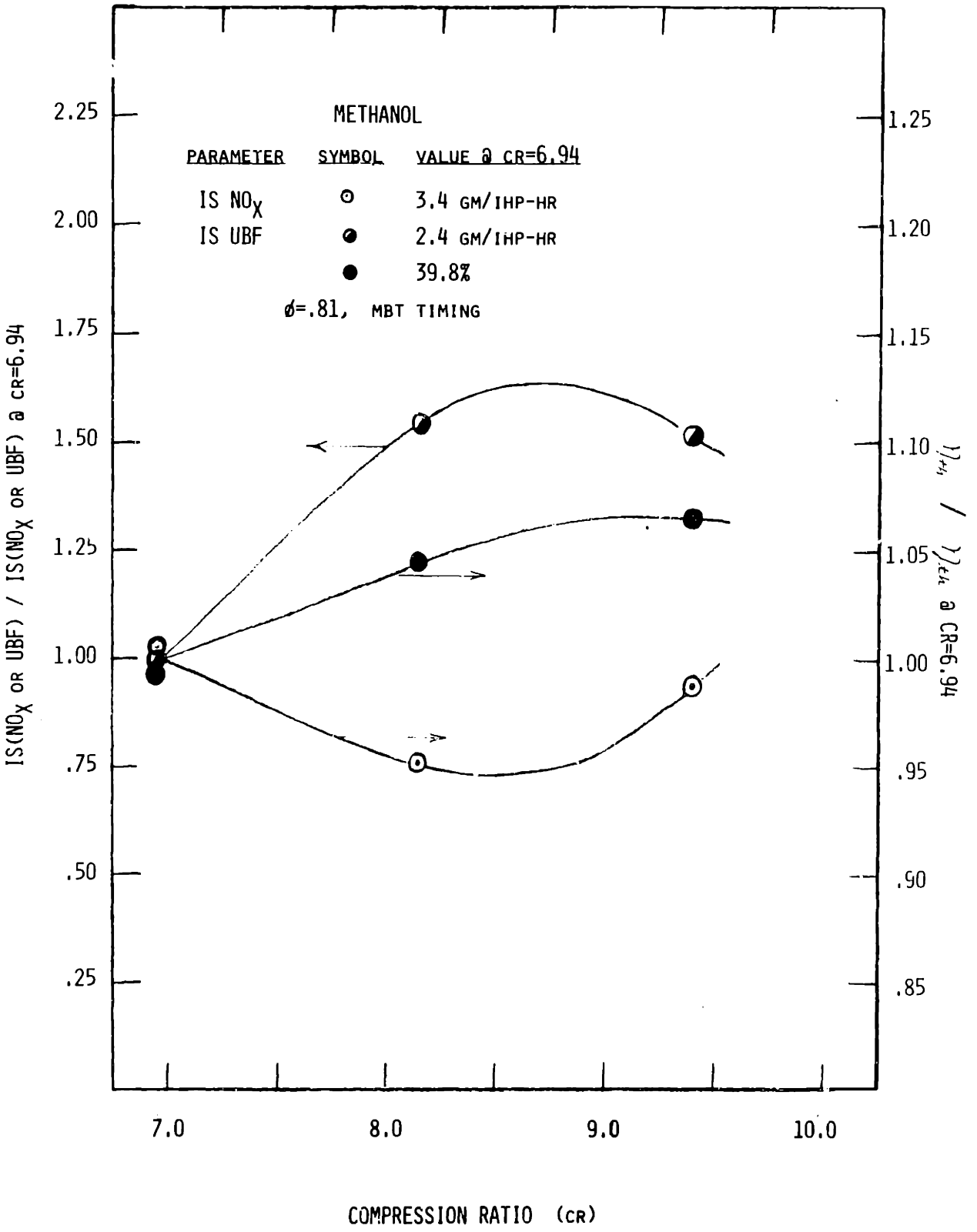

Figure 32 η_{th}, IS NO_x emissions, and IS UBF emissions vs. compression ratio (C.R.) for methanol

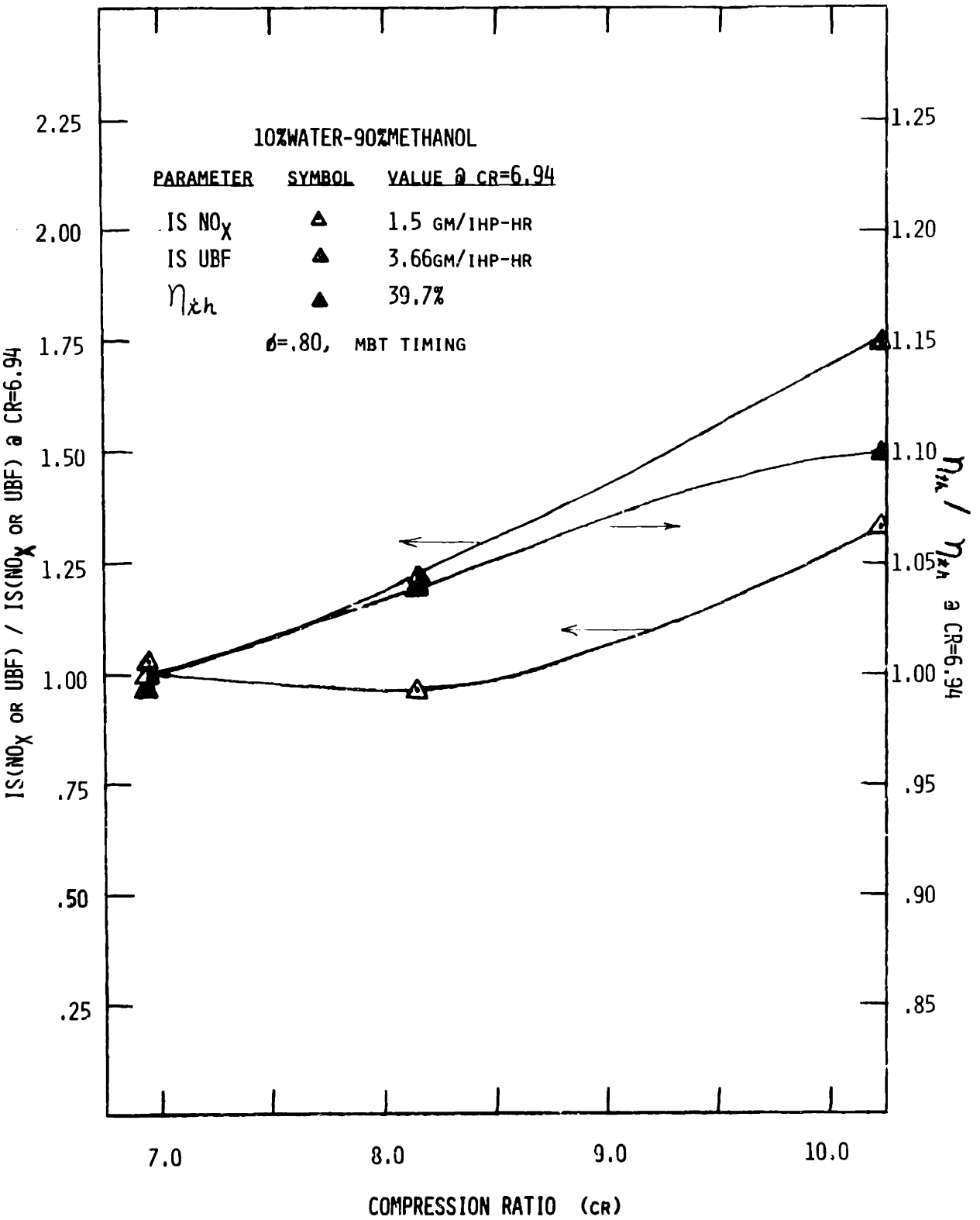

Figure 33 η_{th}, IS NO_x emissions, and IS UBF emissions vs. compression ratio (C.R.) for 10% water-90% methanol

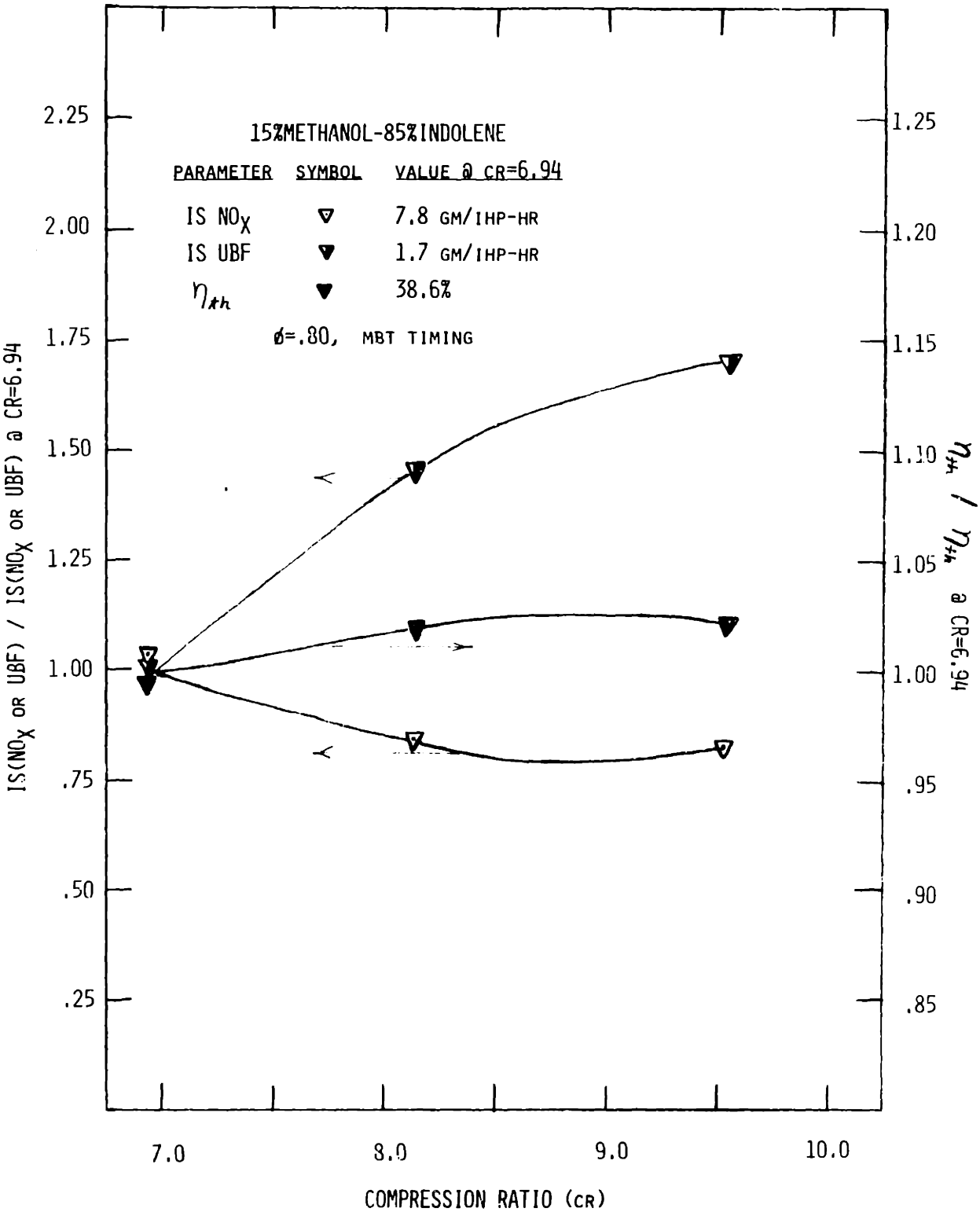

Figure 34 η_{th} IS NO_x emissions, and IS UBF emissions vs. compression ratio (C.R.) for 15% methanol-85% indolene

Figure 35A

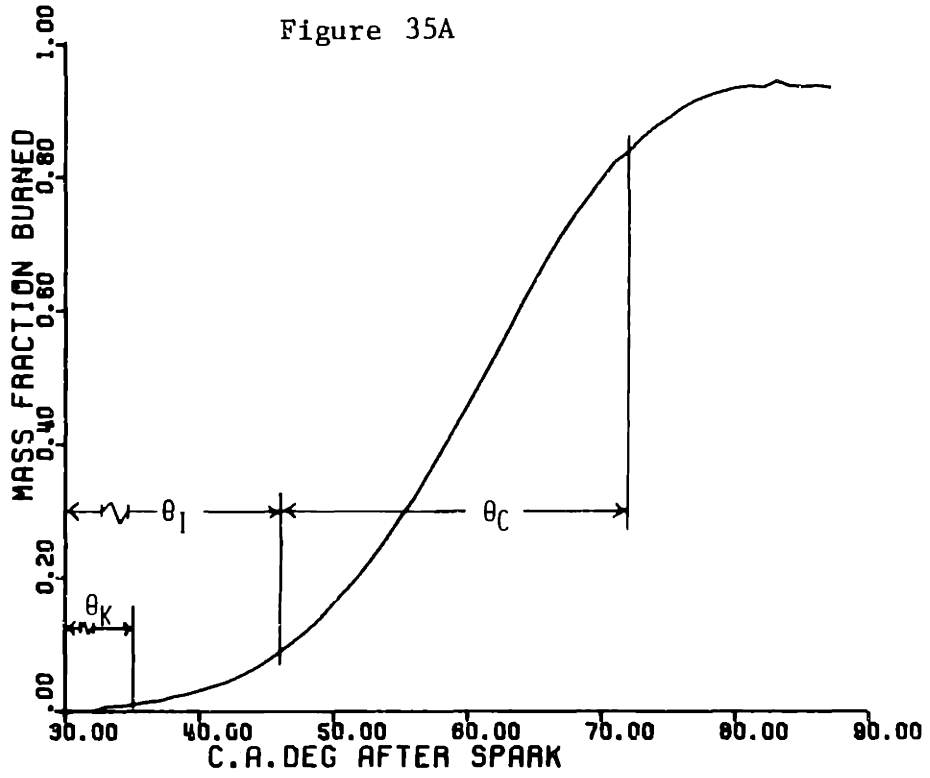

Figure 35B

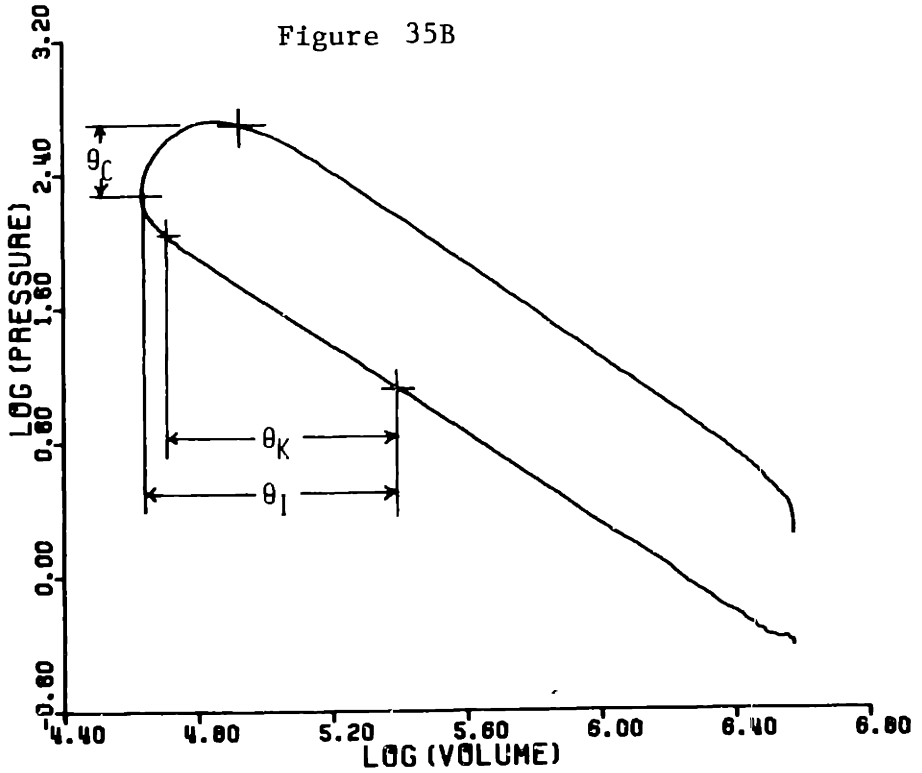

Figure 35 Definition of kernel development (θ_k), ignition delay (θ_I), and combustion duration intervals (θ_c) on mass fraction burned (x) vs log (Volume) diagrams (35A and 35B) for case #35, ϕ=.57, lean limit, methanol

APPENDIX A

Thermodynamic Properties of Unburned and Burned Gases During Combustion When Using Oxygenated Organic Fuels

A.1 Calculation of Unburned Mixture Properties - (Oxidant, Fuel Vapor, Residual Gas)

When oxygenated organic fuels are used, the computation of thermodynamic properties for the unburned and burned gases requires additional analysis compared with analyses for pure hydrocarbon fuels. This section presents an overview of the modified analysis for a general fuel containing oxygen and nitrogen following methods in references (22, 37, 38).

During spark ignition engine combustion the unburned mixture in the cylinder consists of oxidant, fuel vapor, and residual gas. The concentrations of major species present depend upon whether the mixture is fuel lean or fuel rich; i.e.,

for $\phi \leq 1$: H_2O, CO_2, O_2, N_2, Fuel Vapor

for $\phi \geq 1$: H_2O, CO_2, H_2, CO, O_2, N_2, Fuel Vapor.

The fuel composition and the burned gas fraction (R) in the unburned mixture will determine the species concentrations present. Representing the fuel composition as $C_{\chi}H_{\chi\alpha}O_{\chi\beta}N_{\chi\delta}$ for a single- or multi-component fuel, the general combustion equation is of the form;

$$(1 - R)\ \varepsilon\ \phi\ C_{\chi}H_{\chi\alpha}O_{\chi\beta}N_{\chi\delta} + (1 - R)\ (O_2 + \psi N_2)$$

$$+\ R[\tilde{x}_1\ CO_2 + \tilde{x}_2 H_2O + \tilde{x}_3\ CO + \tilde{x}_4 H_2 + \tilde{x}_5 O_2 + \tilde{x}_6 N_2] \qquad \text{(A-1)}$$

$$\longrightarrow\ \tilde{x}_1\ CO_2 + \tilde{x}_2 H_2O + \tilde{x}_3 CO + \tilde{x}_4 H_2 + \tilde{x}_5 O_2 + \tilde{x}_6 N_2$$

where,

R = Residual Gas Mole Fraction

ϕ = mixture fuel/air equivalence ratio

ψ = molar N_2/O_2 ratio in the oxidant (3.764 for air)

$\tilde{x}_i$ = mole fraction of specie i

ε = constant determined from fuel-oxidant stoichiometry

χ = average number of carbon atoms in the fuel

α = H : C ratio in the fuel

β = O : C ratio in the fuel

δ = N : C ratio in the fuel

The mixture is treated differently for fuel lean, stoichiometric, and fuel rich cases. The following assumptions were made to solve for the seven unknowns (ε, $\tilde{x}_1$, $\tilde{x}_2$, $\tilde{x}_3$, $\tilde{x}_4$, $\tilde{x}_5$, $\tilde{x}_6$):

for $\phi \leq 1$ $\quad \tilde{x}_3 = \tilde{x}_4 = 0$ (A-2)

for $\phi > 1$ $\quad \tilde{x}_5 = 0$ (A-3)

for $\phi > 1$ $\quad CO_2 + H_2 \overset{K(T)}{\rightleftarrows} CO + H_2O$ (A-4)

Setting $\phi = 1$ and R = 0 determines the value of ε as

$$\varepsilon = (1 - \beta/2 + \alpha/4)^{-1} \qquad \text{(A-5)}$$

From atomic conservation of Carbon, Hydrogen, Oxygen and Nitrogen in equation (A-1), species concentrations $\tilde{x}_i$ can be computed. Table A-1 gives values of $\tilde{x}_i$ as a function of ϕ, R, and fuel composition.

Table A-1

Composition of Unburned Mixture for a $C_\chi H_{\chi\alpha} O_{\chi\beta} N_{\chi\delta}$ Fuel

i	Specie	$\tilde{x}_i$ (moles $\tilde{x}_i$/(1-R) moles O_2 oxidant	
		$\phi \leq 1$	$\phi > 1$
1	CO_2	$\varepsilon\phi R$	$(\varepsilon\phi - C)\ R$
2	H_2O	$[2(1-\varepsilon)+\varepsilon\beta]\phi R$	$[2(1-\varepsilon\phi)+\beta\varepsilon\phi+C]R$
3	CO	0	CR
4	H_2	0	$[2(\phi-1)-C]R$
5	O_2	$1-\phi R$	$1-R$
6	N_2	$\psi + \frac{R\varepsilon\phi\delta}{2}$	$\psi + \frac{R\varepsilon\phi\delta}{2}$
7	$C_\chi H_{\chi\alpha} O_{\chi\beta} N_{\chi\delta}$	$\frac{\varepsilon\phi(1-R)}{\chi}$	$\frac{\varepsilon\phi(1-R)}{\chi}$
TOTAL MOLES		$(1-\varepsilon)\phi R+\varepsilon\phi(1-R)/\chi$ $+\psi+1+\varepsilon\phi R(\beta+\delta/2)$	$(2-\varepsilon)\phi R+(1+\varepsilon\phi/\chi)(1-R)$ $+\psi+\varepsilon\phi R(\beta+\delta/2)$

The water gas equilibrium constant, K(T), is given by

$$K(T) = \frac{[CO]\ [H_2O]}{[CO_2]\ [H_2]} = \frac{[\tilde{x}_3]\ [\tilde{x}_2]}{[\tilde{x}_1]\ [\tilde{x}_4]} \qquad \text{(A-6)}$$

hence, $\tilde{x}_3$ can be expressed in terms of the values for $\tilde{x}_1$, $\tilde{x}_4$, and $\tilde{x}_2$ in Table A-1. $\tilde{x}_3$ is then equal to the positive root of the following quadratic equation where $\tilde{x}_3$ has been replaced by C:

$$C^2\ (1 - K(T)) + 2C\ (1 - \varepsilon\phi + \frac{\varepsilon\phi\beta}{2} + K(T)\ [\phi - 1 + \frac{\varepsilon\phi}{2}] - 2\ \ K(T)\varepsilon\phi\ (\phi-1) = 0. \qquad \text{(A-7)}$$

The value of K(T) given by Martin (39) as a curve fit to JANAFF table data over the range $400 < T < 3200$ °K is

$$\log_e [K(T)] = 2.743 - 1.761/t - 1.611/t^2 + .2803/t^3 \qquad \text{(A-8)}$$

where $t = T/1000°K$ and T is the temperature in °K.

The equations for the seven unknowns are now solvable with the four atomic conservation equations (Table A-1), and equations (A-5), (A-7), and (A-8). Letting $\tilde{M}_u$,

$$\tilde{M}_u = \varepsilon\ \phi\ (12 + \alpha + 16\ \beta + 14\ \delta) + 32 + 28\psi \qquad \text{(A-9)}$$

represent the total mass of the unburned mixture per (1-R) moles of O_2 oxidant, one can express the specific heat at constant pressure (c_{pu}) and the specific enthalpy (h_u) via the following equations (AVCO Everett Version) (40)

$$\tilde{M}_u\ c_{pu} = \sum_{i=1}^{7}\ \tilde{x}_i \left[\sum_{j=1}^{4}\ a_{ij}\ t^{j-1} + \frac{a_{i5}}{t^2}) \right] \qquad \text{(A-10)}$$

$$M_u\ h_u = \sum_{i=1}^{7}\ \tilde{x}_i \left[\sum_{j=1}^{4} \frac{a_{ij} t^j}{j} - \frac{a_{i5}}{t} + a_{i6} + a_{i8} \right] \qquad \text{(A-11)}$$

where

$t = T(°K)/1000°K$

$[a_{ij}]$ = kcal/gm mole - $(10^3\ °K)^j$

$[a_{i5}]$ = kcal $(10^3\ °K)$/gm-mole

$[a_{i6}], [a_{i8}]$ = kcal/gm mole

$[c_{pu}]$ = cal/gm °K

$[h_u]$ = kcal/gm

Coefficients a_{ij} were obtained by fitting c_{pu} and h_u data from thermochemical tables (41,42,43) to the functional form of equations (A-10) and (A-11). Results given by Hires (38) were used for species 1-6 for two temperature ranges 100°K < T < 500°K, and 500°K < T < 6000°K. Coefficients for various fuel vapors were calculated for one temperature range of 300°K < T < 1000°K (described in more detail in Section A.2).

The unburned mixture is being treated as a mixture of independent ideal gases; hence, in addition to c_{pu} and h_u, the following relationships are calculated via a computer subroutine (37, 39) given pressure P, temperature and volume:

$$C_{Tu} = \left(\frac{\partial h_u}{\partial P}\right)_{T_u} = 0 \qquad \text{(A-12)}$$

$$\rho_u = \frac{\bar{M}_u P}{\tilde{R} T_u} \qquad \text{(A-13)}$$

$$\left(\frac{\partial \rho_u}{\partial T_u}\right)_P = -\rho_u / T_u \qquad \text{(A-14)}$$

$$\left(\frac{\partial \rho_u}{\partial P}\right)_{T_u} = \rho_u / P \qquad \text{(A-15)}$$

where ρ_u is the density of the unburned gas, and $\tilde{R}$ is the universal gas constant. $\bar{M}_u$ is the resultant molecular weight which is a function of ϕ, R, and fuel compostion; i.e.

for $\phi \leq 1$

$$\bar{M}_u = \tilde{M}_u / \left[R\,\phi\,(1-\varepsilon) + 1 + \psi + \varepsilon\,\phi(1-R)/\chi + \varepsilon\phi R(\beta + \delta/2) \right]$$

for $\phi > 1$

$$\bar{M}_u = \tilde{M}_u / \left[2-\varepsilon)\,\phi\,R + \psi + (1 + \frac{\varepsilon\phi}{\chi})\,(1-R) + \varepsilon\phi R(\beta + \delta/2) \right] \qquad \text{(A-16)}$$

where $\psi = 3.764$ for air.

A.2 Calculation of Thermodynamic Properties for the Fuel Vapor

a) General

For multi-component fuels, or fuels such as Indolene which is composed of many different hydrocarbons, additional analysis was done to properly define the fuel's thermodynamic properties. Specifically, the specific heat at constant pressure (c_{pi}), specific enthalpy (h), and entropy (s_i)* of a specie i can be defined via curve fits to thermochemical data tables as shown below:

$$c_{pi} = a_{i1} + a_{i2}t + a_{i3}\,t^2 + a_{i4}\,t^3 + \frac{a_{i5}}{t^2} \qquad \text{(A-17)}$$

$$h_i = a_{i1}t + \frac{a_{i2}\,t^2}{2} + \frac{a_{i3}\,t^3}{3} + \frac{a_{i4}\,t^4}{4} - \frac{a_{i5}}{t} + a_{i6} + a_{i8} \qquad \text{(A-18)}$$

$$s_i = a_{i1}\log_e t + a_{i2}\,t + \frac{a_{i3}\,t^2}{2} + \frac{a_{i4}\,t^3}{3} - \frac{a_{i5}}{2t^2} + a_{i7} - R\log_e P \qquad \text{(A-19)}$$

---

*entropy (s) was not used in our calculations; however, coefficients for various fuel vapors were determined.

where,

[s] = cal/gm mole = °K t, c_{pi}, h_i, a_{ij}, = same as in equation (A-11)

For multi-component fuels represented by $C_\chi H_{\chi\alpha} O_{\chi\beta} N_{\chi\delta}$ thermodynamic properties are defined by summing mole-weighted contributions from its components. Hence, c_{pf} and h_f for a fuel of average molecular weight $\bar{M}_f$ are

$$c_{pf} = \frac{1}{\bar{M}_f} \sum_{k=1}^{n} y_k \left(\sum_{j=1}^{4} (a_{kj} t^{j-1}) + \frac{a_{k5}}{t^2} \right) \qquad \text{(A-20)}$$

and,

$$h_f = \frac{1}{\bar{M}_f} \sum_{k=1}^{n} y_k \left(\sum_{j=1}^{4} \left(\frac{a_{kj} t^j}{j}\right) - \frac{a_{k5}}{t} + a_{k6} + a_{k8} \right) \qquad \text{(A-21)}$$

where

y_k = whole fraction of component K in the fuel $C_\chi H_{\chi\alpha} O_{\chi\beta} N_{\chi\delta}$

$[M_f]$ = gm/gm mole

$[a_{kj}]$ = same as $[a_{ij}]$ in equations (A-10) and (A-11)

b) 100% Indolene Clear

Indolene clear; an unleaded gasoline-type fuel, is principally a mixture of various aromatic, olefin, and paraffin hydrocarbons. A chemical analysis was done on the indolene used to determine hydrogen-to-carbon ratio, average molecular weight, heat of combustion, and weight % aromatics, olefins and paraffins. To define thermodynamic properties of indolene, it was assumed that indolene is composed of average aromatic, olefin, and paraffin hydrocarbons. Properties

such as c_p, h, and s were determined as in equations (A-17) to (A-21) by summing and weighting the contributions of the representative components.

Representing indolene or any multi-hydrocarbon fuel as $C_A H_B$, the general molecular formula for its components are

for Olefins $C_m H_{2m}$

for Aromatics $C_n H_{2n-6}$

for Paraffins $C_p H_{2p+2}$

Hence, Indolene's composition is given by

$$(1)\ C_A H_B \equiv (X_n)\ C_n H_{2n-6} + (Y_m)\ C_m H_{2m} + (Z_p)\ C_p H_{2p+2} \qquad \text{(A-22)}$$

where

$$1 = X_n + Y_m + Z_p \qquad \text{(A-23)}$$

and,

X_n = Mole Fraction Aromatics

Y_m = Mole Fraction Olefins

Z_p = Mole Fraction Paraffins

m = average number of carbons in olefin

n = average number of carbons in aromatic

p = average number of carbons in paraffin

From atomic conservation of carbon and hydrogen, along with measurements of A, B, the weight % aromatics (G), olefins (S), and paraffins (Q) in the fuel, the following equations can be written:

$$A = n X_n + m Y_m + p Z_p \qquad \text{(A-24)}$$

$$B = 2A - 6X + 2Z \qquad \text{(A-25)}$$

$$G/100 = (14 \text{ X } n - 6 \text{ X})/C \quad \text{(A-26)}$$

$$S/100 = (14 \text{ Y } M)/C \quad \text{(A-27)}$$

$$Q/100 = (14 \text{ Z } p + 2 \text{ Z})/C$$

where $C = 14A - 6X_n + 2Z_p$

The six unknowns X_n, Y_m, Z_p, m, n, and p were calculated via a computer solutions of the six nonlinear algebraic equations (A-23) to (A-28). Table A-2 summarizes the results for indolene clear used in the experiments.

Thermodynamic properties c_p, h, and s for the various representative hydrocarbons in indolene were determined by fitting coefficients in equations (A-17), (A-18) and (A-19) to thermochemical data tables in references (41,42,43). The curve fitting was done by a computer program developed to fit coefficients of the form in equations (A-17), (A-18) and (A-19) or of the form of the NASA version in Reference (44). A least squares minimization of the deviation of curve fitted c_p's from tabulated c_p's was the basis for the calculations. Table A-3 lists the coefficients for the representative hydrocarbons used.

After coefficients for the various hydrocarbons were determined, coefficients for calculating indolene's (A-20) and (A-21) by summing weighted contributions of its components. The constant in equation (A-18), a_{i6}, representing the chemical enthalpy of the fuel, was adjusted to agree with the measured heat of combustion of indolene. More specifically, a_{i6} is determined by the definition of the heat of combustion which is given as

Table A-2

Indolene Clear Properties as Defined

in Equations (A-23) to (A-28)

Symbol	Value
From Chemical Analysis	
A	7.26
B	13.87
G	28.1 %
S	3.5 %
Q	68.4 %
From Computer Analysis	
X_n	.32
Y_m	.03
Z_p	.65
m	7.9
n	6.7
p	7.5

Table A-3

Coefficients for Determining Thermodynamic Properties of Various Fuels*

Name	Species**	a_{i1}	a_{i2}	a_{i3}	a_{i4}	a_{i5}	a_{i6}	a_{i7}	a_{i8}***
Methanol	CH_3OH	-2.70585	+44.1677	-27.5009	+7.21927	+.20299	-48.3211	+42.9592	+5.37100
Water	H_2O	+7.05451	+2.18652	+.833211	-.245212	+.0223292	-59.9304	+53.0596	+3.06200
Benzene	C_6H_6	-15.3997	+142.517	-111.628	+34.5597	+.126649	+19.4247	+8.45932	+7.58100
Toluene	C_7H_8	-19.5613	+176.392	-135.306	+41.5736	+.237377	+11.8563	+7.13400	+9.85600
n-Heptane	C_7H_{16}	-15.1162	+210.313	-147.158	+42.8266	+.357146	-47.2987	+29.1065	+17.945
Iso-Octane	C_8H_{18}	-17.9283	+242.674	-172.904	+51.362	+.418388	-56.1743	+16.2871	+20.225
1-Heptene	C_7H_{14}	-11.640	+188.593	-131.279	+37.9584	+.280913	-17.7675	+37.7389	+15.9310
Octene	C_8H_{16}	-13.1677	+215.745	-149.586	+42.9101	+.316535	-23.1793	+38.0527	+18.2040
Propane	C_3H_8	- 1.4867	+ 74.339	-39.0649	+8.05426	+.0121948	-27.3111	+42.22814	+ 8.8500
100% Indolene	$[C_{7.261}H_{13.87}]$	-16.990	+206.805	-149.478	+44.514	+.326768	-55.047	+18.3033	+15.88
10% Water-90% Methanol	$[C_{.777}H_{3.554}O_{.9891}]$	-.52929	+34.8059	-21.1824	+5.55469	+.162703	-50.910	+45.2116	+4.85609
15% Methanol-85% Indolene	$[C_{5.218}H_{10.65}O_{.3409}]$	-12.3291	+153.736	-109.677	+32.3447	+.28638	-52.8523	+26.3485	+12.4509

* $[a_{ij}]$ = kcal/gm mole - $(10^3°K)^j$ $j = 1,4$

$[a_{i5}]$ = kcal $(10^3°K)$/gm mole

$[a_{i6}],[a_{i7}],[a_{i8}]$ = kcal/gm mole See Equations (A-17), (A-18), (A-19)

** Coefficients were fitted over a temperature range $0°K < T < 1000°K$

*** For an absolute enthalpy datum state at T=0°K, a_{i8} is added to a_{i6} in equations (A-11),(A-18), and (A-21). For T = 298°K datum state, a_{i8} is omitted.

$$\Delta H_{C,\ 298°K} = A\ (\Delta H_f)_{CO_2,\ 298°K} + B/2\ (\Delta H_f)_{H_2O_g,\ 298°K} - (\Delta H_f)_{C_AH_B,\ 298°K} \quad \text{(A-29)}$$

where

$\Delta H_{C,\ 298°K}$ = heat of combustion (lower) @ 298°K

$\Delta H_{f_{CO_2},H_2O,298°K}$ = heat of formation @ 298°K

$\Delta H_{fC_AH_B,298°K}$ = heat of formation @ 298°K

Solving for $\Delta H_{fC_AH_B,\ 298°K}$ in (A-29) in terms of the remaining variables determines a_{16} since $\Delta H_{fC_AH_B,\ 298°K}$ is given as the value of h calculated in equation (A-18) with t = T/1000°K = .298 and a_{18} = 0. Table A-3 lists the coefficients used for determining Indolene's thermodynamic properties.

c) Coefficients for the Methanol Blends and Effective Heating Value

Coefficients for the 15% Methanol - 85% Indolene blend, and the 10% Water - 90% Methanol blend were calculated using the same approach outlined above. All results for the determination of thermodynamic properties for these blends are given in Table A-3.

For calculating thermal efficiency when using various methanol blends, the effective heat of combustion (lower) was defined as

$$Q_E \text{ (energy per unit mass)} = \frac{1}{\bar{M}_f} \sum_{k=1}^{n} y_k\ Q_k\ M_k \quad \text{(A-30)}$$

where

n = number of coefficients

y_k, $\bar{M}_k$ = as in equations (A-20) and (A-21)

Q_k, M_k = heat of combustion (lower) and molecular weight, respectively, of component k.

A.3 Calculating Burned Mixture Properties for Oxygenated Fuels Using an Existing Technique for Pure Hydrocarbon Fuels

It is assumed in the thermodynamic model of the combustion process in the engine cylinder (reviewed in Appendix B) that local thermodynamic equilibrium exists for species present in the burned gas region. By knowing temperature, pressure, and composition of the charge, thermodynamic properties can be determined.

A method developed by Martin (44) was used that approximates full equilibrium calculations for pure hydrocarbon-air combustion products via a bulk treatment of the species present into divisions of triatomic, diatomic, and monotomic molecules. The model's computational speed and acceptable accuracy for calculations of thermodynamic properties were important advantages to trade off some of the precision and additional information of the full equilibrium calculations.

For pure hydrocarbon fuels, the model calculates for the products of combustion the enthalpy (h_b), density (ρ_b) as a function of pressure (P), temperature (T_b), and equivalence ratio Φ for a given H : C ratio of the fuel (α') and N : O_2 ratio of the oxidizer Ψ. By direct differentiation, partial derivatives of h_b and ρ_b with respect to P, T_b, and Φ are also calculated. Specifically, input to the model is of the form

$$E\ \Phi\ C\ H_{\alpha'} + O_2 + \Psi N_2 \rightarrow \text{Combustion Products} \qquad \text{(A-31)}$$

where

Φ, α', Ψ = as defined above

E = a constant determined from stoichiometry of combustion.

Since input to the model is essentially temperature, pressure, equivalence ratio, and ratios of hydrogen to carbon and nitrogen to oxygen atoms, the analysis for hydrocarbon-air combustion products can be used for fuels containing oxygen and/or nitrogen (37). The combustion equation for a general $C_{\chi}H_{\chi\alpha}O_{\chi\beta}N_{\chi\delta}$ fuel is rewritten as follows:

$$\varepsilon\ \phi\ C_{\chi}H_{\chi\alpha}O_{\chi\beta}N_{\chi\delta} + O_2 + \psi\ N_2 \rightarrow \text{Combustion Products} \qquad \text{(A-32)}$$

where ϕ, χ, α, β, δ, and ψ are defined as in equation (A-1). By defining an equivalent Φ, E, Ψ, and α', in equation (A-31) in terms of ε, ϕ, α, β, δ, and ψ in equation (A-32), thermodynamic properties of combustion products can be calculated using Martin's model. Specifically, by setting expressions in equations (A-31) and (A-32) equivalent to each other, one obtains for E, Φ and ψ via conservation of C, H, O, and N atoms, given ϕ, ε, α, β, δ:

$$E = \varepsilon / (1 + \beta\varepsilon/2) \qquad \text{(A-33)}$$

$$\Phi = \phi\ (1 + \beta\varepsilon/2)/(1 + \beta\varepsilon\phi/2) \qquad \text{(A-34)}$$

$$\Psi = (\psi + \varepsilon\phi\delta/2)/(1 + \beta\ \varepsilon\phi/2) \qquad \text{(A-35)}$$

and,

$$\alpha' = \alpha \qquad \text{(A-36)}$$

Φ in equation (A-34) can be interpreted as the effective equivalence ratio of the products (the C : O_2 ratio divided by the stoichiometric C : O_2 ratio). This can be different than the mass based equivalence ratio ϕ. Ψ is the molar N : O ratio of the products which can be different than the molar N : O ratio of the oxidizer.

APPENDIX B

Thermodynamic Analysis of the Combustion Process Relating Mass Fraction Burned to Measured Pressure-Time Histories

A computer model developed by Martin (39) describing the thermodynamics of internal combustion was modified for use with fuels containing oxygen and/or nitrogen (see Appendix A). This model was used to obtain a greater insight into the burned and unburned gas properties during combustion, and to provide a basis for calculations of kernel development periods, ignition delay periods, and combustion intervals. Using a model for the structure of the flame front, turbulent flame speeds, flame radii, turbulent entrainment speeds, characterstic burning times, and entrainment f/ront radii are also calculated (see Appendix C). This section presents an overview of the fundamentals of the thermodynamic model.

The combustion process in the spark ignition engine is modeled by assuming the gases can be divided into burned and unburned thermodynamic systems. The volume of the reaction zones is assumed negligible. The unburned gases are assumed frozen at their original composition. Since energy producing reactions in the flame front are sufficiently fast, the burned gases are assumed in local chemical equilibrium. By also assuming the pressure is uniform throughout the cylinder, conditions in the burned and unburned gases are determined by the equation of state for the burned and unburned gases, respectively,

$$P \bar{v}_b = \bar{R}_b \bar{T}_b \qquad \text{(B-1)}$$

$$P \bar{v}_u = \bar{R}_u \bar{T}_u \tag{B-2}$$

where the subscripts b and u refer to burned out unburned gases. Conservation of mass, assuming leakage passed the rings negligible, yields

$$V/M = \bar{v}_b x + \bar{v}_u (1 - x) \tag{B-3}$$

and conservation of energy from the system illustrated in Figure B-1, yields

$$(E_o - W - Q) M = x \bar{e}_b + (1 - x) \bar{e}_u \tag{B-4}$$

where,

P = pressure in the cylinder

v = specific volume

$\bar{R} = \tilde{R} / \bar{M}$

$\tilde{R}$ = universal gas constant

$\bar{M}$ = mean molecular weight of gases in the cylinder

V = cylinder volume

M = total mass of gases in the cylinder

x = mass fraction burned

E_o = initial internal energy

W = commulative work done on the piston

Q = commulative heat loss (see Figure B-1)

e = specific internal energy

Figure B-1 Thermodynamic systems of burned and unburned gases during combustion

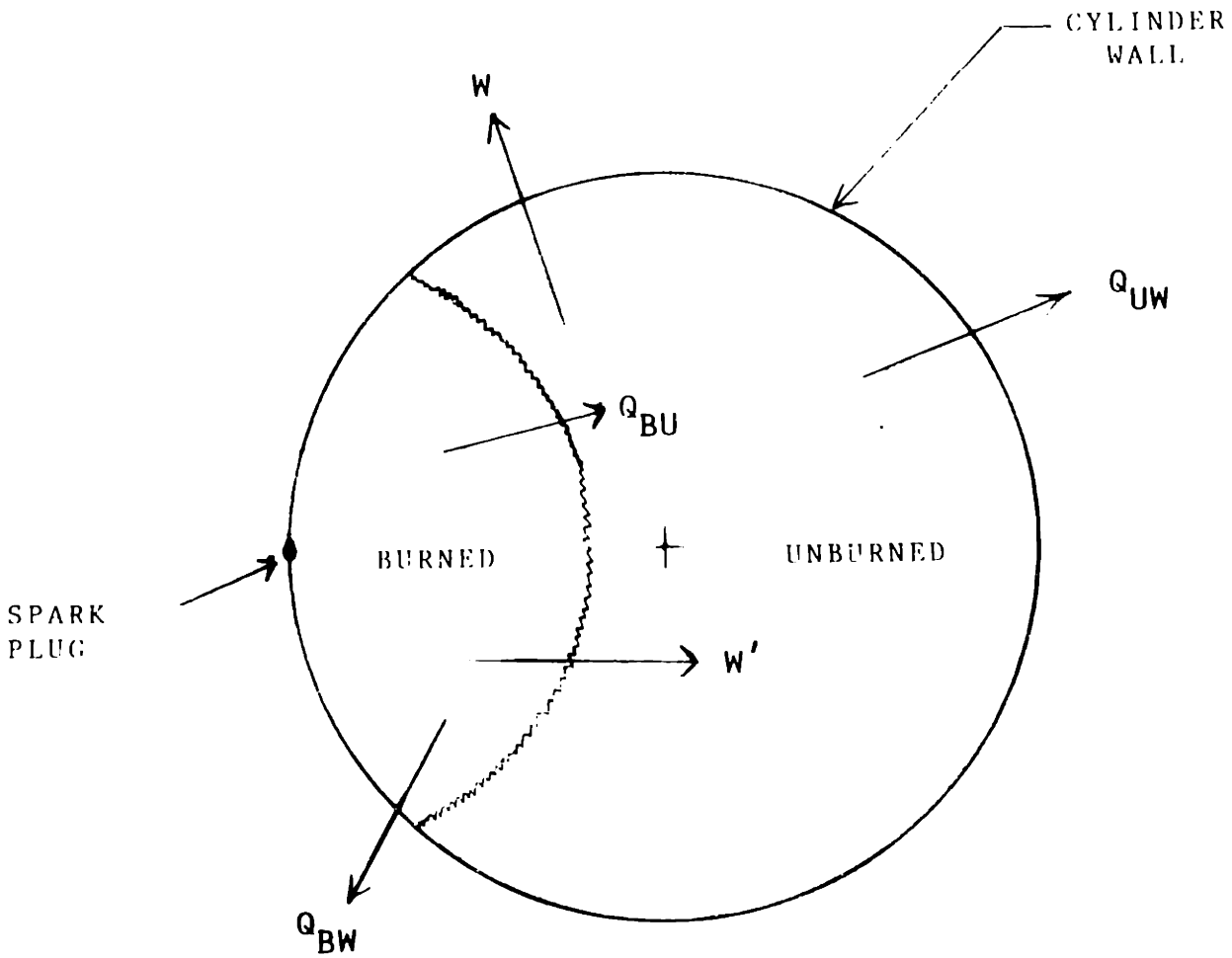

where,

W = cummulative work done on piston

W' = work done on burned compressing unburned gas

Q_{BW} = heat loss from burned gases to wall

Q_{BU} = heat loss from burned gases to unburned gases

Q_{UW} = heat loss from unburned gas to wall.

and b, u refer to burned and unburned gases, respectively. The conceptual definitions of $\bar{v}_b$, $\bar{v}_u$, $\bar{e}_b$, $\bar{e}_u$ are given by

$$\bar{v}_b = \frac{1}{x} \int_o^x v_b \, dx' \tag{B-5}$$

$$\bar{v}_u = \frac{1}{(1-x)} \int_x^1 v_u \, dx' \tag{B-6}$$

$$\bar{e}_b = \frac{1}{x} \int_o^x e_b \, dx' \tag{B-7}$$

and

$$\bar{e}_u = \frac{1}{(1-x)} \int_x^1 e_u \, dx' \tag{B-8}$$

Assuming the unburned charge is composed of oxidant, fuel vapor, and residual gas, the unburned gas properties are determined with the methods described in Appendix A. Specifically for solving equations (B-1) through (B-4),

$$\bar{e}_u = \bar{h}_u - P\bar{v}_u \qquad \text{(B-9)}$$

where $\bar{h}_u$ is calculated by equation (A-11) given P, $\bar{T}_u$, ϕ, R, and composition of the fuel (see Appendix A). The perfect gas assumption allows $\bar{v}_u$ to be calculated via equation (b-2) as a function of P, and $\bar{T}_u$.

$\bar{T}_u$ is specified directly for some initial state of the unburned gas (where x = o) by P_o, V_o, R, ρ_u, and fuel composition via equation (B-2) where $\bar{M}$, the mean molecular weight is given by (A-15) or (A-16). For future states of the unburned gas, an assumption was made for the calculation of $\bar{T}_u$. Heat loss from the unburned gas is of the same order of magnitude as radiative heat loss of the burned gas to the unburned gas (39). This leads to the assumption that the compression and expansion of unburned gases during combustion can be modeled as an isentropic process. From the definition of enthalpy, the change in enthalpy for a change in entropy (s) and pressure (P) is given by

$$dh = T\,ds + v\,dP \qquad \text{(B-10)}$$

The change in temperature with respect to pressure for an isentropic process is given by

$$\left(\frac{\partial T}{\partial P}\right)_s = \left[\bar{v}_u\ (P,\ T) - \left(\frac{\partial h}{\partial P}\right)_T\right] \Big/ \left(\frac{\partial \bar{h}_u}{\partial T}\right)_P \qquad \text{(B-11)}$$

Using an adaptive predictor-corrector method, along with unburned properties defined in Appendix A, $\bar{T}_u$ is determined. Hence, $\bar{v}_u$ and $\bar{e}_b$ are now defined via equations (B-2) and (B-7).

The burned gases are assumed to be in local chemical equilibrium and the thermodynamic properties are calculated using the approximate technique described in Appendix A.3. Specifically,

$$\bar{h}_b,\ (\partial\ h_b/\partial T_b)_P,\ (\partial h_b/\partial P)_{\bar{T}_b},\ \bar{\rho}_b,\ (\partial\bar{\rho}_b/\partial\bar{T}_b)_P,\ \text{and}\ (\partial\bar{\rho}_b/\ P)_{\bar{T}_b}$$

are calculated as a function of P, $\bar{T}_b$, Φ, Ψ, and β' (see Appendix A).

The average specific internal energy, $\bar{e}_b$, and average specific volume, v_b, must be calculated to determine mass fraction burned from either (B-3) or (B-4). To calculate $\bar{v}_b$ and $\bar{e}_b$ the average burned gas temperature $\bar{T}_b$ must be known, implying that some additional assumptions must be made about conditions in the burned gases. Two limiting cases will be considered (28). The first case is called the "fully mixed" case where burned gases are approximated as homogeneous at an equivalence ratio Φ with uniform temperature throughout so that $T_b = \bar{T}_b$. This assumption corresponds to infinite heat conductivity in the burned gas region. The second case is called the "unmixed" case and no mixing of the burned gases occurs. For this assumption, each burned gas element is isentropically compressed after combustion so that

$$T_b\ (x',\ x)/T_b\ (x') = [P(x)/P(x')]^{(\bar{\gamma}_b - 1)/\bar{\gamma}_b} \qquad \text{(B-12)}$$

where T_b (x', x) is the temperature of the element burned at pressure P (x') when the pressure is p(x). T_b (x') is the temperature resulting from isenthalpic combustion of the gas at pressure P (x'), i.e.,

$$T_b (x') = [\Delta h_c + c_{pu} \bar{T}_u (x')]/c_{pb} \quad \text{(B-13)}$$

where, Δh_c is the heat of combustion for the mixture. For the unmixed case, equations (B-12) and (B-13) would give $\bar{T}_b$; hence, the state of the burned gases would be defined.

The "unmixed" case implies zero heat conductivity in the burned gases with no mixing, and is opposite in sense to the"fully-mixed" case (28). Although temperature gradients have been shown to exist in the burned gases (28), turbulent mixing during combustion and heat transfer from the burned gases to the wall do occur. Therefore, the real situation lies somewhere between the two limiting cases. For this work, the various combustion properties presented were calculated using the fully mixed model since heat transfer needed to be incorporated. A description of how burned gas properties were calculated follows.

By solving both equations (B-3) and (B-4) for x and equating their solutions, the function Z ($\bar{T}_b$) is defined as

$$Z (\bar{T}_b) = \frac{(V/M - v_u)(\bar{e}_b - \bar{e}_u)}{(\bar{v}_b - \bar{v}_u)(e_{tot} - \bar{e}_u)} - 1 = 0 \quad \text{(B-14)}$$

where,

$$e_{tot} = (E_o - Q - W)/M \quad \text{(B-15)}$$

and $\bar{T}_b$ is the positive root of $Z(\bar{T}_b) = 0$. A Newton-Raphson iteration is performed given the previous $\bar{T}_b$ as a first estimate; i.e.

$$\bar{T}_b = \bar{T}_{b_{old}} - \left(\frac{Z(\bar{T}_b)}{\frac{\partial Z(\bar{T}_b)}{\partial \bar{T}_b}} \right)_{P,\ \emptyset} \tag{B-16}$$

where,

$$\left(\frac{\partial Z\ (T_b)}{\partial \bar{T}_b} \right)_{P,\ \emptyset} = \frac{(V/M - v_u)}{(\bar{v}_b - \bar{v}_u)^2} \quad \frac{1}{(e_{tot} - \bar{e}_u)} \quad \left[\quad (\bar{v}_b - \bar{v}_u) \left(\frac{\partial \bar{e}_b}{\partial \bar{T}_b} \right)_{P,\ \emptyset} \right.$$

$$\left. - (\bar{e}_b - \bar{e}_u) \left(\frac{\partial \bar{v}_b}{\partial \bar{T}_b} \right)_{P,\ \emptyset} \right] . \tag{B-17}$$

Since, $\bar{e}_b = \bar{h}_b - P/\bar{\rho}_b$ (B-18)

$$\left(\frac{\partial e_b}{\partial \bar{T}_b} \right)_{P,\ \emptyset} = \left(\frac{\partial \bar{h}_b}{\partial \bar{T}_b} \right)_{P,\ \emptyset} - \frac{P}{\rho_b^2} \left(\frac{\partial \bar{\rho}_b}{\partial \bar{T}_b} \right)_{P,\ \emptyset} \tag{B-19}$$

and

$$\left(\frac{\partial \bar{v}_b}{\partial \bar{T}_b} \right)_{P,\ \emptyset} = - \frac{1}{\bar{\rho}_b^{\ 2}} \left(\frac{\partial \bar{\rho} b}{\partial \bar{T}_b} \right)_{P,\ \emptyset} \tag{B-20}$$

The adiabatic flame temperature is calculated for the initial state, P_o, V_o, and the second state, P_1, V_1 to obtain the initial heat transfer rates and starting points for the iteration.

After the iteration for burned gas temperature, $\bar{T}_b$, is completed, burned gas properties are known, and mass fraction burned x is obtained via equation (B-3).

$$x = \frac{(V/M - \bar{v}_u)}{(\bar{v}_b - \bar{v}_u)} \tag{B-21}$$

Note that in the iteration, solving for e_{tot} in equation (B-15) involves knowing the cumulative work done on the piston and cumulative heat loss to the charge. By definition the work is given as

$$W = \int_{V_o}^{V} p \, d \, V \tag{B-22}$$

where V_o is the initial volume. The calculation of cumulative heat transfer, Q, was based upon an empirical correlation developed by Woschni (39). The correlation relates the expected dependence of Nusselt Number with Reynolds Number, i.e.

$$Nu = \frac{h_t \, d}{k} = .035 \, Re^{.8} \tag{B-23}$$

which becomes,

$$h_t = 110 \, d^{-0.2} \, P^{0.8} \, T^{-0.53} \, W^{.8} \tag{B-24}$$

where,

h_t = heat transfer coefficient, kcal - m^{-2} - p^{-1} - $°K^{-1}$

d = cylinder diameter, m

P = absolute cylinder Pressure, KP/cm^2

T = appropriate temperatures (burned or unburned) °K

W = characteristic velocity, m/sec.

Woschni divides the characteristic velocity into two components: a velocity component resulting from piston induced motions, and a velocity component resulting from combustion induced motions. The combustion induced velocity is expressed as

$$w_c = C_2 T_o \left(\frac{V}{V_o}\right) \frac{(P - P_m)}{P_o} \qquad \text{(B-25)}$$

where P_o, V_o, T_o are the pressure, volume, and temperature of the charge at some reference time, and

P_m = pressure in a motored engine at similar conditions

V = combustion chamber volume - M^3

C_2 = 3, 24 x 10^{-3} m/sec - °K (an empirical constant).

The following heat transfer rates are calculated:

$\dot{Q}_{bw}$ = heat transfer rate from burned gas to the wall (cal/sec)

$\dot{Q}_{uw}$ = heat transfer rate from unburned gas to the wall (cal/sec)

$\dot{Q}_{bu}$ = heat transfer rate from burned gas to unburned gas (cal/sec).

The cumulative heat loss Q/M is solved by integration of $\dot{Q}_{bw}$ and $\dot{Q}_{uw}$,

$$Q/M = \int_{\Theta_o}^{\Theta} (\dot{Q}_{bw} + \dot{Q}_{uw}) \frac{d\Theta}{6N} \qquad \text{(B-26)}$$

where N is the engine speed.

Appendix C

Turbulent Flame Speed Calculations from Thermodynamic Properties During Combustion and Spherical Flame Geometry

To obtain a more qualitative insight into how varying fuel type affects the heat release rate in the combustion cycle, turbulent flame speeds were calculated using the thermodynamic properties calculated from the analysis described in Appendix B.

Using a method described by Lancaster et al. (21) for calculation of turbulent flame speed (Su_T), the continuity equation for entrainment of unburned mixture into the turbulent flame front can be written as

$$M \dot{x} = Su_T \quad A_T \quad \rho_u \tag{C-1}$$

or

$$Su_T = \frac{M \dot{x}}{A_T \rho_u} \tag{C-2}$$

where M is the charge mass, $\dot{x}$ is the first time derivative of mass fraction burned, ρ_u is the density of the unburned mixture, and A_T is the turbulent flame front area*. In the computation of flame front area (A_T), a spherical flame geometry model by Blizard and Keck (20,37) is used. Assumptions inherent in the use of the model in Equation (C-2) for calculation of Su_T are (20, 21)**.

---

*From ionization probe measurements of flame (or entrainment front radius) versus crank angle, turbulent entrainment speed (U_e), characteristic time (τ), and entrainment front radius (A_e) of the Blizard and Keck model can also be calculated (20,37,45) in addition to S_{u_T} and A_T .

**Refer to Figure C-1.

1) flame propagation process as a spherical wave from the point of ignition until truncated by the combustion chamber,
2) thickness of the flame front is negligible,
3) no heat release occurs in any element of charge before it is engulfed by the flame front,
4) a cylindrically shaped combustion chamber with the spark plug located on the edge of the upper surface of the head (see Figure 1) is used, and
5) spherical flame geometry is still valid with the use of a shrouded intake valve.

The assumption of infinitely thin flame thickness is an idealization of the real case where an entrainment front with finite thickness exists. The radius of the entrainment front (r_e) would be greater than the radius of the turbulent flame front (r_T). It is anticipated that computed flame speeds will be affected mostly by r_e versus r_T during the initiation and termination of the combustion cylce (21).

Figure C-1 Turbulent flame front during combustion with spherical geometry

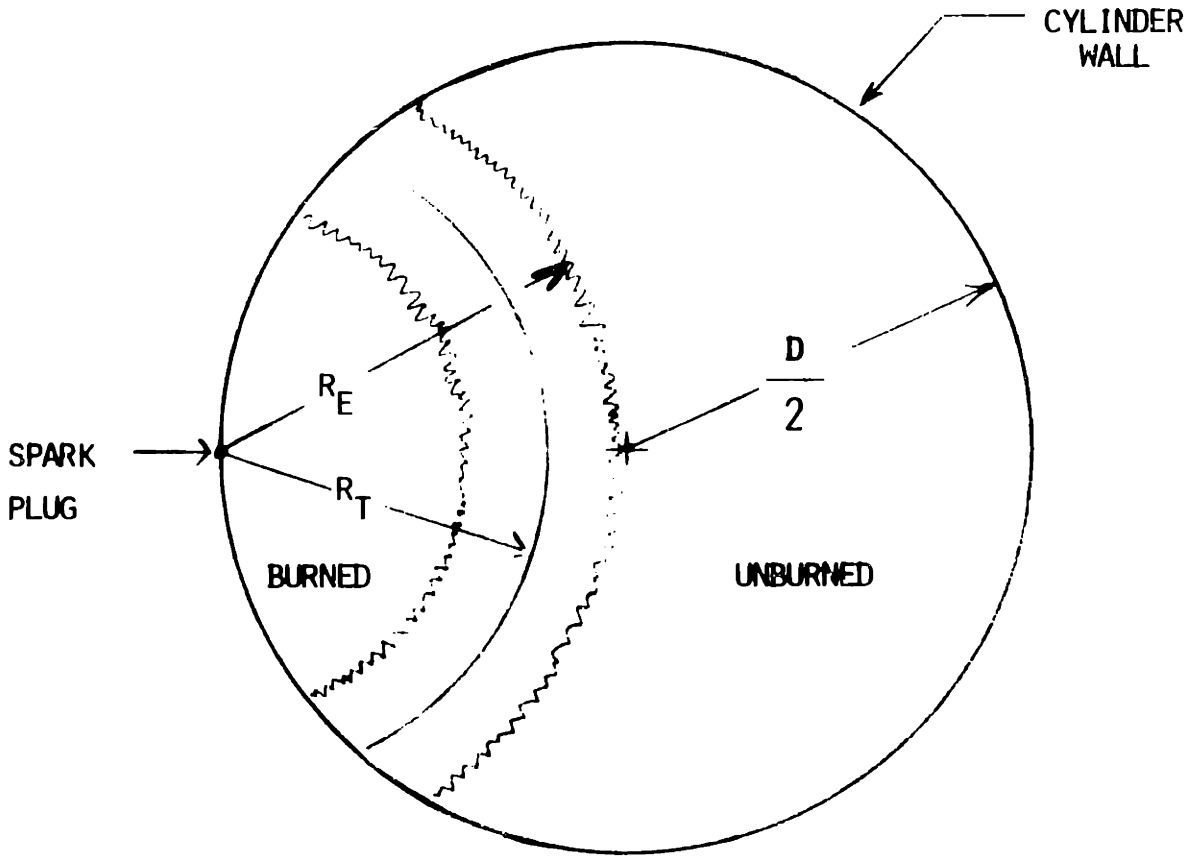

R_E = Turbulent entrainment front radius

R_T = Calculated turbulent flame front radius

d = Diameter of cylinder

Appendix D

Equivalence Ratios from Exhaust Gas Analysis when Burning Fuels Containing Oxygen and/or Nitrogen

A check of the accuracy of fuel flow, air flow, and exhaust gas specie concentration measurements can be made by comparing measured ($\phi_{measured}$) and calculated ($\phi_{calculated}$) equivalence ratios. The general combustion equation for fuels containing oxygen and/or nitrogen is similar to that for pure hydrocarbon fuels given in references (46,47)

$$(1 - \beta/2 + \alpha/4)^{-1}\ \phi\ CH_\alpha O_\beta N_\delta + O_2 + \psi\ N_2 \longrightarrow$$

$$T\ [\tilde{x}_1\ CO_2 + \tilde{x}_2\ H_2O + \tilde{x}_3\ CO + \tilde{x}_4\ H_2 + \tilde{x}_5\ O_2 + \tilde{x}_6\ N_2 + \tilde{x}_7\ C_rH_sO_tN_v] \qquad (D\text{-}1)$$

where $CH_\alpha O_\beta N_\delta$ defines the fuel composition, and

α = H : C ratio in the fuel

β = O : C ratio in the fuel

δ = N : C ratio in the fuel

ψ = N_2:O_2 ratio in the oxidant (3.764 for air)

$\tilde{x}_i$ = mole fraction of specie i

T = total moles in exhaust gases per one mole O_2

ϕ = mixture fuel/air equivalence ratio

It is assumed that the composition of unburned fuel emissions measured from the FID are equal to the fuel composition

(D-2)

$$(S/r = \alpha,\ t/r = \beta,\ v/r = \delta) \tag{D-3}$$

(D-4)

Known quantities from exhaust gas measurements and fuel analysis in Equation (D-1) are $\tilde{x}_1$, $\tilde{x}_3$, $\tilde{x}_5$, $\tilde{x}_7/r$, α, β, δ, $\psi = 3.764$ for air. The unknowns are ϕ, T, $\tilde{x}_2$, $\tilde{x}_4$, $\tilde{x}_7/s$, $\tilde{x}_7/t$, $\tilde{x}_7/v$.

Using atomic conservation of carbon, hydrogen, oxygen, and nitrogen, and assuming the water gas species in the exhaust are governed by the following equations

$$CO_2 + H_2 \overset{\tilde{k}}{\rightleftarrows} CO + H_2O \tag{D-5}$$

and

$$\tilde{k} = \frac{\tilde{x}_2\,\tilde{x}_3}{\tilde{x}_1\,\tilde{x}_4} = 3.5^{*} \tag{D-6}$$

the following set of equations were derived to calculate equivalence ratio ($\phi_{calculated}$) from exhaust gas specie concentrations

$$[H_2O] = \frac{k}{k+1} \tag{D-7}$$

where

$$k = \frac{\alpha}{2}\ \frac{([CO_2]_{dry} + [CO]_{dry})}{\left[1 + \frac{1}{3.5}\ \frac{[CO]_{dry}}{[CO_2]_{dry}}\right]} \tag{D-8}$$

and

$$\phi_{calc} = \frac{2\left(1 + \frac{\alpha}{4} - \frac{\beta}{2}\right)}{\left[\frac{\left[(1-[H_2O])\ (2[CO_2]_{dry}+[CO]_{dry}+2[O_2]_{dry}) + \alpha[UBF]_{wet}+[H_2O]\right]}{\left[(1-[H_2O])\ ([CO_2] + [CO]_{dry}) + [UBF]_{wet}\right]} - \beta\right]} \tag{D-9}$$

---

*k = 3.5 determined empirically by Spindt (49)

Appendix E

Indicated Specific Unburned Fuel Concentrations for Oxygenated Hydrocarbons

The FID response to unburned fuel components in the exhaust gases represents mole fraction carbon atoms of the unburned fuel composition*. This implies that the mass of fuel per mole carbon in the fuel ($M_{f/c}$) must be known. Specifically

for indolene ($C_{7.57}H_{15.21}$) $M_{f/c}$ = 14.0

for methanol (CH_3OH) $M_{f/c}$ = 32.0

for 15% methanol-85% indolene ($C_{5.218}H_{10.65}O_{.3409}$) $M_{f/c}$ = 15.1

and for 10% water-90% methanol ($C_{.777}H_{3.554}O_{.9891}$) $M_{f/c}$ = 32.0

Since the sensitivity of a total hydrocarbon analyzer to oxygenated hydrocarbons is not 100% when calibrated with a pure hydrocarbon calibration gas (12, 15). the following correction is used for all IS UBF results presented for methanol or an indolene-methanol blend

$$\text{Correction} = \frac{\text{actual ppm UBF}}{\text{measured ppm UBF}} = \left(\frac{x}{S} + 1 - x\right) \qquad \text{(E-1)}$$

where

x = mole fraction methanol in the fuel**

S = FID sensitivity for methanol

$= \frac{\text{ppm methenol measured}}{\text{ppm actual}}$

---

*Note that in the case of methanol-water blends, the only specie detected by the FID would be methanol and water would not be considered part of the measured UBF emissions.

**For methanol-water blends x = 1

For all experiments, propane was the calibration gas and s was determined to be roughly equal to .9 for all cases (see Table 3).

Indicated specific unburned fuel emissions were then calculated as follows

$$ISUBF = \frac{(\frac{x}{s} + 1-x)\ [UBF]_{wet}\ (\dot{M}_F + \dot{M}_A)\ M_{f/c}}{IHP \qquad M_{total}} \tag{E-2}$$

where

x,s = as described in Equation (E-1)

$[UBF]_{wet}$ = wet mole fraction reading from total hydrocarbon analyzer

$\dot{M}_F$ = mass flow rate of fuel

$\dot{M}_A$ = mass flow rate of air

$M_{f/c}$ = mass of fuel per mole carbon in fuel

IHP = indicated horsepower

M_{total} = average molecular weight of products (taken as 28.95)

Appendix F

Instrumentation

This section was added to include additional information on special instrumentation designed for the experiments.

Figure F-1 shows a logic schematic diagram of the electronic processor designed* to process the 5 volt pulses from the pulse generator mounted to the engine shaft and display pulses either every 10 and 60 crank angle degrees, or every 20 and 120 crank angle degrees. A 5 volt step scope trigger which remains + 5 volts for one cycle is also in the design.

*Designed and built by Fee Q. Yee, Sloan Laboratory, MIT, 1976.

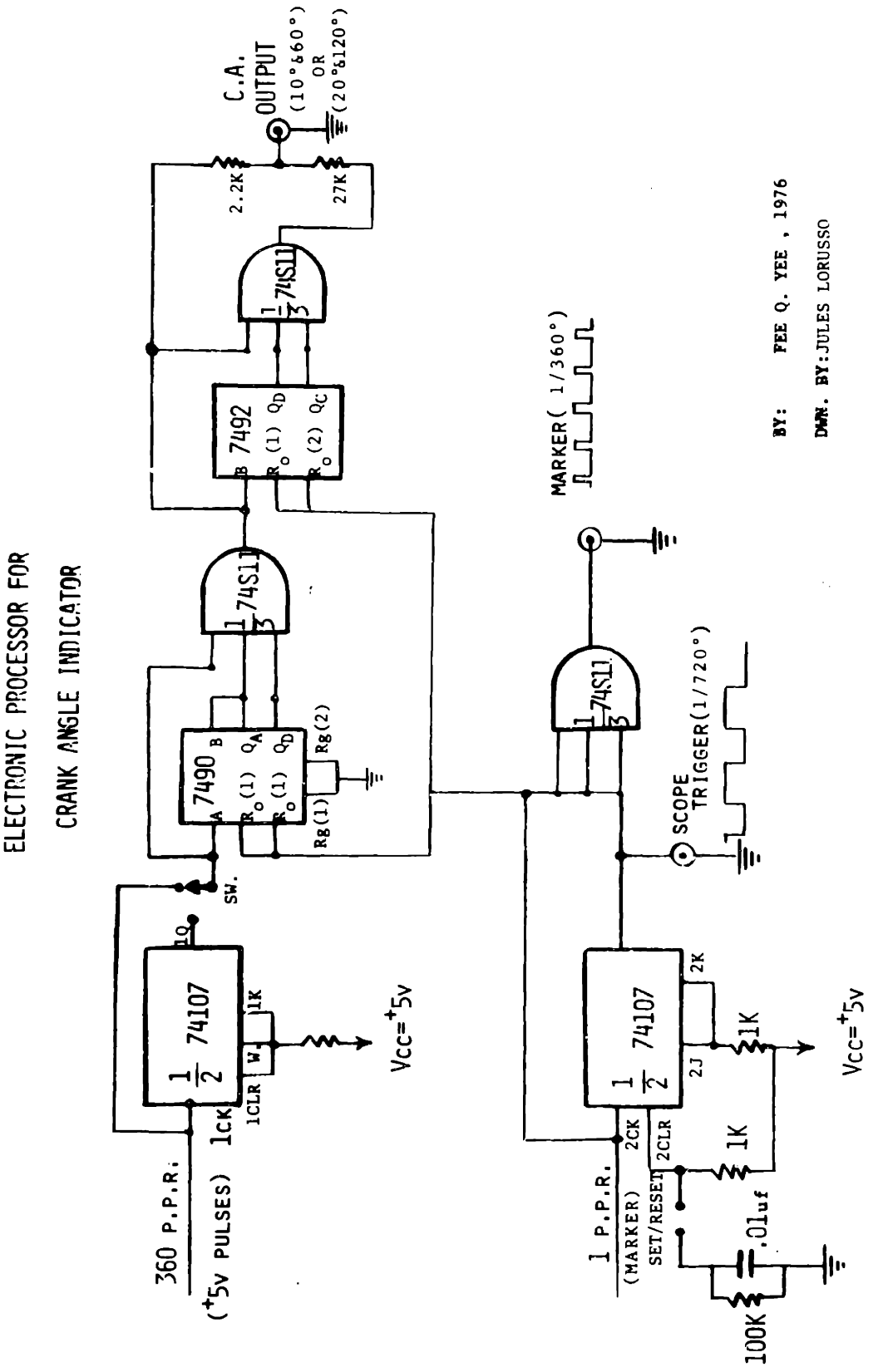

Figure F-1 Electronic processor for crank angle indicator